Master's thesis

NTNU
Norwegian University of Science and Technology
Faculty of Information Technology and Electrical Engineering
Department of Electronic Systems

Konstantin Jordal

Moisture detection in waste materials using electromagnetic waves in the GHz domain

Master's thesis in Electronic Systems Design and Innovation
Supervisor: Dag Roar Hjelme
June 2021

NTNU
Norwegian University of Science and Technology

Konstantin Jordal

Moisture detection in waste materials using electromagnetic waves in the GHz domain

Master's thesis in Electronic Systems Design and Innovation
Supervisor: Dag Roar Hjelme
June 2021

Norwegian University of Science and Technology
Faculty of Information Technology and Electrical Engineering
Department of Electronic Systems

NTNU
Norwegian University of
Science and Technology

Abstract

This master's thesis addresses whether electromagnetic waves in the GHz domain can be used to determine moisture levels of waste materials at Waste-to-Energy plants. This could be achieved in a setup where waste materials are illuminated by GHz waves, followed by analysing the response of the system for patterns related to the moisture level. A theoretical model based on this setup was developed and implemented with MATLAB to assess water contents of homogeneous materials. Where the theoretical model consisted of three layers, with two layers of air separated by the middle layer characterised by experimental values of the frequency-dependent complex refractive index $\underline{n}(\nu)$ of water. Imposing the Fresnel equations at each boundary between the different media combined with matrix-theory and the effective media approximation, determined how electromagnetic waves would propagate through the system as the moisture level changed. Which was demonstrated by simulating the reflection and transmission spectra of the layered media for different moisture levels. The resulting theoretical model proved to be suitable for moisture detection. Especially for certain frequencies in the range 1-35 GHz, where substantial differences in the detected reflection of the incident waves was strongly correlated to changes in moisture levels. By interpreting the reflection spectra simulated from the theoretical model, the moisture level in the effective medium was detected with an average certainty of 86%.

To determine the validity and accuracy of the theoretical model, dielectric properties of a sponge sample filled with different volumetric moisture contents were measured experimentally in the lab using the DAKS-3.5 measurement setup. The experimentally measured dielectric properties were then used to simulate the corresponding reflection spectra following the same method described for the theoretical model. The reflection intensity in the resulting reflection spectra was strongly correlated to changes in the volumetric moisture content of the sample material, especially for frequencies in the range 3-14 GHz. By interpreting the simulated reflection spectra, the volumetric moisture content of the sample material was determined with an average certainty of 70.38%.

Sammendrag

Denne masteroppgaven tar for seg om elektromagnetiske bølger i GHz-domenet kan brukes til å detektere fuktighetsnivået i avfall ved Waste-to-Energy anlegg. Dette kan oppnås i et oppsett der avfallsmaterialer blir belyst av GHz-bølger, etterfulgt av å analysere systemets respons for mønstre relatert til fuktighetsnivået. En teoretisk modell basert på dette oppsettet ble utviklet og implementert med MATLAB for å detektere vanninnholdet i homogene materialer. Hvor den teoretiske modellen besto av tre lag med materialer, to lag med luft adskilt av det midterste laget karakterisert av eksperimentelle verdier av den frekvensavhengige komplekse brytningsindeksen $\underline{n}(\nu)$ av vann. En beskrivelse av hvordan de elektromagnetiske bølgene ville forplante seg gjennom systemet ved endringer i fuktighetsnivå ble etablert ved å bruke Fresnel-ligningene på hver grense mellom forskjellige medier kombinert med matriseteori og effektiv medie-tilnærming. Som ble demonstrert ved å simulere refleksjon og transmisjon spekter av lagdelte medier for forskjellige fuktighetsnivåer. Den resulterende teoretiske modellen viste seg å være egnet for fuktdeteksjon. Spesielt for visse frekvenser i området 1-35 GHz, hvor vesentlige forskjeller i den observerte refleksjonen av de innfallende bølgene var sterkt korrelert med endringer i fuktighetsnivåer. Ved å tolke refleksjonsspektrene simulert av den teoretiske modellen ble fuktighetsnivået i det effektive mediet detektert med en gjennomsnittlig sikkerhet på 86%.

For å avgjøre gyldigheten og nøyaktigheten til den teoretiske modellen, ble dielektriske egenskaper til en svamp fylt med forskjellige volumetriske fuktighetsinnhold målt eksperimentelt i laboratoriet ved hjelp av DAKS-3.5 måleoppsett. De målte eksperimentelle dielektriske egenskapene ble deretter brukt til å simulere de tilsvarende refleksjonsspektrene ved å bruke samme metode beskrevet for den teoretiske modellen. Refleksjonsintensiteten i de resulterende refleksjonsspektrene var igjen sterkt korrelert med endringer i volumetrisk fuktighetsinnhold i prøvematerialet, spesielt for frekvenser i området 3-14 GHz. Ved å tolke de simulerte refleksjonsspektrene, ble volumetrisk fuktighetsinnhold i prøvematerialet detektert med en gjennomsnittlig sikkerhet på 70,38%.

Contents

List of Tables

List of Figures

Nomenclature

κ	Extinction coefficient
R	Power reflectance
r	Reflection coefficient
T	Power transmittance
t	Transmission coefficient
θ_1	Angle of incidence
θ_2	Angle of refraction
θ_w	Volumetric moisture content
ε	Complex permittivity
ε''	Dielectric loss factor
ε'	Dielectric constant
$\underline{n}$	Complex refractive index
n	Real refractive index
DAK	Dielectric Assessment Kit
$DAKS$	Dielectric Assessment Kit System
MSW	Municipal Solid Waste
TE	Transverse Electric
TM	Transverse Magnetic
VNA	Vector Network Analyser
WtE	Waste-to-Energy

1 Introduction

As an introduction to this master's thesis, background research is provided to motivate why the research conducted is of interest to the Waste-to-Energy (WtE) industry. Followed by investigating previous findings in the field to establish a reference point for the following research. Lastly, formulating the objective and outlining how the work is structured to reach the objective. WtE is a EnergiX KPN project co-funded by the Research Council of Norway and industry partners.

1.1 Background

In today's society, the primary source of energy stems from fossil fuels and still provide the best part of the current global energy demand. However, it is generally known that traditional fossil fuels are not environmentally sustainable and have limited reserves. As the global energy demand is only expected to increase in the future, there is a growing need for developing alternative sources of energy which are more sustainable and environmentally friendly. As stated by Kumar and Samadder (2017), Waste-to-Energy can be considered as a potential alternative source of energy, which is economically viable and environmentally sustainable" [7]. WtE plants would not only serve the purpose of meeting future energy demand, but also handle waste disposal. However, there are some challenges and problems that should be addressed in order to improve the efficiency of such WtE plants.

A current problem encountered in WtE plants that employs incineration as a method to both recover energy and minimise the waste volume and mass is the presence of moisture in the municipal solid waste (MSW) and not being able to differentiate dry from moist waste. According to Komilis et al. (2014), higher concentrations of moisture in the MSW will decrease the calorific value of the waste as a result of the latent heat of vaporisation and thus have an adverse affect on the self-sustained combustibility [6]. Not only will moisture in the MSW decrease the efficiency in energy conversion, but also lead to higher emissions and an increase of flue gases. If the moisture content for a given amount of waste could somehow be determined before combustion, the waste-to-energy process could be improved by increasing the energy conversion and simultaneously reducing emissions. For this reason, it is advantageous to develop a sensor system which serves the purpose of measuring moisture contents of waste materials.

A natural starting point arises from the fact that electromagnetic radiation in the millimetre wavelength range has high absorption in water and high transmission in most materials expect metals. With this in mind, one can imagine that for a given amount of waste material with an unknown water content, the water content could be determined by sending an input signal in the millimetre wavelength range through the waste. Followed by a sensor receiving the output signal and determining the water content of the waste based of the response of the system. As the water content directly influences factors such as how much of the input signal was lost due to absorption or how well the material reflects the incident waves. This is however only a simplified representation of the

idea, where other factors such as temperature and reflection from metals is not considered and may cause issues with the accuracy of the measurements.

1.2 Previous work

In a paper published in 2011, Paz et al. measured the dielectric properties of sawdust samples with different moisture content levels between 13% and 45% at 20°C [13]. The purpose of the research was to provide knowledge of material characteristics to better assess pricing, quality control and energy-conversion processes in sawdust employed as biofuel. The dielectric properties were measured both by an open-ended coaxial-line dielectric probe and a free-space transmission method for frequencies between 0.5 and 15 GHz. For the free-space transmission method, the dielectric properties were determined from the measurements of the attenuation and phase shift of waves propagating through a layer of material. This method could be of interest in determining moisture contents of waste materials in WtE plants. Furthermore, measurements of the sawdust samples at 9 GHz showed a strongly linear relation between the dielectric constant ε', the dielectric loss factor ε'', and θ_w, where θ_w is a volumetric representation of the moisture content. Namely the fact that both the dielectric constant ε' and the dielectric loss factor ε'' increased with moisture content. [13]

Another paper was published in 2009 in relation to frequent collapses by degradation of building blocks [12]. Determining material characteristics of building blocks was urgently required for strength inspection of built constructions. Moisture content in timber was one of the material characteristics provided in the paper, where a 200 GHz semiconductor electromagnetic wave source was used to inspect timbers with moisture content between approximately 0% and 25% at room temperature. According to Oyama et al. (2009), sub-THz inspection of moisture content proved to be practical as it demonstrated a linear relationship between the absorption coefficient and moisture content [12].

A master's thesis by Segelstein (1981) reported the experimental values for the complex refractive index of water for a wide spectre of frequencies. The real and imaginary part of the complex refractive index is represented by the real refractive index n and the extinction coefficient κ, respectively. These properties are used to describe the dielectric properties of water, and will be essential for the research conducted in this paper. Namely, to develop the theoretical model describing the interaction between the electromagnetic waves and materials containing moisture. Specifically, to compute the reflectance and transmittance of electromagnetic waves in the specified frequency range for homogeneous materials. [15]

1.3 Problem statement

The problem addressed in this paper will therefore be whether electromagnetic waves in the frequency range of 0.1-1000 GHz can be used to detect moisture in waste materials. The aim is to investigate how different volumes of water influence the electromagnetic wave and use that as a basis to build a theoretical model to assess water volumes in materials, then investigate whether

the theoretical results are consistent with reality by performing measurements in the lab. The project can be divided into two parts, where the first part involves building a theoretical model to describe how the electromagnetic signal interacts with materials of different water contents. It is worth mentioning that the model is limited to homogeneous materials (i.e. uniform materials). However, materials that do not have a uniform composition, formally known as heterogeneous, can be approximated and treated as homogeneous by applying effective medium approximation. In the second part of the thesis the purpose is to investigate whether the theoretical model is consistent with measurements performed in the lab, and then make a judgement on whether the theoretical model can be used as a tool at WtE plants to indicate unknown water contents in waste materials. The DAKS-3.5 setup consisting of an open ended coaxial probe and the R140 Vector Network Analyser was the measurement method used to experimentally measure dielectric properties of a sponge sample filled with different volumetric moisture contents.

Theory needed to understand the properties of water and how it interacts with electromagnetic radiation is introduced first. Followed by how the different theories were implemented to develop a theoretical model for assessing water concentrations. Lastly, the validity of the theoretical model is verified by measurements in the lab to evaluate whether it is a viable solution for moisture detection.

2 Theory

The aim for the first part of the project is to build a theoretical model used for detecting moisture levels of waste materials in the frequency domain of 0.1 - 1000 GHz, which may be considered to be the microwave region. Before it is possible to build such a theoretical model, it is necessary to describe the system to be analyzed and determine what theory is needed to understand how the system behaves. Understanding how the system behaves provides insight to make predictions about the system, where predicting moisture levels is of particular interest. Before explaining in detail the theories used for the research in this master's thesis, a short summary of each theory and why it is useful is provided.

Figure 1 shows the layered medium considered in this master's thesis. Here the two layers of air, represented by the refractive index n_1, are separated by a layer of distance d with a material containing an arbitrary amount of water. This layer is characterised by the frequency-dependent complex refractive index $\underline{n}_2(\nu)$. The mentioned terms of the refractive index of air n_1, complex refractive index of water $\underline{n}_2(\nu)$ and distance d may be considered as some of the initial conditions for the system illustrated in figure 1. Each of these conditions plays a role in how the electromagnetic wave behaves as it propagates through the system. A natural starting point would therefore be to explain what the dielectric property referred to as the complex refractive index describes and how it influences light-matter interaction. Followed by what importance the distance d has for electromagnetic waves propagating through a material with the dielectric properties of water.

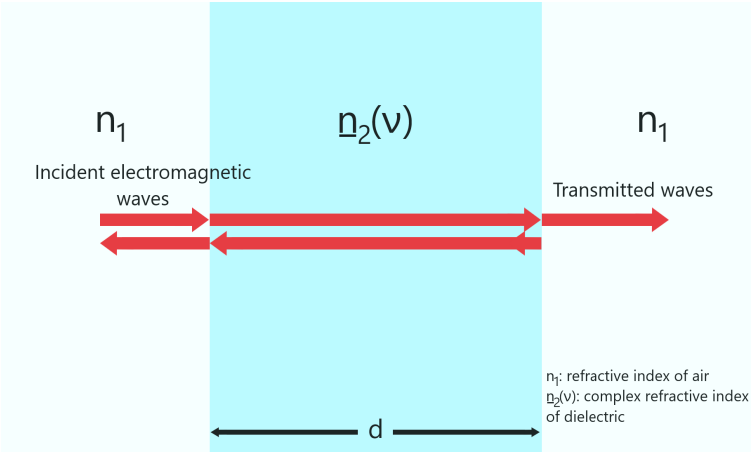

Figure 1: Model of the multilayered medium. Adapted from *Fundamentals of Photonics* (p. 256), by B. E. A. Saleh and M. C. Teich, 2013, Hoboken, New Jersey: John Wiley & Sons, Incorporate. Copyright 2007 John Wiley & Sons, Inc.

Furthermore, understanding what happens with the electromagnetic wave when incident on a boundary between two layers in the multilayered structure is essential for understanding how the system behaves. At the boundary, the difference in refractive index causes the electromagnetic wave to either be reflected or transmitted, where the resulting waves also undergo their own reflections and transmissions in the layered structure. Resulting in a rather complex problem with an endless

amount of waves travelling in each direction due to the many reflections and transmissions at each boundary, as illustrated by figure 2(a). The problem is simplified by considering all the contributions of the waves travelling forward as a single collected forward travelling wave $U^{(+)}$ and similarly for the backward travelling wave $U^{(-)}$, as shown in figure 2(b). It is worth mentioning that the boundaries between the different media in figure 1 are assumed to be planar. In reality, all surfaces are rough and may therefore contribute to scattering effects when the roughness of the surface is at a similar scale or smaller compared to the wavelength λ of the incident electromagntic wave. This is however not considered in this master's thesis.

With the knowledge of the refractive index associated with the materials at each side of a boundary, the Fresnel equations of reflection and transmission is applied to find the relationship between the waves at each side of the boundary. Making it possible to determine the overall reflectance and transmittance at a boundary. As the system in figure 1 consists of three layers with two boundaries, matrix theory is used to monitor the complex amplitudes of the forward and backward travelling waves as they propagate through the multilayered structure. The use of matrix theory also allows the overall reflectance and transmittance to be determined for the entire system in figure 1 in the desired frequency range. [14, p. 245-246]

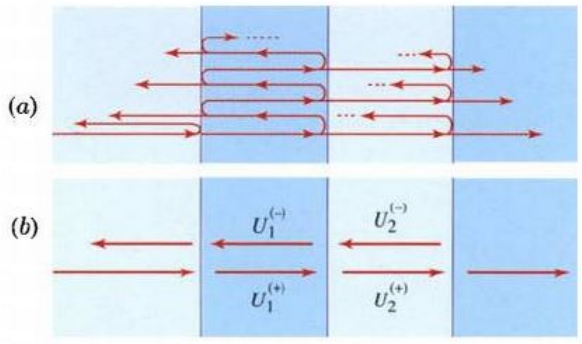

Figure 2: (a) Representation of how a single wave is transmitted or reflected at each boundary in a multilayered medium.
(b) All the forward travelling waves represented by a single forward collected wave $U^{(+)}$, and all the backward travelling waves represented by a single backward collected wave $U^{(-)}$ in each layer of the system. Reprinted from *Fundamentals of Photonics* (p. 246), by B. E. A. Saleh and M. C. Teich, 2013, Hoboken, New Jersey: John Wiley & Sons, Incorporate. Copyright 2007 John Wiley & Sons, Inc.

As it is desirable to analyze how the system in figure 1 behaves for different moisture levels, the concept of effective media approximation is introduced. This is necessary in order to approximate the dielectric properties of a media with an arbitrary moisture level. The last theory worth mentioning is an observable effect of how the system in figure 1 behaves. Part of the electromagnetic waves transmitted through the first boundary is reflected at the second boundary, where a part of these waves travel back across the middle layer and again be transmitted through the first boundary. The interaction between these waves and the waves being reflected off the first boundary is a physical phenomena known as interference. Understanding interference patterns provide useful insight when analyzing how the system behaves in section 4.

2.1 Dielectric properties

Establishing how the water molecule interacts with electromagnetic radiation in the mentioned frequency range is useful when assessing moisture content. For the chosen frequency range, the water

molecule has some interesting properties that cause the incident radiation to either be scattered, absorbed or transmitted. Each of these transitions have a likelihood of occurring as the electromagnetic waves interact with water, where the likelihood of each action is dependent on factors such as temperature, frequency, angle of incidence, polarisation, etc. The refractive index is an important property in light and matter interaction, and measures the velocity of light c in a specified medium compared to the speed of light in free space c_0. It is defined as

$$n = \frac{c_0}{c} = \sqrt{\frac{\varepsilon\mu}{\varepsilon_0\mu_0}}. \quad \text{[14, p. 158]} \tag{1}$$

For nonmagnetic material, such as water, the magnetic permeability of the material is simply $\mu = \mu_0$. Hence the refractive index n is only dependent on the factor known as the dielectric constant or relative permittivity ε_r of the material. Equation (1) is therefore written as

$$n = \sqrt{\frac{\varepsilon}{\varepsilon_0}} = \sqrt{\varepsilon_r}. \tag{2}$$

The relative permittivity ε_r is another dielectric property that describes how the medium responds to an applied electric field, discussed in section 2.1.2. The type of response the relative permittivity ε_r describes is sensitive to frequency, meaning that the refractive index n is also frequency-dependent. This implicates that electromagnetic waves of different frequencies propagates at different velocities c through a dielectric medium. Phase velocity is a term commonly used to describe the velocity at which one frequency-component is propagating through the medium, hence the refractive index n is used to determine the phase velocity. As the name suggests, the refractive index n is also used to describe how the electromagnetic wave is refracted when entering a medium. Even more compelling is the fact that the refractive index n can be used to determine the amount of electromagnetic radiation that is reflected or transmitted at the interface between two media of different refractive index. This is achieved by imposing the Fresnel's equations at boundaries between media of different refractive indices, described in further detail in section 2.3.

Considering the fact that water is an absorbing material, the complex refractive index is a more suitable property as it accounts for the phase velocity component as well as the attenuation of the electromagnetic wave as it propagates through the medium. According to the University of Reading (2019), the complex refractive index $\underline{n}(\nu)$ can be written in terms of a real part related to the phase velocity and an imaginary part related to the decay or damping of the oscillation amplitude of the incident electric field [16]. Thus complex refractive index is defined by the equation

$$\underline{n}(\nu) = n(\nu) - i\kappa(\nu), \tag{3}$$

where the real and imaginary part of the complex refractive index are formally known as the

refractive index n and the extinction coefficient κ, respectively.

Just like the refractive index $n(\nu)$, the extinction coefficient $\kappa(\nu)$ is also frequency-dependent. As water is an absorbing material, it has certain frequencies where the incident electromagnetic waves are absorbed a substantial amount, causing a damping of the oscillation amplitude of the incident electric field. This well known phenomena is what constitutes the heating process in microwave ovens, as the water molecule has a peak in the absorption spectra for the specific frequencies used in microwave ovens.

2.1.1 Experimental values of the refractive index and extinction coefficient of water

The frequency dependent parameters $n(\nu)$ and $\kappa(\nu)$ used in this master's thesis were obtained from previous studies and measurements conducted in regards to the interaction between water and electromagnetic radiation. In particular, the real and imaginary part of the complex refractive index $\underline{n}(\nu)$ for the desired spectrum was obtained from Segelstein (1981) [15]. Figure 3 shows experimental values of the real and imaginary part of the complex refractive index of water between 0.1 and 1000 GHz at the temperature 25 °C. Due to the highly temperature dependent nature of the dielectric properties showcased in figure 3, small temperature variations could drastically change the values of the real and imaginary part of the complex refractive index $\underline{n}(\nu)$.

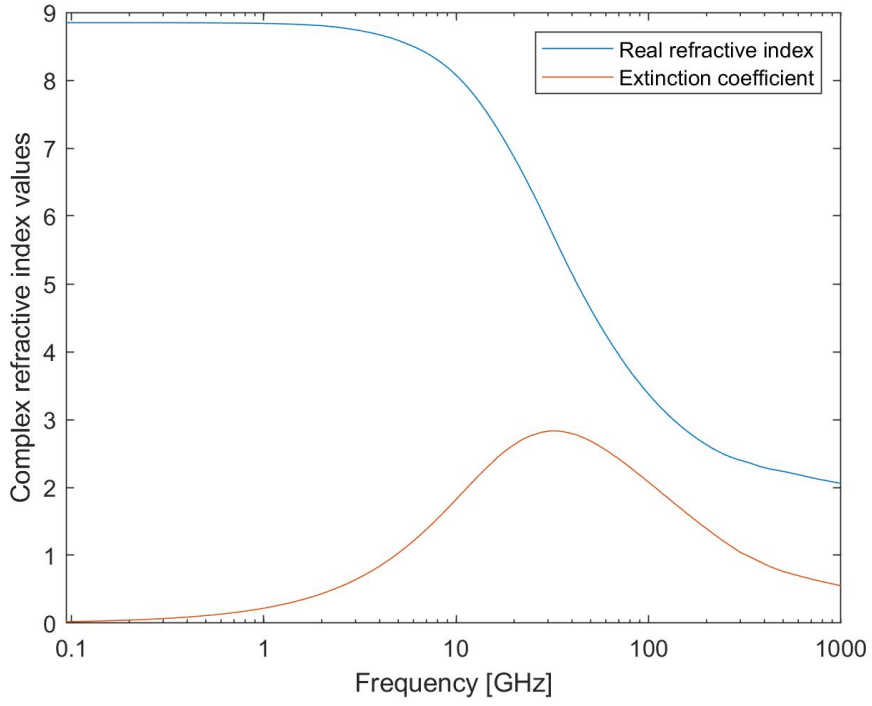

Figure 3: The real and imaginary part of the complex refractive index $\underline{n}(\nu)$ of water as function of frequency at 25 °C, gathered from Segelstein (1981) [15].

Upon inspection of figure 3, it is clear that the real part represented by the refractive index $n(\nu)$ dominates for most of the spectrum, especially for the lower frequencies. The refractive index directly influences both the reflection and transmission of the incident electromagnetic waves at the boundary between media, as well as how the waves travel through the media with regards to velocity. As mentioned previously, the refractive index is related to the velocity at which the light travels through the media, which in this case is water. By looking at equation (1), $n = 1$ when the velocity of light in the media is equal to the speed of light in free space (i.e. $c = c_0$). When the refractive index n is increased beyond unity, the velocity of light in the media c is reduced compared to the speed of light in free space c_0. With this in mind, one can conclude from figure 3 that the light velocity in the media increases with frequency.

The extinction coefficient $\kappa(\nu)$ is most influential at its peak, meaning that electromagnetic waves for these frequencies are more likely to be attenuated by water. According to Kupfer (2005), absorption in the microwave and infrared ranges are caused by the significantly high dipole forces that materialise as a result of the water molecules structure [8]. The exact origin of electromagnetic absorption for specified frequencies has been subject to discussion, where the microscopic interpretation of absorption spectra is still considered controversial [10]. However, the main purpose of this master's thesis is to investigate whether transmission and reflection spectra can be used for moisture detection, where the exact causes for absorption at specified frequencies is less important.

2.1.2 Dielectric permittivity

In some cases it is useful to describe the dielectric properties of water in terms of the complex permittivity. Especially since a considerable amount of research and studies conducted in the field use the complex permittivity to describe the dielectric properties of water. Before considering the complex nature of this property, the physical quantity of permittivity describes how a dielectric medium responds to an external electric field. In electromagnetism, the permittivity ε is a material property that describes the relation between the electric flux density $\mathbf{D}$ inside a medium and the electric field $\mathbf{E}$. Considering a homogeneous isotropic medium, the relation is given by the equation

$$\mathbf{D} = \varepsilon \mathbf{E}, \tag{4}$$

where ε represents the absolute permittivity of the medium. Applying an electric field to a dielectric causes a change in charge distribution, whereby charged particles inside the dielectric orientate according to the applied electric field. Meaning that the charged particles become polarised, where the permittivity ε is considered the quantity that describes how much the electric charge in a medium is polarised by an applied electric field.

The traditional capacitor model showcased in figure 4 is useful to provide insight to how the dielectric medium responds to an external electric field. In this example, the two capacitor plates are separated

by a dielectric region. Applying charge to the capacitor plates induces an electric field across the dielectric region. The applied electric field then polarises the electric charges, creating dipole moments which align themselves parallel to the applied field. By measuring the capacitance C associated with a dielectric medium and comparing it to the capacitance C_0 of a test capacitor, the capacitor model in figure 4 may be employed to define the relative permittivity ε_r. Resulting in the following equation

$$\varepsilon_r = \frac{C}{C_0} = \frac{\varepsilon}{\varepsilon_0}, \tag{5}$$

where ε is the permittivity of the medium and ε_0 is the vacuum permittivity.

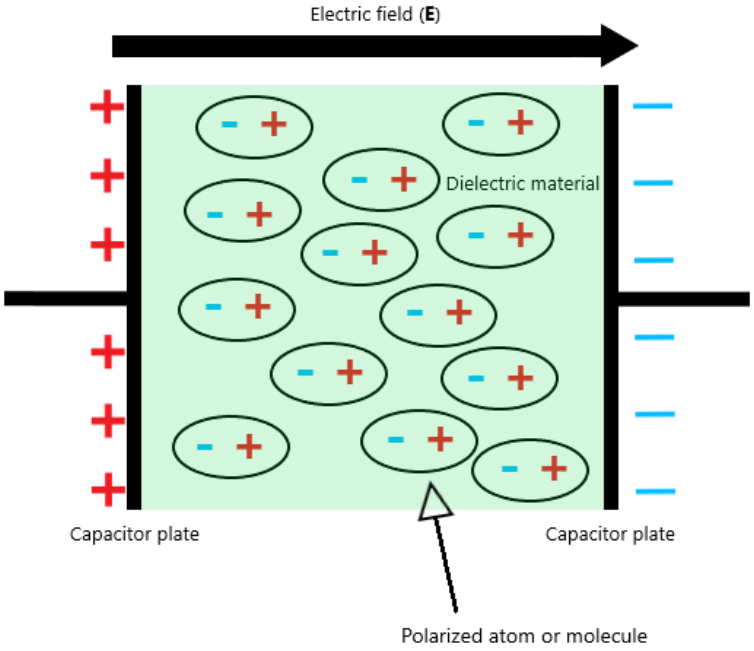

Figure 4: Polarisation effects in a dielectric material induced by an applied electric field.

By imposing an external electric field on a dielectric media, the response is generally frequency-dependent and must not violate causality. Meaning that the response cannot precede the application of the external electric field. Considering the frequency-dependent nature of a dielectric's response to an external electric field implicates that the polarisation of electric charges within the dielectric is not instantaneous. Introducing a phase difference is therefore necessary to ensure that causality is not violated. Hence the dielectric property of permittivity is represented by a frequency-dependent complex function, as complex numbers provide information about both amplitude and phase. The complex permittivity can be expressed by

$$\varepsilon(\nu) = \varepsilon'(\nu) - i\varepsilon''(\nu). \tag{6}$$

The complex permittivity $\varepsilon(\nu)$ consists of the real part formally known as the relative permittivity or dielectric constant $\varepsilon'(\nu)$ and describes the mediums energy storing abilities. While the imaginary part of the complex permittivity is known as the dielectric loss factor $\varepsilon''(\nu)$. As the name suggests, the dielectric loss factor describes the loss of electric energy due to the movement of electrically charged particles induced by the continually changing external electric field. When the electric field alternates, the dipole moments in the medium respond by realigning themselves parallel to the electric field. Resulting in energy loss due to heat generation caused by friction, as the rotation of dipole moments accelerate and decelerate in response to the alternating electric field. How much the dipole moment is out of phase with the electric field is indicated by the imaginary part of the complex permittivity $\varepsilon(\nu)$. High loss materials are charcterized by greater values of the dielectric loss factor $\varepsilon''(\nu)$. This property is particularly interesting in relation to determining moisture content of a medium, as the damping effect of the electromagnetic wave is related to the moisture level of the media.

As stated in Lunkenheimer et al. (2017), the dielectric loss factor $\varepsilon''(\nu)$ is an important property for daily-life applications such as microwave cooking, airport body scanners, and even has an affect on communication and radar devices as the electromagnetic waves experience a damping effect as they travel through fog and clouds [10]. The complex permittivity of water is a dielectric property which has been experimentally measured by various sources in recent history, but can also be calculated from other dielectric properties. According to Wooten (1972), the dielectric constant $\varepsilon'(\nu)$ and the dielectric loss factor $\varepsilon''(\nu)$ can both be derived from the refractive index $n(\nu)$ and the extinction coefficient $\kappa(\nu)$ by the following equations

$$\varepsilon'(\nu) = n^2(\nu) - \kappa^2(\nu), \tag{7}$$

$$\varepsilon''(\nu) = 2n(\nu)\kappa(\nu). \quad [17, \text{ p. } 45] \tag{8}$$

Using the already measured values of the refractive index $n(\nu)$ and extinction coefficient $\kappa(\nu)$ by Segelstein (1981), the relative permittivity $\varepsilon'(\nu)$ and the dielectric loss factor $\varepsilon''(\nu)$ of water was calculated from the relations in equation (7) and (8) [15]. Figure 5 displays the resulting values of the real and imaginary part of the complex permittivity $\varepsilon(\nu)$ for frequencies between 0.1 and 1000 GHz at the temperature 25 °C.

The ability to convert between the complex permittivity $\varepsilon(\nu)$ and the complex refractive index $\underline{n}(\nu)$ and vice versa is useful in this master's thesis. Where the real and imaginary part of the complex refractive index $\underline{n}(\nu)$ can be expressed in terms of the real and imaginary parts of the complex permittivity $\varepsilon(\nu)$ by the following expressions

$$n(\nu)^2 = \frac{1}{2}\left(\left(\varepsilon'(\nu)^2 + \varepsilon''(\nu)^2\right)^{\frac{1}{2}} + \varepsilon'(\nu)\right), \tag{9}$$

$$\kappa(\nu)^2 = \frac{1}{2}\left(\left(\varepsilon'(\nu)^2 + \varepsilon''(\nu)^2\right)^{\frac{1}{2}} - \varepsilon'(\nu)\right). \tag{10}$$

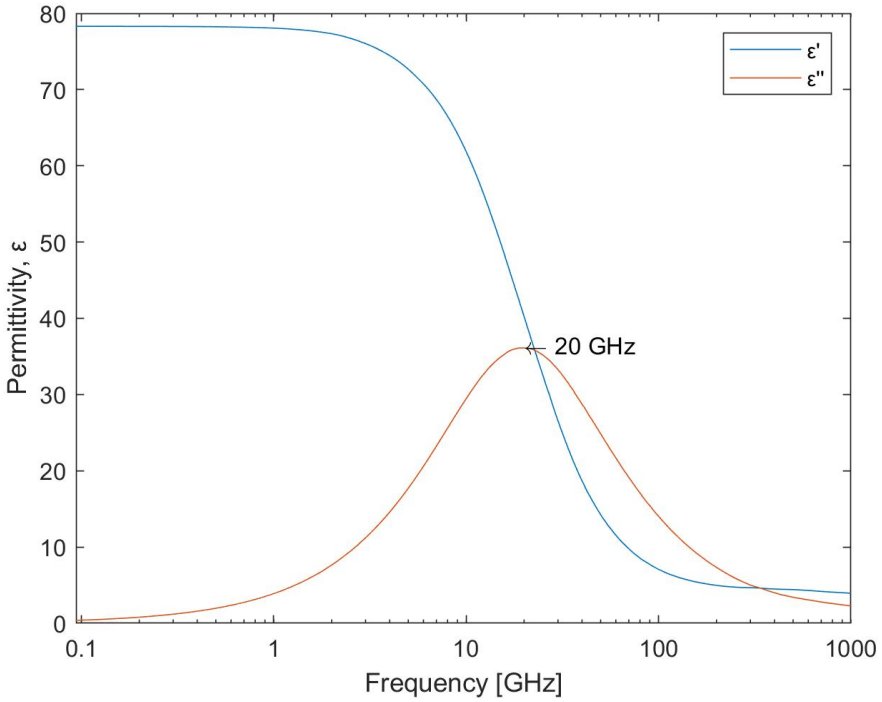

Figure 5: The relative permittivity $\varepsilon'(\nu)$ and the dielectric loss factor $\varepsilon''(\nu)$ as a function of frequency at 25 °C.

According to Lunkenheimer et al. (2017), a peak in the absorption spectra at 20 GHz is considered to be the dominating absorption mode or main relaxation peak, which is strongly temperature dependent [10]. This is consistent with figure 5, where the peak of the dielectric loss factor $\varepsilon''(\nu)$ is seen at 20 GHz. As described in Paz et al. (2011), the relative permittivity $\varepsilon'(\nu)$ is high for frequencies below the relaxation frequency of 20 GHz due to dipole polarization [13]. Furthermore, there is a phase shift between the electric field and the electric polarization of the water molecule in the relaxation region, where energy of the external electromagnetic field dissipates as heat resulting in a peak for $\varepsilon''(\nu)$ [8, p. 21]. Vibration-related processes causing absorption have also been detected, mainly located at the higher frequencies 150 - 940 GHz and 1.3 - 1.9 THz [10]. These processes are less influenced by temperature compared to the main relaxation peak. A research paper by Ellison et al. (1996) provides an extensive report of the permittivity of water in the frequency range 0 - 1000 GHz and temperature range 0° - 100°C. Comparing with the figure for the complex

permittivity presented by Ellison et al. (1996), it is reasonable to assume that the values for the dielectric constant $\varepsilon'(\nu)$ and the dielectric loss factor $\varepsilon''(\nu)$ in figure 5 are relatively accurate [3, p. 177].

2.2 Skin depth

The skin depth [1] of a material is another physical property which is useful when analyzing the interaction between electromagnetic waves and water. As mentioned, water is an absorbing material, which means that some of the optical intensity of the electromagnetic wave is lost as the wave propagates through water due to absorption. The amount of absorption in a specific medium is governed by the absorption coefficient α. According to the University of Reading (2019), the absorption coefficient is given by the following equation

$$\alpha(\nu) = \frac{4\pi}{\lambda}\kappa(\nu), \tag{11}$$

where λ and $\kappa(\nu)$ is the wavelength and extinction coefficient, respectively [16]. The skin depth δ represents the depth at which the optical intensity of the incident electromagnetic wave is attenuated by a factor $1/e$ and is defined by the equation

$$\delta(\nu) = \frac{1}{\alpha(\nu)} = \frac{\lambda}{4\pi\kappa(\nu)}. \tag{12}$$

By using the extinction coefficient $\kappa(\nu)$ from Segelstein (1981), the skin depth $\delta(\nu)$ was calculated by the expression in equation (12) for the desired frequency domain [15].

Figure 6 shows the skin depth $\delta(\nu)$ of water in millimetres for frequencies between 0.1 and 1000 GHz at the temperature 25 °C . There is a clear relationship between the skin depth δ and frequency, namely the fact that the skin depth $\delta(\nu)$ decreases with frequency. This should be kept in mind when analyzing the reflection and transmission spectra for water later on. An argument can already be made that for the higher frequencies, the skin depth $\delta(\nu)$ is very short and therefore make it difficult for the electromagnetic wave to penetrate through a medium containing water. As the lower frequencies have greater skin depth, it seems reasonable to assume that these frequencies are better suited for detecting moisture levels in media where the electromagnetic waves travel for longer distances through media containing water.

[1] Not to be confused with the skin depth in relation to the skin effect regarding the current density in conductors

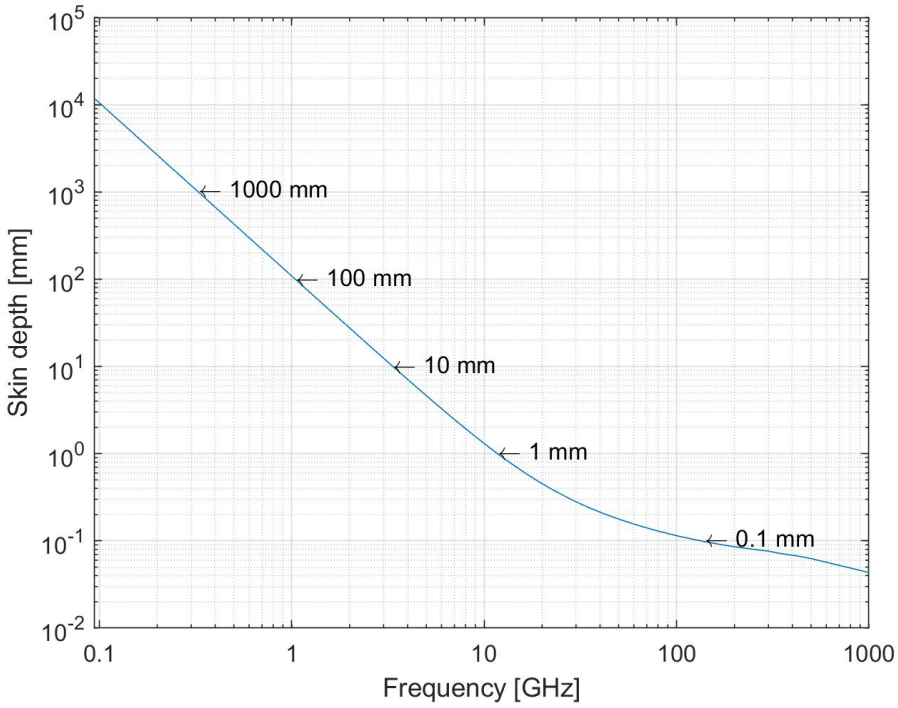

Figure 6: Skin depth $\delta(\nu)$ for water as a function of frequency at 25 °C.

However, it is worth mentioning that the skin depth $\delta(\nu)$ displayed in figure 6 only serves to provide a qualitative measure of the relationship between the skin depth and frequency. Considering that in equation (12), the skin depth $\delta(\nu)$ is determined by the extinction coefficient $\kappa(\nu)$ of a media with the dielectric properties of water. Adjusting the moisture level in a media means changing its dielectric properties, hence changing the extinction coefficient $\kappa(\nu)$ and thereby the skin depth $\delta(\nu)$. On the basis of the evidence currently available, it seems fair to suggest that media with lower levels of moisture attenuate the electromagnetic field to a lesser degree and therefore result in a greater skin depth $\delta(\nu)$ compared to that of media with higher concentrations of moisture.

2.3 Reflection and transmission of waves in layered media

At the planar boundary between two dielectric media with different refractive index, the incident electromagnetic wave can either be reflected or transmitted. As stated in Saleh and Teich (2013), the incident wave is assumed to be a monochromatic plane wave of arbitrary polarisation and the two media are assumed to be linear, homogeneous, and isotropic with refractive indexes n_1 and n_2 [14, p. 209]. In this case, the Fresnel equations are used to determine the amount of radiation from the incident wave that is reflected at the boundary between the two media. Consider an electromagnetic field consisting of the transverse electric (TE) and transverse magnetic (TM) polarisation is propagating through a material with refractive index n_1 and is then incident on a material with refractive index $\underline{n}_2(\nu)$, as illustrated in figure 7. According to Saleh and Teich (2013),

the reflection $\mathfrak{r}$ and transmission $\mathfrak{t}$ coefficient for TE and TM polarised light is given by the following equations

$$\mathfrak{r}_{\mathrm{TE}} = \frac{n_1 \cos\theta_1 - n_2 \cos\theta_2}{n_1 \cos\theta_1 + n_2 \cos\theta_2}, \quad \mathfrak{t}_{\mathrm{TE}} = 1 + \mathfrak{r}_{\mathrm{TE}}, \tag{13.1}$$

$$\mathfrak{r}_{\mathrm{TM}} = \frac{n_1 \sec\theta_1 - n_2 \sec\theta_2}{n_1 \sec\theta_1 + n_2 \sec\theta_2}, \quad \mathfrak{t}_{\mathrm{TM}} = (1 + \mathfrak{r}_{\mathrm{TM}}) \frac{\cos\theta_1}{\cos\theta_2}, \tag{13.2}$$

where the angles θ_1, θ_2 are the angles of the incident and refracted wave, respectively [14, p. 211].

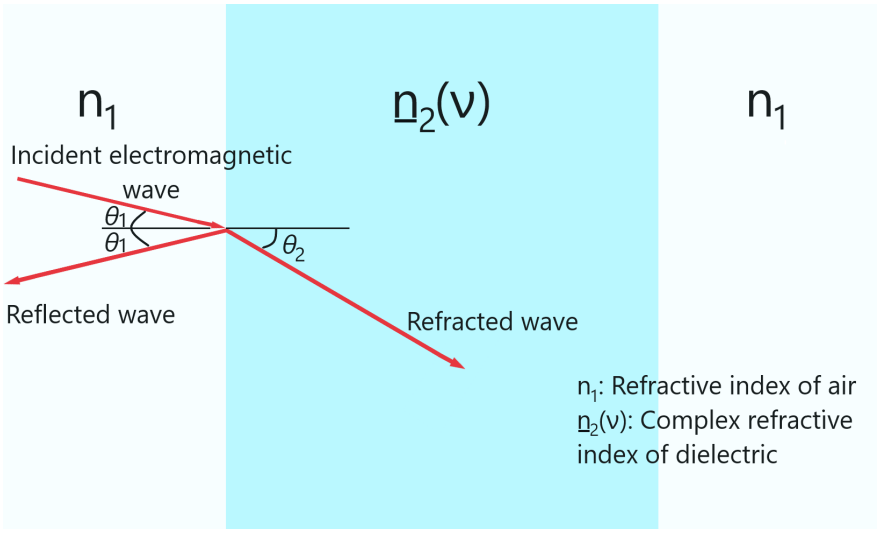

Figure 7: Reflection and refraction of an electromagnetic wave incident on the boundary between a material with refractive index n_1 and complex refrative index $\underline{n}_2(\nu)$. Adapted from *Fundamentals of Photonics* (p. 210), by B. E. A. Saleh and M. C. Teich, 2013, Hoboken, New Jersey: John Wiley & Sons, Incorporate. Copyright 2007 John Wiley & Sons, Inc.

Using the trigonometric relation $\sec\theta = \frac{1}{\cos\theta}$, the expression for $\mathfrak{r}_{\mathrm{TM}}$ may be rewritten as

$$\mathfrak{r}_{\mathrm{TM}} = \frac{n_1 \cos\theta_2 - n_2 \cos\theta_1}{n_1 \cos\theta_2 + n_2 \cos\theta_1}. \tag{13.3}$$

Snell's law describes the relation between the angle of incidence θ_1 and angle of refraction θ_2 by the following expression

$$n_1 \sin\theta_1 = n_2 \sin\theta_2. \tag{14}$$

If only normal incidence is considered, that is where both angles θ_1 and θ_2 are equal to zero, the expression for the reflection coefficient can be simplified to

$$\mathfrak{r} = \frac{n_1 - n_2}{n_1 + n_2}, \ |\mathfrak{t}|^2 + |\mathfrak{r}|^2 = 1, \tag{15}$$

which applies to both TE and TM polarizations. The expressions for the reflection and transmission coefficients $\mathfrak{r}$ and $\mathfrak{t}$ in equation (15) represent ratios of complex amplitudes. To gain an understanding from a more physical perspective, it is desirable to represent how much of the incident radiation is reflected or transmitted by some real physical quantity. Thus the power reflectance $\mathfrak{R}$ and power transmittance $\mathfrak{T}$ are introduced, which represent the ratio between power flow of the incident wave compared to the reflected and transmitted waves. The power reflectance $\mathfrak{R}$ is related to the reflection coefficient $\mathfrak{r}$ in equation (15) by the following expression

$$\mathfrak{R} = |\mathfrak{r}|^2 = \left(\frac{n_1 - n_2}{n_1 + n_2} \right)^2, \tag{16.1}$$

whereas the power transmittance $\mathfrak{T}$ is simply determined from the power reflectance $\mathfrak{R}$ by the relation

$$\mathfrak{T} = 1 - \mathfrak{R}. \quad [14, \text{ p. } 213\text{-}214] \tag{16.2}$$

2.4 Matrix theory

So far, the interaction between an incident electromagnetic wave onto a material with different refractive index has only been addressed at one boundary. Figure 1 illustrates the system considered in this master's thesis, consisting of a layered medium with three layers. Where the electromagnetic wave first propagates through a layer of air denoted by the refractive index n_1. As the wave reaches the first boundary between the different layers, the wave is partially reflected and transmitted which is determined by the first boundary determined by the Fresnel equations (15). Figure 2(a) shows how the incident wave undergoes an endless amount of reflections and transmissions at each boundary in the layered medium, resulting in a rather complex problem. By considering water as a homogeneous material, the layered medium formed by layers of air and water is treated as a multilayered structure. Thus, the described problem is simplified by the use of matrix theory, allowing for a systematic treatment of the multiple reflections that occur at each boundary in the layered media. Figure 2(b) shows that all the forward and backward travelling waves are represented by one single forward $U^{(+)}$ and backward wave $U^{(-)}$, respectively. Making it possible to impose the Fresnel equations (15) at each boundary to determine the relationship between the forward $U^{(+)}$ and backward $U^{(-)}$ at each side of the boundary.

By imposing the Fresnel equations at each boundary coupled with matrix theory to combine all the boundaries and layers of medium into one system, the overall transmittance and reflectance of the entire multilayered structure is determined. As the reflectance and transmittance are both

dependent on the refractive index of the materials, they are also frequency-dependent, making it possible to create reflectance and transmittance spectra for this sort of system.

2.4.1 Wave-Transfer Matrix

Two types of matrices needs to be defined to charcterize the layered medium as described. The first is known as the wave-transfer matrix and is denoted by $\mathbf{M}$. This matrix is used to determine the forward and backward travelling waves $U_2^{(+)}$, $U_2^{(-)}$ in medium 2 from the initial forward and backward travelling waves $U_1^{(+)}$, $U_1^{(-)}$ in medium 1. As described in Saleh and Teich (2013), the amplitudes of the forward and backward collected waves in medium 1 $U_1^{(+)}$, $U_1^{(-)}$ forms a plane 1 [14, p. 247]. An equivalent situation in medium 2 forms the second plane from the amplitudes $U_2^{(+)}$, $U_2^{(-)}$. The elements of matrix $\mathbf{M}$ are defined as A, B, C and D and are related to the optical properties of the layered medium between the two planes. Hence the following matrix equation is defined

$$\begin{bmatrix} U_2^{(+)} \\ U_2^{(-)} \end{bmatrix} = \mathbf{M} \begin{bmatrix} U_1^{(+)} \\ U_1^{(-)} \end{bmatrix} = \begin{bmatrix} A & C \\ B & D \end{bmatrix} \begin{bmatrix} U_1^{(+)} \\ U_1^{(-)} \end{bmatrix} \tag{17}$$

If a system is comprised of three layers, one wave-wave transfer matrix is needed to represent each layer. The product of these three matrices results in one single matrix $\mathbf{M}$, relating the amplitudes of the forward and backward collected waves at each end of the entire system. [14, p. 247]

2.4.2 Scattering Matrix

The other type of matrix is known as the scattering matrix and is denoted $\mathbf{S}$, where the elements are directly related to the physical parameters of the system. These four elements constitutes of the two reflection $\mathfrak{r}_{12}$, $\mathfrak{r}_{21}$ coefficients and the two transmission $\mathfrak{t}_{12}$, $\mathfrak{t}_{21}$ coefficients. Here the subscript $_{12}$ denotes reflection or transmission from medium 1 onto medium 2, and vice versa for the subscript $_{21}$. Yielding the following matrix equation

$$\begin{bmatrix} U_2^{(+)} \\ U_1^{(-)} \end{bmatrix} = \mathbf{S} \begin{bmatrix} U_1^{(+)} \\ U_2^{(-)} \end{bmatrix} = \begin{bmatrix} \mathfrak{t}_{12} & \mathfrak{r}_{21} \\ \mathfrak{r}_{12} & \mathfrak{t}_{21} \end{bmatrix} \begin{bmatrix} U_1^{(+)} \\ U_2^{(-)} \end{bmatrix}, \tag{18}$$

where the reflection $\mathfrak{r}_{12}$, $\mathfrak{r}_{21}$ and transmission $\mathfrak{t}_{12}$, $\mathfrak{t}_{21}$ coefficients are found from the Fresnel equations (15), which is valid when considering normal incidence. Looking at the matrix operations in equation (18), the forward travelling wave in plane 2 is given by $U_2^{(+)} = \mathfrak{t}_{12}U_1^{(+)} + \mathfrak{r}_{21}U_2^{(-)}$. This makes sense as the forward travelling wave $U_2^{(+)}$ in plane 2 should consist of two contributions, the transmitted part of the forward travelling wave $\mathfrak{t}_{12}U_1^{(+)}$ in plane 1 and the reflected part of the backward travelling wave $\mathfrak{r}_{21}U_2^{(-)}$ in plane 2. Similarly, the backward travelling wave $U_1^{(-)}$ in plane 1 is given by $U_1^{(-)} = \mathfrak{r}_{12}U_1^{(+)} + \mathfrak{t}_{21}U_2^{(-)}$. Meaning that the backward travelling wave $U_1^{(-)}$ in plane 1 is found from

the reflected forward travelling wave $\mathfrak{r}_{12}U^{(+)}$ in plane 1 and the transmitted backward travelling wave $\mathfrak{t}_{21}U_2^{(-)}$ in plane 2. [14, p. 247]

2.4.3 Relation between Scattering Matrix and Wave-Transfer Matrix

A combination of both **S** and **M** matrices are needed to represent the described layered medium. As mentioned, the elements of matrix **S** contain direct physical properties of the system, which is not the case for the elements in the **M** matrix. However, the **S** matrices do not have the ability to be cascaded in the same manner as the **M** matrices. In order to find the overall reflectance and transmittance of the layered medium, it is necessary to convert between the **S** and **M** matrices and vice versa. The conversion equations described in Saleh and Teich (2013) are given by the following

$$\mathbf{M} = \begin{bmatrix} A & C \\ B & D \end{bmatrix} = \frac{1}{\mathfrak{t}_{21}} \begin{bmatrix} \mathfrak{t}_{12}\mathfrak{t}_{21} - \mathfrak{r}_{12}\mathfrak{r}_{21} & \mathfrak{r}_{21} \\ -\mathfrak{r}_{12} & 1 \end{bmatrix}, \tag{19.1}$$

$$\mathbf{S} = \begin{bmatrix} \mathfrak{t}_{12} & \mathfrak{r}_{21} \\ \mathfrak{r}_{12} & \mathfrak{t}_{21} \end{bmatrix} = \frac{1}{D} \begin{bmatrix} AD - BC & B \\ -C & 1 \end{bmatrix} \quad \text{[14, p. 248].} \tag{19.2}$$

2.4.4 Propagation through a homogeneous medium

As stated by Saleh and Teich (2013), the **S** and **M** matrices for an electromagnetic wave propagating through a homogeneous medium of distance d with refractive index n are given by

$$\mathbf{M} = \begin{bmatrix} e^{(-j\varphi)} & 0 \\ 0 & e^{(j\varphi)} \end{bmatrix}, \quad \mathbf{S} = \begin{bmatrix} e^{(-j\varphi)} & 0 \\ 0 & e^{(-j\varphi)} \end{bmatrix}, \quad \varphi = nk_0 d \quad \text{[14, p. 248].} \tag{20}$$

Here $k_0 = \frac{2\pi}{\lambda}$ is the wavenumber of free space.

2.5 Propagation by off-axis waves through layered media

Similarly to the situation illustrated in figure 2(a) for normal incidence, figure 8(a) demonstrates that an oblique wave incident on a layered media is reflected and transmitted at each boundary in the same manner. Due to laws of reflection and refraction, waves travelling in the same direction in each layer of the structure are parallel with each other. Meaning that the same approach used for normally incident waves can also be applied for oblique waves. Which is demonstrated by figure 8(b), where all the forward and backward travelling waves are represented by one forward collected wave $U^{(+)}$ and one backward collected $U^{(-)}$, respectively.

Figure 9 showcases an oblique wave incident from a media with refractive index n_1 onto a media

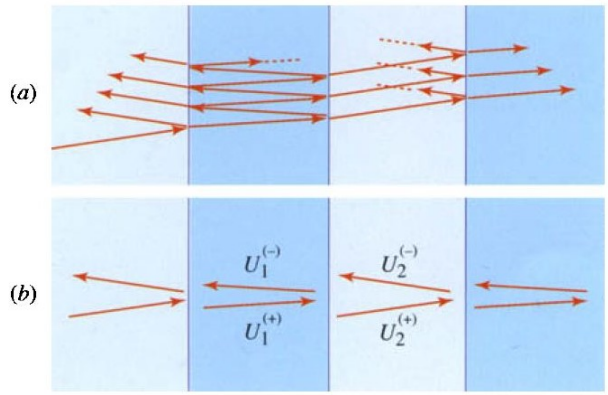

Figure 8: (a) Representation of how a single oblique wave is reflected or transmitted at each boundary in a multilayered medium.
(b) All the forward travelling waves represented by a single forward collected wave $U^{(+)}$, and all the backward travelling waves represented by a single backward collected wave $U^{(-)}$ in each layer of the system. Reprinted from *Fundamentals of Photonics* (p. 252), by B. E. A. Saleh and M. C. Teich, 2013, Hoboken, New Jersey: John Wiley & Sons, Incorporate. Copyright 2007 John Wiley & Sons, Inc.

with complex refractive index $\underline{n}_2(\nu)$ at an angle θ_1. Naturally, the amount of the incident waves that are either reflected or refracted at each boundary is found by imposing the Fresnel equations (13.1)-(13.2) for TE and TM polarised waves, respectively. Where the angle of incidence θ_1 is related to the angle of refraction θ_2 by Snell's law (14). According to Saleh and Teich (2013), an oblique wave incident and transmitted from the media with refractive index n_1 to complex refractive index $\underline{n}_2(\nu)$ at angles θ_1 and θ_2, is represented by the following $\mathbf{S}$ and corresponding $\mathbf{M}$ matrix

$$\mathbf{S} = \begin{bmatrix} \mathfrak{t}_{12} & \mathfrak{r}_{21} \\ \mathfrak{r}_{12} & \mathfrak{t}_{21} \end{bmatrix} = \frac{1}{\widetilde{n}_1 + \widetilde{n}_2} \begin{bmatrix} 2a_{12}\widetilde{n}_1 & \widetilde{n}_2 - \widetilde{n}_1 \\ \widetilde{n}_1 - \widetilde{n}_2 & 2a_{21}\widetilde{n}_2 \end{bmatrix}, \tag{21.1}$$

$$\mathbf{M} = \begin{bmatrix} A & B \\ C & D \end{bmatrix} = \frac{1}{2a_{21}\widetilde{n}_2} \begin{bmatrix} \widetilde{n}_1 + \widetilde{n}_2 & \widetilde{n}_2 - \widetilde{n}_1 \\ \widetilde{n}_2 - \widetilde{n}_1 & \widetilde{n}_1 + \widetilde{n}_2 \end{bmatrix} \quad [14, \text{ p. } 253]. \tag{21.2}$$

The $\mathbf{S}$ and $\mathbf{M}$ matrix in equations (21.1)-(21.2) can be adapted for TE and TM polarised waves by the following expressions

$$\begin{aligned} &\text{TE}: \ \widetilde{n}_1 = n_1 \cos\theta_1, \ \ \widetilde{n}_2 = \underline{n}_2(\nu)\cos\theta_2, \ \ a_{12} = a_{21} = 1, \\ &\text{TM}: \ \widetilde{n}_1 = n_1 \sec\theta_1, \ \ \widetilde{n}_2 = \underline{n}_2(\nu)\sec\theta_2, \ \ a_{12} = \frac{\cos\theta_1}{\cos\theta_2} = \frac{1}{a_{21}}. \end{aligned} \tag{22}$$

As the oblique wave enters the media with complex refractive index $\underline{n}_2(\nu)$ and distance d, the wave-transfer matrix $\mathbf{M}$ describing the propagation through the media is given by equation (20) where the phase is defined as $\varphi = \underline{n}_2(\nu)k_0 d\cos\theta_2$. [14, p. 253]

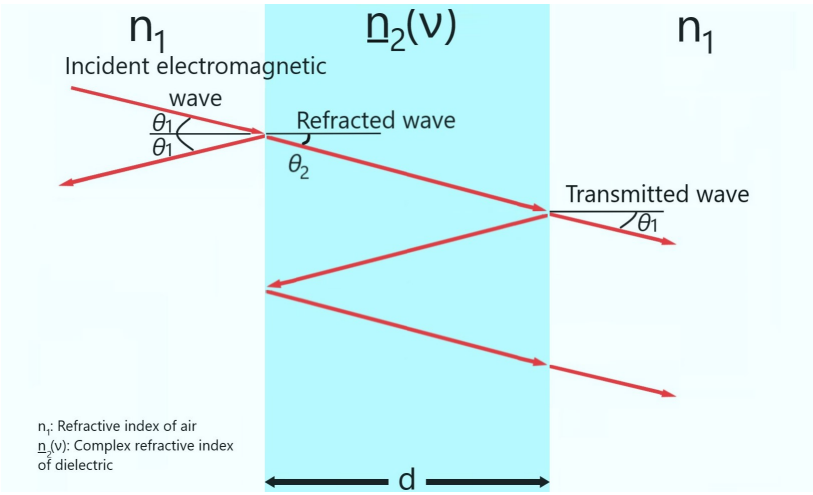

Figure 9: Propagation of an oblique electromagnetic wave on the boundary between a material with refractive index n_1 and complex refractive index $\underline{n}_2(\nu)$ with distance d. Adapted from *Fundamentals of Photonics* (p. 253), by B. E. A. Saleh and M. C. Teich, 2013, Hoboken, New Jersey: John Wiley & Sons, Incorporate. Copyright 2007 John Wiley & Sons, Inc.

2.6 Effective medium approximation

Effective medium approximation is a method used to treat heterogeneous media as homogeneous media. As one of the main purposes of the research conducted in this master's thesis is to determine moisture content in waste materials, it is convenient to represent the mix of different materials as one effective medium with a given effective refractive index. As stated in Chýlek et al. (1988), effective medium approximations are considered to lack mathematical and physical justifications and their accuracy and range of validity are not easily established [2]. However, when considering scattering and absorption of electromagnetic radiation in composite materials, no other methods to solve the problem are readily available. The effective medium approximation serves as an approximate solution and is able to provide relatively reasonable results. There are several different effective medium approximations available, where a paper by Hutchinson et al. (2009) provides a detailed description of some of the different effective media approximations [5]. The one employed in this master's thesis is the volume average of refractive indexes given by

$$n_{eff} = v_1 n_1 + v_2 n_2, \tag{23}$$

where n_{eff} is the effective refractive index of the composite material, n_1 and n_2 are the refractive indices of a non-absorbing and absorbing material, respectively. Lastly, v_1 and v_2 are the corresponding volume fractions of each material, where the total volume is $v_1 + v_2 = 1$. [2]

2.7 Interference

The purpose of the theory described in this chapter so far has mainly been to understand how an electromagnetic wave behaves as it propagates through the mentioned multilayered structure and how this knowledge is useful in determining moisture levels. Whereas this section provides a description of a physical phenomena known as interference which arises as a result of the interaction between the electromagnetic wave and the multilayered structure. Understanding the principle of interference is not only useful when interpreting the data and simulations provided in section 4, but is also used to determine the distance d of the middle layer in the system shown in figure 10.

Interference of waves requires that two or more optical waves are present simultaneously in the same location of space and time, implicating that the total wavefunction is determined by summing the wavefunctions of the individual waves. Considering the situation illustrated in figure 10, the first wave emerges as the incident electromagnetic wave is partially reflected at the first boundary. The remaining part is transmitted through the first boundary and propagates across the middle layer until it is partially reflected at the second boundary. Part of this reflected wave is then transmitted back through the first boundary. Thus at least two different waves originating from the initial incident electromagnetic wave is present in the leftmost layer of the multilayered structure. Considering that the wave entering the middle layer travels a greater distance in comparison to the other wave, the two waves may be in or out phase, implicating that they interfere with each other. How these waves interfere with one another is dependent on the phase difference between them, as well as their respective optical intensity. [14, p. 58]

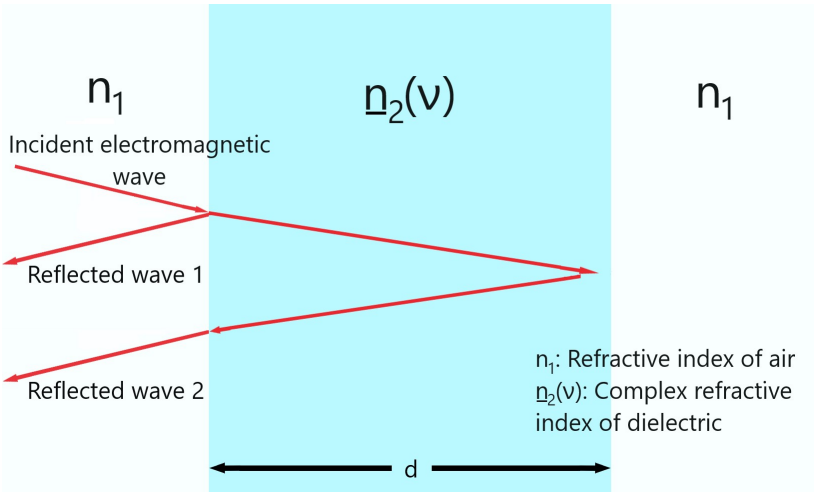

Figure 10: Interference between two waves. The first wave is partially reflected and refracted at the first boundary. The second wave is partially reflected at the second boundary and then transmitted back through the first boundary, where interaction with the first waves causes interference patterns.

When interference between two optical waves occurs, the total intensity I is according to Saleh and Teich (2013) determined from the interference equation given by

$$I = I_1 + I_2 + 2\sqrt{I_1 I_2}\cos\varphi, \text{ where } \varphi = \varphi_2 - \varphi_1 \text{ [14, p. 58].} \tag{24}$$

Here I_1, I_2 and φ_1, φ_2 represents the intensity and phase of wave 1 and 2, respectively. Even though the optical intensity of the two waves in figure 10 is not equal, setting $I_1 = I_2 = I_0$ simplifies equation (24), making it easier to determine what values of the phase difference φ causes constructive and destructive interference. The resulting expression is given by

$$I = 2I_0(1 + \cos\varphi) \tag{25}$$

It is clear from equation (25) that constructive interference occurs when the two waves are in phase (i.e. $\varphi = 0$), resulting in a total intensity of $I = 4I_0$. While destructive interference occurs at $\varphi = \pi$, where the superposed waves cancel each other out and the resulting intensity is $I = 0$. These values of intensity are however not representative for the waves shown in figure 10, they are only meant to show a qualitative representation of the total intensity I for the two cases of constructive and destructive interference.

The ratio between the distance d of the middle layer and the wavelength λ of the incident wave is an important factor in regards to interference. Relating this factor to interference patterns is useful when interpreting the reflection and transmission spectra for different distances d, see section 4. Looking at figure 10, determining the conditions that must be satisfied for constructive interference to occur is simplified by assuming normal incidence of the electromagnetic wave. The path-length difference $\triangle$ between the two waves is then simply $\triangle = 2d$. As constructive interference occurs when the two waves are in phase, it might seem reasonable to assume that this is satisfied for $\triangle = m\lambda_n$, where m is an integer and $\lambda_n = \frac{\lambda}{n}$ is the wavelength in a medium of refractive index n. This is not the case. Reason being is that an additional phase shit of 180° or $\frac{\lambda_n}{2}$ is introduced as an electromagnetic wave reflects of a medium with a greater refractive index relative to the refractive index of the medium where it is propagating. Given that $n_2 > n_1$ means that the wave reflecting off the first boundary is phase shifted by $\frac{\lambda_n}{2}$. To account for this additional phase difference in the circumstance of constructive interference, the difference in path-length $\triangle$ between the two waves must therefore be given by

$$\triangle = 2d = (m + \frac{1}{2})\lambda_n. \tag{26}$$

Equation (26) is used to interpret the reflection and transmission spectra in section 4, where the distance d of the middle layer is determined from the wavelength λ and refractive index n. An interference pattern consists of constructive and destructive interference fringes, where the integer m in equation (26) can be thought of as an index of the constructive interference fringes. For instance, $m = 0$ and $m = 1$ represents the first and second constructive interference fringes. [4, p.

237]

3 Methodology

3.1 Development and implementation of the theoretical model

This section is for the most part dedicated to how the multilayered structure described in section 2 was charcterized by the physical properties of the system, combined with matrix theory and effective medium approximation. The development of the scattering **S** matrices for each individual boundary between the different layers in the layered medium and then the scattering **S** matrix describing the entire multilayered structure is explained in detail. As well as the implementation of effective media approximation to represent media of different moisture levels. The end result was used to simulate the reflection and transmission spectra in the desired frequency range for media with different moisture levels and varying distance d of the middle layer in the layered medium. Matlab was used to process the experimental data of the complex refractive index collected from Segelstein (1981), produce the reflection and transmission spectra and present them in an understandable manner [15]. Lastly, a description of assumptions and limitations of the principles and the model used is provided.

3.1.1 Determining scattering and wave-transfer matrices

Figure 1 shows the layered medium to be charcterized. By inspection of this model, three **S** matrices is needed to represent the reflections and transmissions at each of the two boundaries and the last one to represent the propagation of the electromagnetic wave through the middle layer.

The system was first implemented with the assumption that the electromagnetic wave was normally incident on the boundaries between the different media. At the first boundary between air and water, the $\mathbf{S_1}$ matrix is given by the matrix equation (18) which yields

$$\mathbf{S_1} = \begin{bmatrix} \mathfrak{t}_{12} & \mathfrak{r}_{21} \\ \mathfrak{r}_{12} & \mathfrak{t}_{21} \end{bmatrix}, \tag{27}$$

where the different reflection $\mathfrak{r}_{12}, \mathfrak{r}_{21}$ and transmission $\mathfrak{t}_{12}, \mathfrak{t}_{21}$ coefficients are found from the Fresnel equations (15). The Fresnel equations (15) were adapted to the layered medium in figure 1 by setting the refractive indices n_1 and n_2 equal to the refractive index of air and the complex refractive index of water (i.e. $n_1 \approx 1$ and $n_2 = \underline{n}_2(\nu)$ gathered from Segelstein (1981)), respectively [15]. The second boundary in the layered medium is charcterized by the $\mathbf{S_3}$ matrix given by

$$\mathbf{S_3} = \begin{bmatrix} \mathfrak{t}_{21} & \mathfrak{r}_{12} \\ \mathfrak{r}_{21} & \mathfrak{t}_{12} \end{bmatrix}. \tag{28}$$

The last scattering matrix $\mathbf{S_2}$ represents the electromagnetic wave propagating through the middle

layer containing water. The $\mathbf{S_2}$ matrix is found from equation (20), which yields

$$\mathbf{S_2} = \begin{bmatrix} e^{(-j\varphi)} & 0 \\ 0 & e^{(-j\varphi)} \end{bmatrix}, \text{ where } \varphi = n_2(\nu)k_0 d. \tag{29}$$

By using the conversion relation in equation (19.1), the scattering matrices $\mathbf{S_1}$, $\mathbf{S_2}$ and $\mathbf{S_3}$ are all converted to their corresponding wave-transfer matrix (i.e. $\mathbf{M_1}$, $\mathbf{M_2}$, and $\mathbf{M_3}$). The product of the three resulting wave-transfer matrices is thus one single wave-transfer matrix $\mathbf{M} = \mathbf{M_3}\mathbf{M_2}\mathbf{M_1}$, which represents the whole system in figure 1. Using the conversion relation in equation (19.2), the wave-transfer matrix $\mathbf{M}$ representing the whole system is then converted back to a scattering matrix. The overall reflectance and transmittance of the entire system is found from the elements of the final scattering matrix, as well as the corresponding power reflectance $\mathfrak{R}$ and transmittance $\mathfrak{T}$ from equations (16.1) and (16.2). As the mentioned matrix operations can become rather tedious to do by hand, Matlab was used to do these steps. Matlab also allowed for the operations to be done for all the frequencies of interest in the domain of 0.1-1000 GHz, and thereby find the overall reflectance and transmittance spectra of the system. The Matlab code used for this part is given in appendix A.

3.1.2 Adapting the theoretical model for off-axis waves

The method described in the previous section is adapted for oblique waves incident at an angle θ_1 on the layered medium by modifying the scattering $\mathbf{S}$ and wave-transfer $\mathbf{M}$ matrices accordingly. Using the expression for the scattering matrix in equation (21.1) yields the following scattering matrices for the first and second boundary

$$\mathbf{S_1} = \begin{bmatrix} \mathfrak{t}_{12} & \mathfrak{r}_{21} \\ \mathfrak{r}_{12} & \mathfrak{t}_{21} \end{bmatrix} = \frac{1}{\widetilde{n}_1 + \widetilde{n}_2} \begin{bmatrix} 2a_{12}\widetilde{n}_1 & \widetilde{n}_2 - \widetilde{n}_1 \\ \widetilde{n}_1 - \widetilde{n}_2 & 2a_{21}\widetilde{n}_2 \end{bmatrix}, \tag{30}$$

$$\mathbf{S_3} = \begin{bmatrix} \mathfrak{t}_{21} & \mathfrak{r}_{12} \\ \mathfrak{r}_{21} & \mathfrak{t}_{12} \end{bmatrix} = \frac{1}{\widetilde{n}_1 + \widetilde{n}_2} \begin{bmatrix} 2a_{21}\widetilde{n}_2 & \widetilde{n}_1 - \widetilde{n}_2 \\ \widetilde{n}_2 - \widetilde{n}_1 & 2a_{12}\widetilde{n}_1 \end{bmatrix}. \tag{31}$$

Using equation (21.2) yields the corresponding $\mathbf{M}$ matrices

$$\mathbf{M_1} = \begin{bmatrix} A & B \\ C & D \end{bmatrix} = \frac{1}{2a_{21}\widetilde{n}_2} \begin{bmatrix} \widetilde{n}_1 + \widetilde{n}_2 & \widetilde{n}_2 - \widetilde{n}_1 \\ \widetilde{n}_2 - \widetilde{n}_1 & \widetilde{n}_1 + \widetilde{n}_2 \end{bmatrix} \tag{32}$$

$$\mathbf{M_3} = \begin{bmatrix} A & B \\ C & D \end{bmatrix} = \frac{1}{2a_{12}\widetilde{n}_1} \begin{bmatrix} \widetilde{n}_1 + \widetilde{n}_2 & \widetilde{n}_1 - \widetilde{n}_2 \\ \widetilde{n}_1 - \widetilde{n}_2 & \widetilde{n}_1 + \widetilde{n}_2 \end{bmatrix}. \tag{33}$$

Matrix $\mathbf{M_1}$ and $\mathbf{M_3}$ is valid for both TE and TM polarisation by applying the relations in equation (22). The final matrix required to describe the propagation through the layered media is the wave-transfer matrix $\mathbf{M_2}$, which determines the propagation through the middle layer in figure 9 and is given by equation (20) where the phase is $\varphi = \underline{n}_2(\nu)k_0 d\cos\theta_2$.

Similarly to the method described in the previous section, the product of the three wave-transfer matrices is thus one single wave-transfer matrix $\mathbf{M} = \mathbf{M_3}\mathbf{M_2}\mathbf{M_1}$, which represents the whole system in figure 9. Using the conversion relation in equation (19.2), the wave-transfer matrix $\mathbf{M}$ representing the whole system is then converted back to a scattering matrix. The overall reflectance and transmittance of the entire system is found from the elements of the final scattering matrix, as well as the corresponding power reflectance $\mathfrak{R}$ and transmittance $\mathfrak{T}$ from equations (16.1) and (16.2). By implementing the mentioned matrices into the MATLAB code provided in appendix A, the matrix operations were handled by MATLAB and used to simulate the resulting reflection and transmission spectra in section 4.2 through the structure for both TE and TM polarised light at two different angles of incidence θ_1.

3.1.3 Implementation of effective media approximation

With the method for determining the overall reflectance and transmittance of the system in figure 1 established, the only missing part was how to account for materials with different concentrations of water in the middle layer of the system. A problem solved by implementing the effective medium approximation from equation (23) into the Matlab code. Research in regards to moisture levels in MSW by Cheng et al. (2007), as well as Mohee and Mudhoo (2012), found that the moisture level was typically 20-30% in the U.S. and European countries [1][11]. With that in mind, reflection and transmission spectra were simulated for moisture levels in the region of 10-40% by adjusting the two volume fractions v_1 and v_2 in equation (23) accordingly.

In equation (23), n_2 represents the frequency-dependent complex refractive index of water, whereas n_1 was simply set to the same refractive index as air (i.e. $n_1 \approx 1$). This was done based on the assumption that millimetre waves only have high absorption in water and high transmittance in most other materials except metals. Thus the material mixed with water was assumed to have the same impact on the electromagnetic wave as air. Consequently, the refractive index of the material mixed with water was chosen to be the same as air. This might not be the most accurate approach, and could certainly deviate from reality. The effective medium approximation itself has limitations. There are many different effective medium approximations used in literature to treat heterogeneous material as homogeneous materials with an effective refractive index. A specific medium approximation may only be defined for certain materials and conditions. Meaning that the

approach used in this paper may not represent an exact model of how the system would interact with electromagnetic radiation in reality. On the other side, this approach is less complex and still provided quantitative data about the water concentration in materials.

3.1.4 Interpreting interference patterns in the simulated reflection and transmission spectra

With the presence of an interference pattern in the simulated reflection and transmission spectra provided in section 4, equation (26) proved useful in determining the distance d of the middle layer in the layered medium. This was done by first identifying the frequency ν at which the first constructive interference fringe m emerged in the simulated reflection spectra, as well as the corresponding real part of the complex refractive index $\underline{n_2}(\nu)$. Followed by converting to the corresponding wavelength λ using the relation $\lambda = \frac{c_0}{\nu}$, where c_0 is the velocity of light in vacuum. Dividing this wavelength λ with the corresponding real part of the complex refractive index $\underline{n_2}(\lambda)$ gave the wavelength λ_n in the medium (i.e. $\lambda_n = \frac{\lambda}{real(\underline{n_2}(\lambda))}$). Finally, inputting the values of λ_n and m into equation (26) yielded the distance d. The mentioned steps were all implemented into the Matlab code provided in appendix A.

3.1.5 Assumptions made for the theoretical model

Several assumptions of the system were made in order to simplify the problem. Including the assumption that the incident electromagnetic wave was a plane wave, that is only dependent on one spatial dimension, with normal incidence on the different layers. In reality, the angle of incidence may vary, where normal incidence was chosen for the sake of simplicity. To give an idea of how varying the angle of incidence influences the reflection and transmission spectra, a few simulations with non-normal incidence are provided in section 4. This was done by using the Fresnel equations (13.1) and (13.3), where the angle of incidence θ_1 could be set as desired.

The electromagnetic wave can also have different polarisation configurations, which is not considered in this paper. Another assumption used in the development of the theoretical model was that the countless number of backwards and forwards waves caused by the endless reflections at the boundaries between the different materials could all be summed up into one forward moving wave and one backward moving wave. Although this assumption is reasonable, some information might be lost by this simplification and cause the final results to deviate from reality. It was also assumed that the temperature of the system was set at 25 °C, as the experimental values of the complex refractive index of water used in this paper were all measured at this temperature. Variations in variables such as temperature and pressure directly impact the dielectric properties of water and therefore affect the detected response of the system. The last assumption worth mentioning is related to the system itself, where the system only consists of three layers of material. In reality, an electromagnetic wave would rarely travel through these three layers alone. The wave would most likely be reflected and transmitted at countless number of interfaces between materials, where the

interfaces could also have different cross-sectional areas or have a non-planer surface. Differences in cross-sectional area or shape of the surface where the electromagnetic wave is incident directly influences scattering processes at boundaries, which has also not been considered in this paper. As mentioned earlier, the main focus of this master's thesis is to address the most fundamental system described by figure 1.

3.2 Experimental measurement method

To determine the accuracy and validity of the theoretical results produced by the method described in the previous section, experimental measurements were performed in the lab. This section explains what equipment was used and how it was set up to collect experimental data, as well as how the data was interpreted.

3.2.1 Measurement setup

For this master's thesis, a Dielectric Assessment Kit System (DAKS) from SPEAG was used to measure dielectric properties in a material with varying concentrations of water. The setup consisted of an open ended coaxial probe from DAKS-3.5 connected to the R140 Vector Network Analyser (VNA) from Copper Mountain Technologies, allowing for measurements of the complex reflection coefficient $S11$ by pressing the probe against the sample material. The VNA was connected to a computer via USB to communicate with the DAKS software (DAK 2.4.0), which determined the complex permittivity $\varepsilon(\nu)$ of the sample material from the measured complex reflection coefficient $S11$. The DAKS-3.5 is limited to the frequency range of 85 MHz - 14 GHz. Considering that the aim of this master's thesis is to investigate moisture detection in the GHz domain (i.e. 0.1-1000 GHz), the limited frequency range of the DAKS-3.5 is not ideal. Still, the resulting experimental measurements in section 4.3 provided enough data to give an indication of the moisture level in the sample material.

3.2.2 Calibrating the VNA and probe system

Before any measurements could be executed, the VNA and probe system needed to be calibrated in the mentioned frequency range of 85 MHz - 14 GHz. This required three types of calibration measurements, commonly known as a short, an open and a load calibration. The short calibration was done by attaching a copper strip to the open end of the probe. Followed by the open circuit calibration, where the probe was simply suspended in mid-air. The load calibration was performed by immersing the open end of the probe in battery water at approximately room temperature of 24.7°C. Where the resulting measurement of the complex permittivity $\varepsilon(\nu)$ of battery water was compared to the target values of water available in the DAK software to confirm that the system had been calibrated properly, see section 4.3.1. Battery water is also commonly known as distilled water and is characterised by its low conductivity, typically in the range 0.5 to 3 μmhos/cm.

3.2.3 Measurements using a sponge as sample material

A sponge made of polyurethane with dimensions 164x88x45 mm was used as a sample material to measure dielectric properties in a material with varying concentrations of water. As mentioned previously, dielectric properties are sensitive to changes in temperature. In an attempt to reduce temperature variations in the sponge sample, the tap water used to regulate the level of moisture in the sponge was kept in a bucket overnight. In doing so, the tap water adjusted to approximately room temperature. Making for more comparative results to the results determined from the theoretical model described in section 3.1, which is based on dielectric properties of water measured at 25°C.

With the theoretical model based on the assumption that most materials except water and metals have approximately the same dielectric properties as air, the dielectric properties of a dry sponge were measured first. Confirming that the dry sponge exhibited roughly the same dielectric properties as air (i.e. $\varepsilon \approx 1$) in the considered frequency range. Using the mentioned DAKS-3.5 setup, the dielectric properties of the sponge were measured at different levels of moisture ranging from $10-40\%$ with frequency intervals of a 100 MHz between 85 MHz and 14 GHz.

The amount of water needed for the sponge to contain a specific moisture content was determined from the volumetric moisture content θ_w defined as

$$\theta_w = \frac{v_w}{v_s} = \frac{m_w}{\rho_w v_s} = \frac{m - m_s}{\rho_w v_s}. \tag{34}$$

In equation (34), v_w and v_s represents the water and sponge volume, respectively. m_w represents the water mass and m_s represents the mass of a dry sponge measured to be 0.015 kg, whereas m is the total mass of a wet sponge. The water density ρ_w is identified to be 997 kg/m^3, and the volume of the sponge v_s is found by $v_s = 164 \cdot 88 \cdot 45$ mm $= 6.49 \cdot 10^{-4}$ m^3. The total mass of a wet sponge m for a given volumetric moisture content θ_w was determined by expressing equation (34) in terms of m. Table 1 shows the resulting total mass of a wet sponge m at the different volumetric moisture contents θ_w ranging from $10 - 40\%$.

Table 1: Total mass of wet sponge m for different volumetric moisture contents θ_w ranging from $10 - 40\%$

Volumetric moisture content θ_w	Mass of wet sponge m_w [kg]
0.10	0.08
0.20	0.145
0.30	0.209
0.40	0.273

Figure 11 shows a picture of the described setup, where the probe connected to the VNA is resting on top of the sponge. For each moisture level, a total of 10 measurements were performed at arbitrary locations at the surface of the sponge. The DAK software converted the measured reflection coefficient $S11$ to the corresponding real and imaginary parts of the complex permittivity $\varepsilon(\nu)$, which then were exported to Excel. Where the average of the 10 measurements was calculated and considered as the dielectric constant $\varepsilon'(\nu)$ and dielectric loss factor $\varepsilon''(\nu)$ of the specific moisture level. MATLAB was then used to compare the measured results for different levels of moisture to the corresponding results derived from the theoretical model by plotting them as a function of frequency, provided in section 4.3.2.

By using equations (9) and (10), the experimentally measured values of the dielectric constant $\varepsilon'(\nu)$ and dielectric loss factor $\varepsilon''(\nu)$ were converted to the refractive index $n(\nu)$ and extinction coefficient $\kappa(\nu)$. Where the resulting refractive index $n(\nu)$ and extinction coefficient $\kappa(\nu)$ was used to simulate the corresponding reflection spectra following the same method described in section 3.1 for the theoretical model. Making it possible to compare between the reflection spectra based on the theoretical model and the experimentally measured properties of the sponge sample, provided in section 4.3.3.

3.2.4 Measurement method considerations

There are several methods available for measuring the dielectric properties of a sample material, where each method has its advantages and disadvantages. In this master's thesis, the experimental measurements of the complex permittivity ε were performed by making use of the open ended coaxial probe method. According to La Gioia et al. (2018), the open ended coaxial probe method is popular as it requires minimal sample preparation and has the ability to perform a large amount of sample measurements in a short period of time. This does however come at a price, as the method assumes that the sample is homogeneous and in good contact with the probe. Where the presence of air bubbles and uneven sample surfaces can be to the detriment of accurate measurements. The sample material used in this master's thesis is also heterogeneous, which is not ideal when using this measurement method. Impurities in the tap water, as well as the non-uniform nature of a wet sponge may also introduce unwanted effects in the measurements. However, this was the only measurement method readily available. [9]

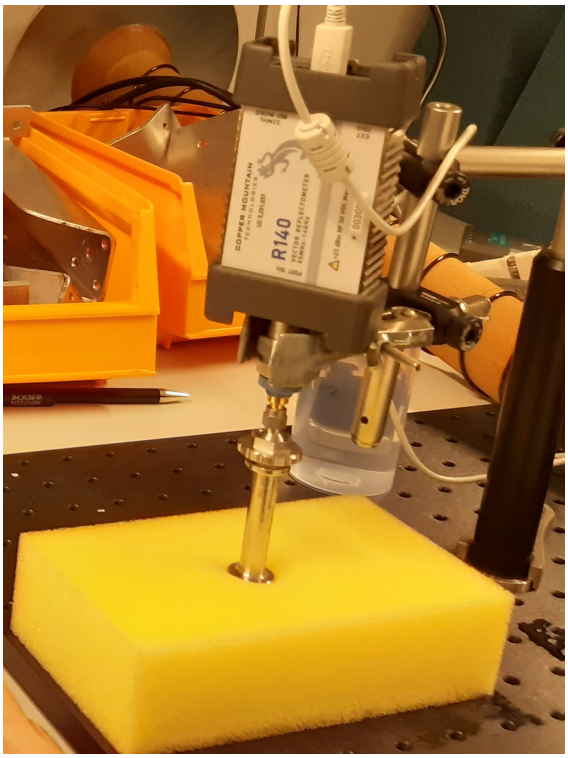

Figure 11: DAKS-3.5 measurement setup with R140 VNA connected to the open ended coaxial probe resting on top of a sponge.

4 Results

4.1 Reflection and transmission spectra simulated from the theoretical model at normal incidence

The overall reflectance and transmittance spectra of the system described by figure 1 for the chosen frequency range of 0.1-1000 GHz is presented in this section. Using the effective media approximation, the system was simulated for media with different moisture levels, as well as varying the distance d of the middle layer in figure 1. Since the values of the complex refractive index of water presented in figure 3 were measured only for the temperature of 25 °C, the resulting spectra presented in this section are also only valid for the same temperature. For all the following simulations provided in this section, the reflection and transmission through the considered system is represented in terms of the power reflectance $\mathfrak{R}$ and power transmittance $\mathfrak{T}$ given by equations (16.1)-(16.2), respectively. As explained in section 2.3, the power reflectance $\mathfrak{R}$ and power transmittance $\mathfrak{T}$ were introduced to relate the reflection and transmission coefficients $\mathfrak{r}$ and $\mathfrak{t}$ to some real physical quantity instead of referring to ratios of complex amplitudes.

4.1.1 Simulated reflection and transmission through a material of distance 1 mm

Figure 12 shows the simulated reflection and transmission spectra of the considered system in figure 1. The middle layer is in this case a distance of $d = 1$ mm, where figure 12(a) and 12(b) corresponds to moisture levels of 10 and 20%, respectively. For this distance d and moisture levels, the reflectance is close to zero and hence the transmittance is close to unity for the entire spectrum, with the exception of a spectral feature in the region of 10-100 GHz. Figure 3 demonstrates a similar spectral feature for the extinction coefficient $\kappa(\nu)$ in the same frequency range. An increase of the extinction coefficient $\kappa(\nu)$ leads to loss of field energy due to absorption, causing the transmission intensity to be reduced. As expected, a clear reduction in transmission intensity is observed in figure 12 between the frequencies of 10-100 GHz. Increasing the moisture level from 10% in figure 12(a) to 20% in figure 12(b), makes the spectral feature more prominent. Showcasing that an increase in moisture level implicates an increase of the extinction coefficient $\kappa(\nu)$, which entails a further reduction in transmission intensity.

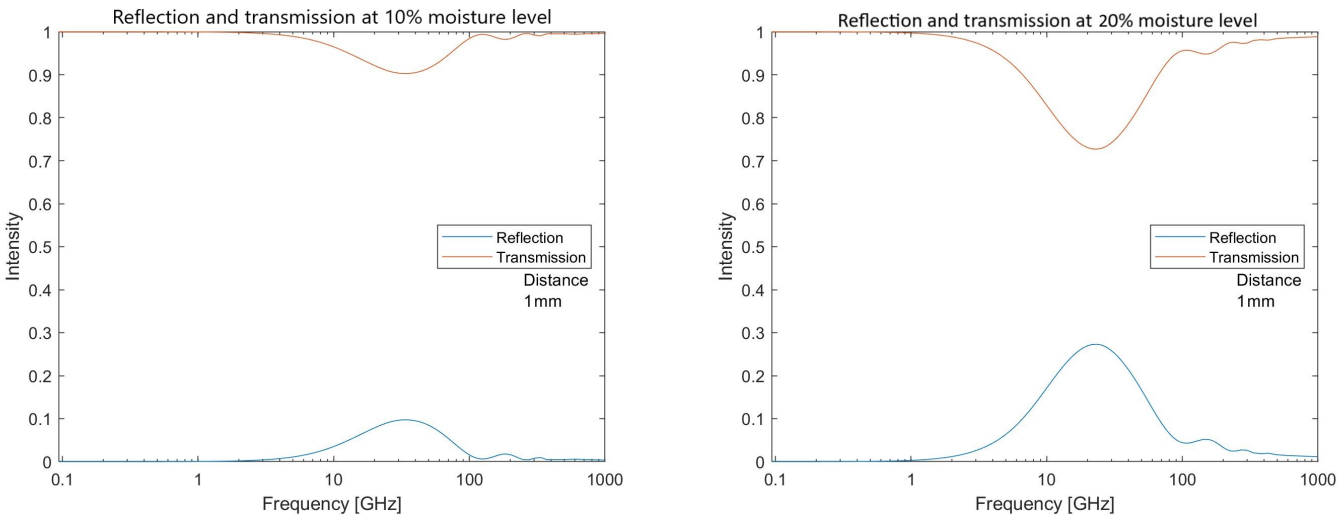

(a) 10% moisture level

(b) 20% moisture level

Figure 12: Reflection and transmission intensity of incident radiation as a function of frequency through a material of a distance 1 mm with moisture levels of 10 and 20%.

Similarly to figure 12, figure 13 shows the simulated reflection and transmission spectra for the same distance d of the middle layer, where 13(a) and 13(b) corresponds to moisture levels of 30 and 40%, respectively. From figure 12(a) and 12(b) to figure 13(a) and 13(b), there is a clear connection in the reflection and transmission spectra as the moisture level increases from 10 to 40%. Namely, the fact that the mentioned spectral feature becomes more prominent and sharper around the 20 GHz mark with higher levels of moisture. Looking at figure 12(a) and 12(b) to figure 13(a) and 13(b), there is also a second peak in the reflectance and transmittance spectra at slightly higher frequencies above 100 GHz. This second peak is substantially smaller and less prominent in contrast to the main absorption mode. These spectral features can be explained by considering the simulated reflection spectra in figure 14, where the extinction coefficient κ is set to zero. The resulting reflection spectra can be understood by considering interference effects, where the peaks and valleys in the reflection intensity corresponds to constructive and destructive interference, respectively. The strange features at frequencies above 100 GHz in figure 14 are due to the sample resolution being too low to plot the reflection values properly.

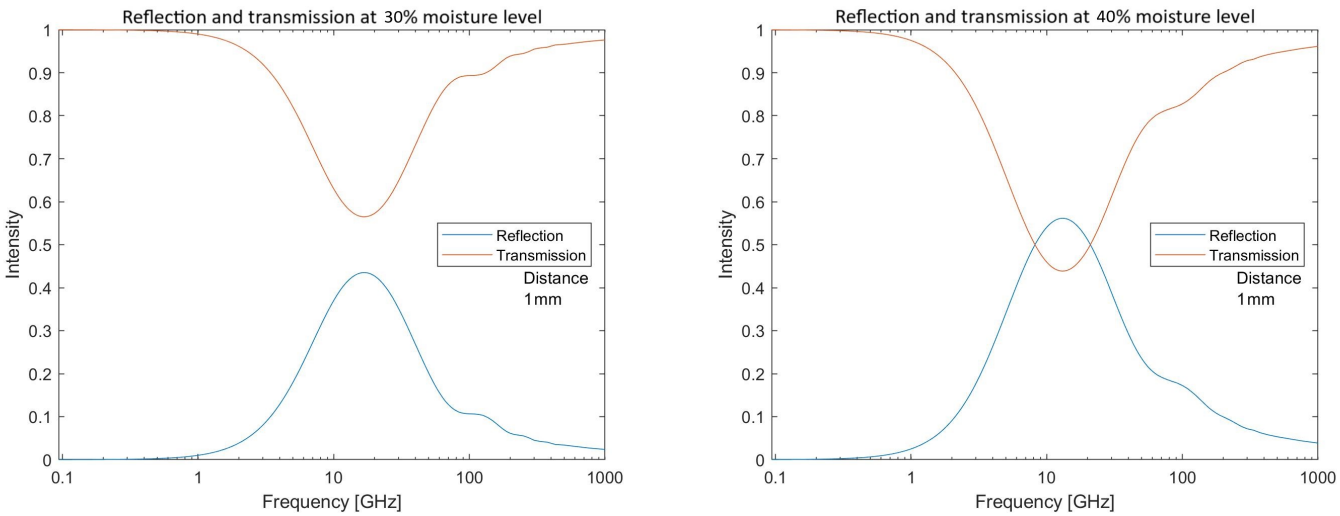

(a) 30% moisture level

(b) 40% moisture level

Figure 13: Reflection and transmission intensity of incident radiation as a function of frequency through a material of a distance 1 mm with moisture levels of 30 and 40%.

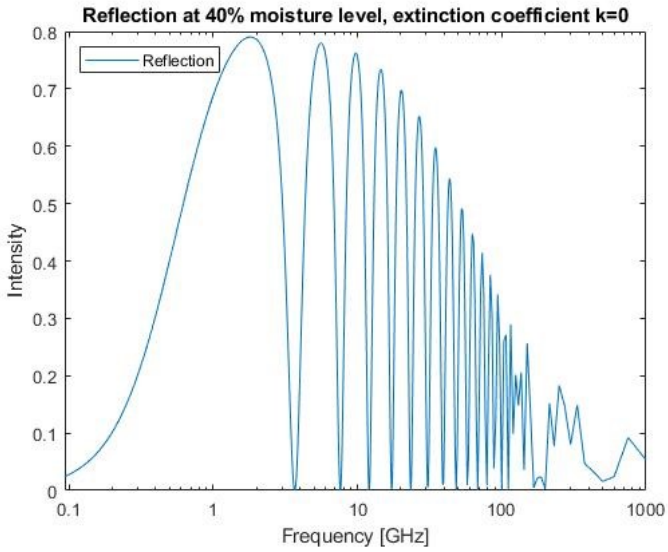

Figure 14: Reflection intensity of incident radiation as a function of frequency through a material of a distance 1 mm with moisture level of 40% and the extinction coefficient $\kappa = 0$.

4.1.2 Simulated reflection and transmission through a material of distance 10 mm

Figure 15 shows the simulated reflection and transmission spectra through the system described in figure 1, where the middle layer is in this case a distance of $d = 10$ mm. Figure 15(a) and 15(b) corresponds to moisture levels of 10 and 20%, respectively. For frequencies lower than 20 GHz, some new spectral features have appeared which were not previously present in the spectra for $d = 1$ mm in figure 12 and 13. These spectral features can be understood by considering a physical phenomena

that often occurs when waves are reflected. Although it might not be immediately apparent, these spectral features are in fact interference patterns. As explained in section 2.7, the peaks and valleys in the reflection spectra are caused by constructive and destructive interference between the waves reflected at the first and second boundary of the system in figure 1.

Why the interference pattern is not as prominent in the spectra for $d = 1$ mm can be understood by first considering the interference equation (26). In equation (26), the difference in path-length $\triangle$ is directly proportional to the wavelength λ_n in a medium with refractive index n (i.e. $\lambda_n = \frac{\lambda}{n}$). The wavelength λ_n is again inversely proportional to the frequency ν given by the relation $\lambda = \frac{c_0}{\nu}$, where c_0 is the velocity of light in vacuum. To sum up, a smaller difference in path-length $\triangle$ requires a shorter wavelength λ_n and therefore a higher frequency ν, meaning that the interference pattern is shifted towards the higher frequencies as the difference in path-length $\triangle$ is shortened. Figure 3 shows that the real part of the complex refractive index $\underline{n}(\nu)$ of water is decreased considerably for the higher frequencies, implicating a smaller difference in refractive index between the media at each side of a boundary in the multilayered system. This in turn results in less of the incident electromagnetic field reflecting off the different boundaries in the layered structure and thereby reducing the amount of interference effects.

The frequency of the first constructive interference fringe denoted by $m = 0$ is marked in figures 15 and 16. Following the steps described in section 3.1.4 for figure 15(a), yielded a path-length difference $\triangle_{10\% \text{ moisture}} = 21.8$ mm corresponding to a distance $d = \frac{\triangle_{10\% \text{ moisture}}}{2} = 10.9$ mm. Repeating the same process for the constructive interference fringe in figures 15(b) and 16(a)-(b), yielded the respective path-length difference of $\triangle_{20\% \text{ moisture}} = 22$ mm, $\triangle_{30\% \text{ moisture}} = 22.1$ mm, and $\triangle_{40\% \text{ moisture}} = 22.1$ mm. Resulting in a distance $d \approx 11$ mm for all the spectra in figures 15 and 16. The actual distance d used to simulate the reflection and transmission spectra was set at $d = 10$ mm. Showcasing that the distance d of the middle layer was in this case determined with an uncertainty of 10% using the procedure described in section 3.1.4.

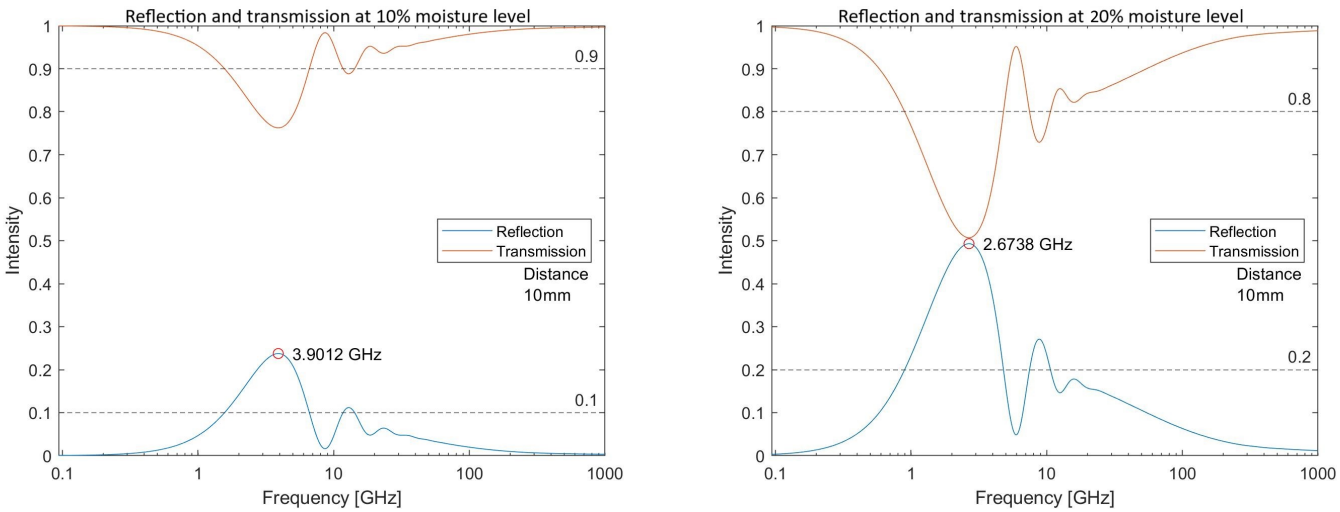

(a) 10% moisture level

(b) 20% moisture level

Figure 15: Reflection and transmission intensity of incident radiation as a function of frequency through a material of a distance 10 mm with moisture levels of 10 and 20%.

Similarly to figure 15, figure 16 shows the simulated reflection and transmission spectra for the same distance d of the middle layer, where 16(a) and 16(b) corresponds to moisture levels of 30 and 40%, respectively. The same oscillations in the reflectance and transmittance for frequencies lower than 20 GHz are also present in figure 16(a) and 16(b). However, as the moisture level increases, the oscillations are more prominent and has sharper features. This is explained by considering the Fresnel equations (15), where higher levels of moisture leads to a greater difference in refractive index between the materials at each side of a boundary. Resulting in more of the incident electromagnetic waves to be reflected at the boundary between the different layers.

At approximately 20 GHz, the oscillations in the reflectance and transmittance spectra in figures 15(a)-(b) and 16(a)-(b) concludes, where the reflection and transmission curves evens out. From this point, the transmittance curve follows a smooth increase with frequency to almost unity at a frequency of 1000 GHz. Whereas the reflectance curve follows a smooth decrease to almost zero at 1000 GHz. One key takeaway from the plots in figure 15 and 16 is the fact that the point where the oscillations concludes and the curves even out, the transmittance is decreased with every level the moisture is increased. This seems reasonable, as higher concentrations of moisture will increase the likelihood of absorption of the electromagnetic waves and hence decrease the transmittance.

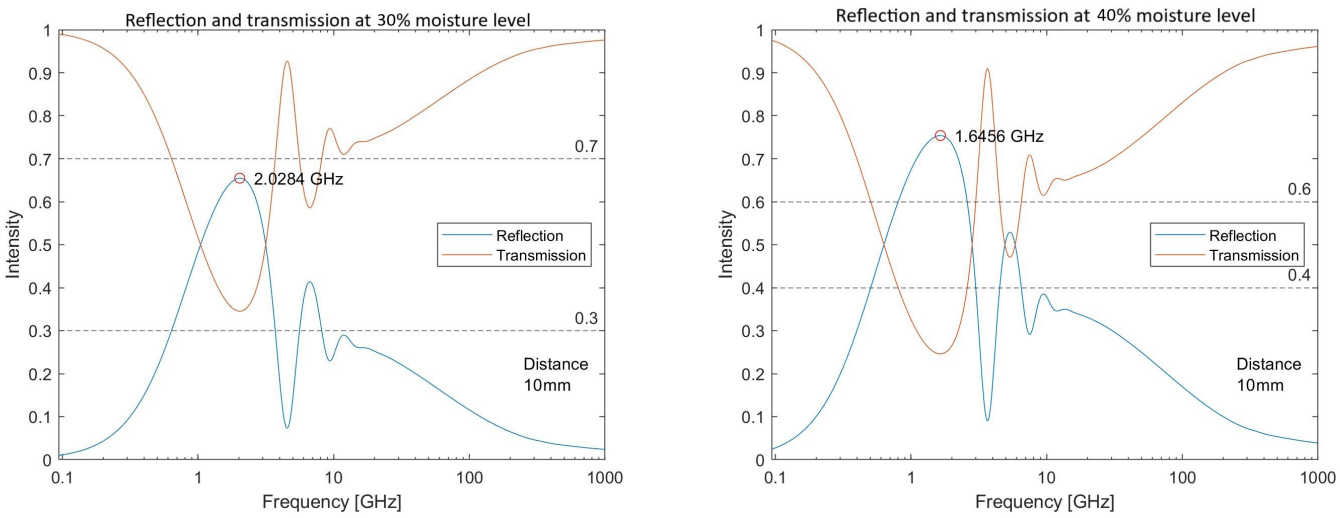

(a) 30% moisture level

(b) 40% moisture level

Figure 16: Reflection and transmission intensity of incident radiation as a function of frequency through a material of a distance 10 mm with moisture levels of 30 and 40%.

Table 2 shows the power reflectance $\mathfrak{R}$ at $d = 10$ mm measured from the spectra in figures 15(a)-(b) and 16(a)-(b) for frequencies in the region where the reflection curve evens out. The power reflectance $\mathfrak{R}$ values in table 2 represents what percentage of the incident electromagnetic wave is reflected by the multilayered media. Even though there is a discrepancy between the moisture level in the media and the measured power reflectance $\mathfrak{R}$ in terms of percentage, these values still give an indication of the moisture level in the media. The average deviation between the actual moisture level in the effective medium and the measured power reflectance values $\mathfrak{R}$ in table 2 was found to be 23.96%. Ideally the deviation should be as close to 0% as possible, but a deviation of 23.96% is still relatively accurate. Hence the theoretical model was in this instance used to detect the moisture level in the effective medium to a certainty of 76.04%.

Table 2: Power reflectance $\mathfrak{R}$ for a material of distance $d = 10$ mm in the frequency region where the reflection intensity curve evens out.

Frequency [GHz]	Moisture level [%]	Power reflectance $\mathfrak{R}$ [intensity]
33	10	0.05 (i.e. 5%)
21	20	0.16 (i.e. 16%)
17	30	0.26 (i.e. 26%)
13.6	40	0.35 (i.e. 35%)

4.1.3 Simulated reflection and transmission through a material of distance 100 mm

Figure 17(a)-(b) and 18(a)-(b) shows the simulated reflection and transmission spectra through the system described in figure 1 with $d = 100$ mm and moisture levels ranging from 10 to 40%. As the distance d is increased from 10 mm to 100 mm, the interference pattern was both shifted towards the lower frequencies as well as the oscillations appearing considerably more frequent. Both of these factors can be explained by expressing equation (26) in terms of the wavelength λ, resulting in the following equation

$$\lambda = \frac{n\triangle}{m + \frac{1}{2}}, \text{ where } \triangle = 2d. \tag{35}$$

The wavelength λ now represents the wavelength at which the constructive interference fringe m emerges. First, the shift of the interference pattern towards the lower frequencies stems from the fact that the path-length difference $\triangle$ is directly proportional to the wavelength λ, which again is inversely proportional to the frequency ν. Implicating that an increase in path-length difference $\triangle$ causes the interference pattern to be shifted towards a lower frequency. Secondly, the more frequent oscillations in the interference pattern is also due to the increase of distance d. As the path-length difference $\triangle$ increases, the expression in equation (35) is dominated by the factor $\triangle$ and becomes less sensitive to changes in the integer m. Hence the wavelengths of the different constructive interference fringes denoted by the integer m are separated by smaller differences in wavelength λ and in turn also frequency ν.

Additionally, the wavelength λ in equation (35) is also directly proportional to the refractive index n. An increase in moisture level coincides with an increase in refractive index n of the effective medium. Meaning that an increase in moisture level produces a similar response as increasing the distance d in terms of shifting the interference pattern towards the lower frequencies, as well as contributing to the oscillations in the interference pattern appearing more frequently.

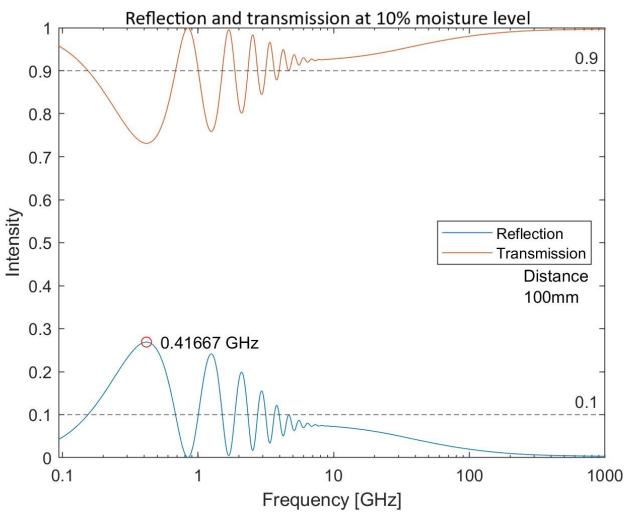

(a) 10% moisture level

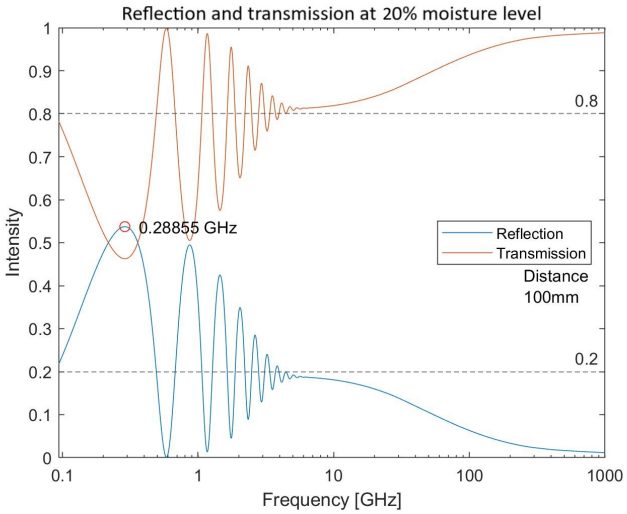

(b) 20% moisture level

Figure 17: Reflection and transmission intensity of incident radiation as a function of frequency through a material of a distance 100 mm with moisture levels of 10 and 20%.

The distance d of the middle layer was determined from the marked frequency of the first constructive interference fringe in figures 17 and 18 and following the steps described in section 3.1.4. Resulting in the distances $d_{10\%\text{ moisture}} = 100.9$ mm, $d_{20\%\text{ moisture}} = 101.2$ mm, $d_{30\%\text{ moisture}} = 101.3$ mm, and $d_{40\%\text{ moisture}} = 101.4$ mm. Showcasing that the distance d of the middle layer was in this case determined with an uncertainty of less than 2% using the procedure described in section 3.1.4.

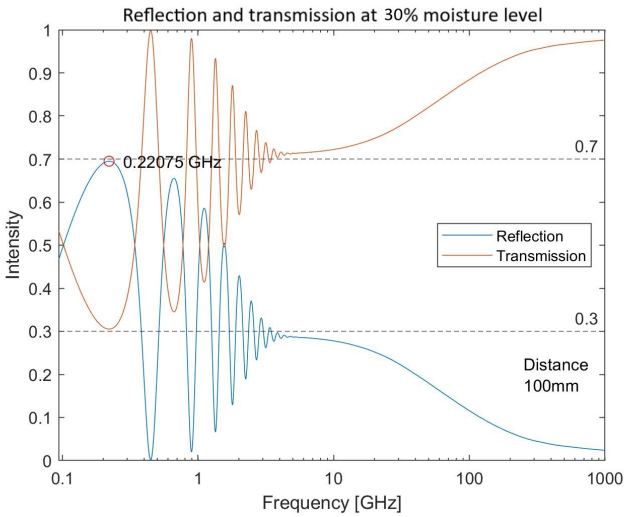

(a) 30% moisture level

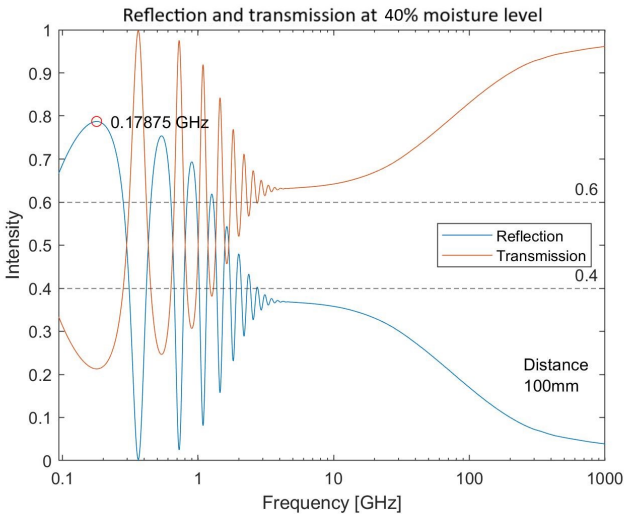

(b) 40% moisture level

Figure 18: Reflection and transmission intensity of incident radiation as a function of frequency through a material of a distance 100 mm with moisture levels of 30 and 40%.

Table 3 shows the power reflectance $\Re$ at $d = 100$ mm measured from the spectra in figures 17(a)-(b)

and 18(a)-(b) at the frequency of 9 GHz. Similarly to the measured values in table 2 for $d = 10$ mm, the power reflectance $\mathfrak{R}$ showcased in table 3 is increased accordingly with an increase in moisture level. Although the frequency region where the power reflectance $\mathfrak{R}$ was measured in table 3 is slightly lower compared to the corresponding measurements in table 2. The average deviation between the actual moisture level in the effective medium and the measured power reflectance values $\mathfrak{R}$ in table 3 was found to be 14.17%. Hence the theoretical model was in this instance used to detect the moisture level in the effective medium to a certainty of 85.83%.

Table 3: Power reflectance $\mathfrak{R}$ for a material of distance $d = 100$ mm in the frequency region where the reflection intensity curve evens out.

Frequency [GHz]	Moisture level [%]	Power reflectance $\mathfrak{R}$ [intensity]
9	10	0.07 (i.e. 7%)
9	20	0.18 (i.e. 18%)
9	30	0.28 (i.e. 28%)
9	40	0.36 (i.e. 36%)

4.1.4 Simulated reflection and transmission through a material of distance 1000 mm

Figure 19(a)-(b) and 20(a)-(b) shows the simulated reflection and transmission spectra through the system described in figure 1 with $d = 1000$ mm and moisture levels ranging from 10 to 40%. The spectra in figures 19 and 20 demonstrates the same response to the increase in distance d as described in section 4.1.3. Where the interference pattern is once again shifted towards the lower frequencies with the interference fringes emerging more frequently compared to the spectra in figures 17 and 18 for $d = 100$ mm. In fact, the interference pattern is shifted to the point where the first interference fringe denoted by $m = 0$ is no longer visible for the simulated frequency range. Meaning that determining the distance d by following the steps described in section 3.1.4 is not as easily achieved in this case. It is still possible, but additional information is needed about what number m the first constructive interference fringe actually signifies in figures 19 and 20. Assuming the reflection and transmission spectra is simulated only for the given frequency range, this is information is not readily available.

If it was somehow possible to determine what number m the first constructive interference fringe actually signified in figures 19 and 20, applying the method described in section 3.1.4 would yield the distance d. Testing for different values of m eventually resulted in the distances $d_{10\%\text{ moisture}} = 1000.9$ mm, $d_{20\%\text{ moisture}} = 1001.1$ mm, $d_{30\%\text{ moisture}} = 1001.3$ mm, and $d_{40\%\text{ moisture}} = 1001.2$ mm. Where $d_{10\%\text{ moisture}}$ was determined using $m = 1$, while $m = 2$ was used for $d_{20\%\text{ moisture}}$ and $d_{30\%\text{ moisture}}$. Lastly, $d_{40\%\text{ moisture}}$ was determined from $m = 3$. The resulting distances d of the middle layer were all determined with an uncertainty of less than 0.2%.

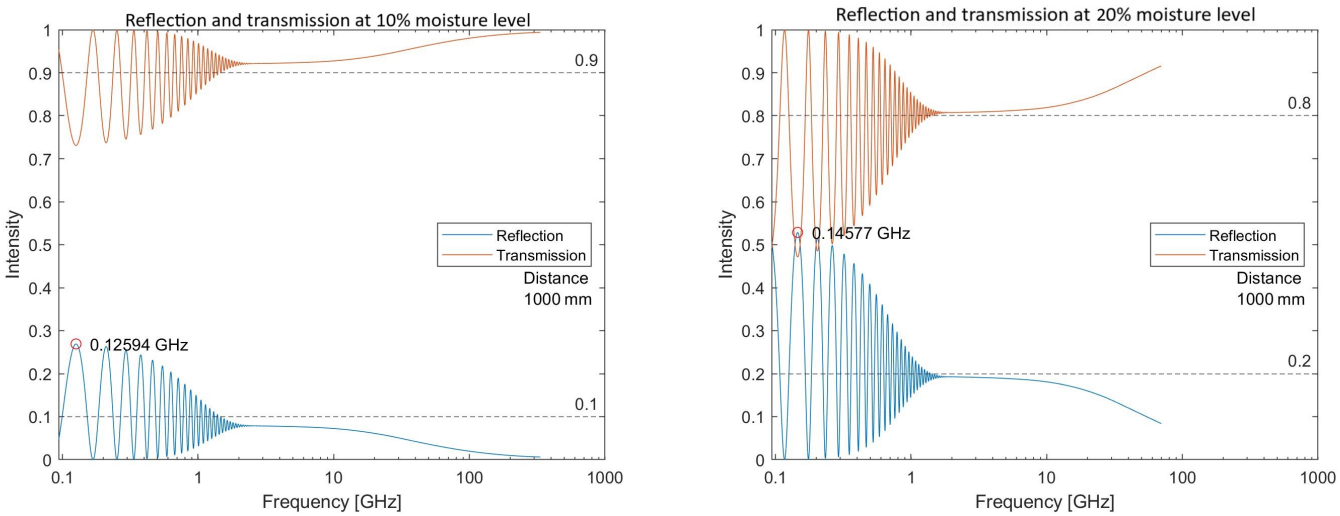

(a) 10% moisture level

(b) 20% moisture level

Figure 19: Reflection and transmission intensity of incident radiation as a function of frequency through a material of a distance 1000 mm with moisture levels of 10 and 20%.

Figures 19 and 20 exhibit a new characteristic which was not previously present, namely that the reflection and transmission curve is undefined for the higher frequencies close to 100 GHz. This can be understood mathematically by considering the exponential term $e^{(-j\varphi)}$ in equation matrix equation (29), where $\varphi = n_2(\nu)k_0 d$ and $k_0 = \frac{2\pi}{\lambda}$ represents the wavenumber of free space. Meaning that φ is inversely proportional to the wavelength λ, which in turn means that φ is directly proportional to frequency. When φ approaches infinity, the exponential term $e^{(-j\varphi)} \to 0$. With the distance set at $d = 1000$ mm and the frequency increased to approximately 100 GHz, φ takes on a sufficiently large number for the MATLAB script to regard $e^{(-j\varphi)}$ as negligible and set it to zero. Which is why the reflection and transmission spectra in figures 19 and 20 have regions above approximately 100 GHz where they are undefined.

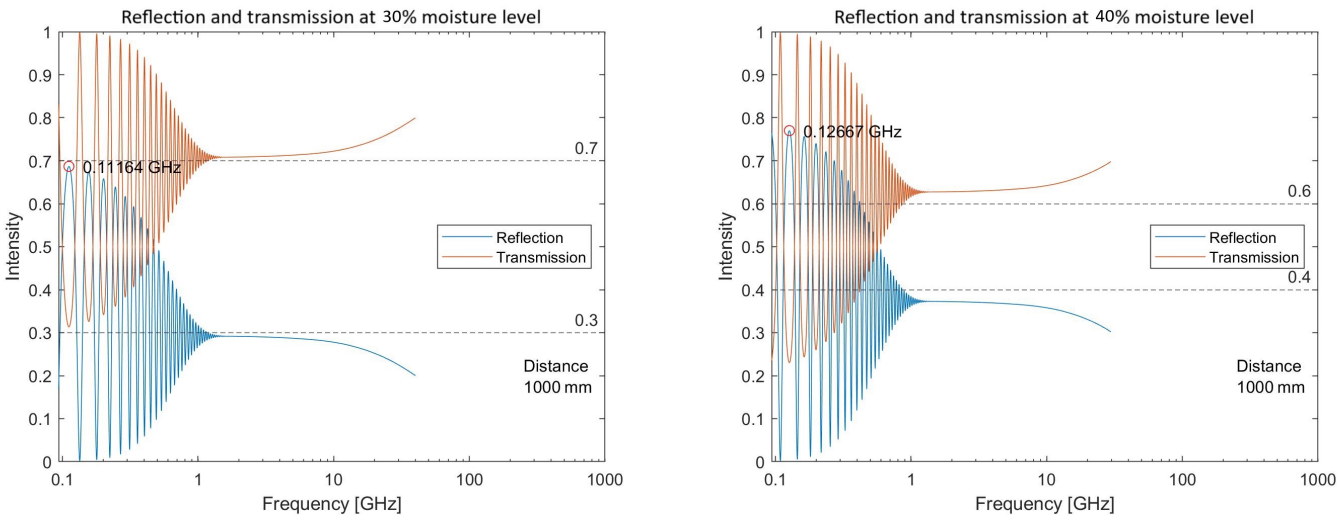

(a) 30% moisture level

(b) 40% moisture level

Figure 20: Reflection and transmission intensity of incident radiation as a function of frequency through a material of a distance 1000 mm with moisture levels of 30 and 40%.

Figure 21 shows that the missing parts of the reflection and transmission spectra in figures 19 and 20 are found and simulated using the Fresnel equations (15). From a physical perspective, when the wavelength λ of the incident wave is sufficiently small compared to the distance d, the incident wave behaves as if the distance d of the material was of infinite length. Which is essentially what happens in this situation, where the resulting reflection and transmission through the material is determined by imposing the Fresnel equations (15) at the first boundary between the different layers.

Table 4 shows the power reflectance $\mathfrak{R}$ at $d = 1000$ mm measured from the spectra in figures 19(a)-(b) and 20(a)-(b) for frequencies in the region where the reflection curve evens out. Similarly to the data presented in table 2 and 3, the power reflectance $\mathfrak{R}$ showcased in table 4 is increased accordingly with an increase in moisture level. Again the frequency region is slightly lower where the power reflectance $\mathfrak{R}$ was measured in table 4 compared to the corresponding measurements in table 2 and 3. The average deviation between the actual moisture level in the effective medium and the measured power reflectance values $\mathfrak{R}$ in table 4 was found to be 8.96%. Hence the theoretical model was in this instance used to detect the moisture level in the effective medium to a certainty of 91.04%.

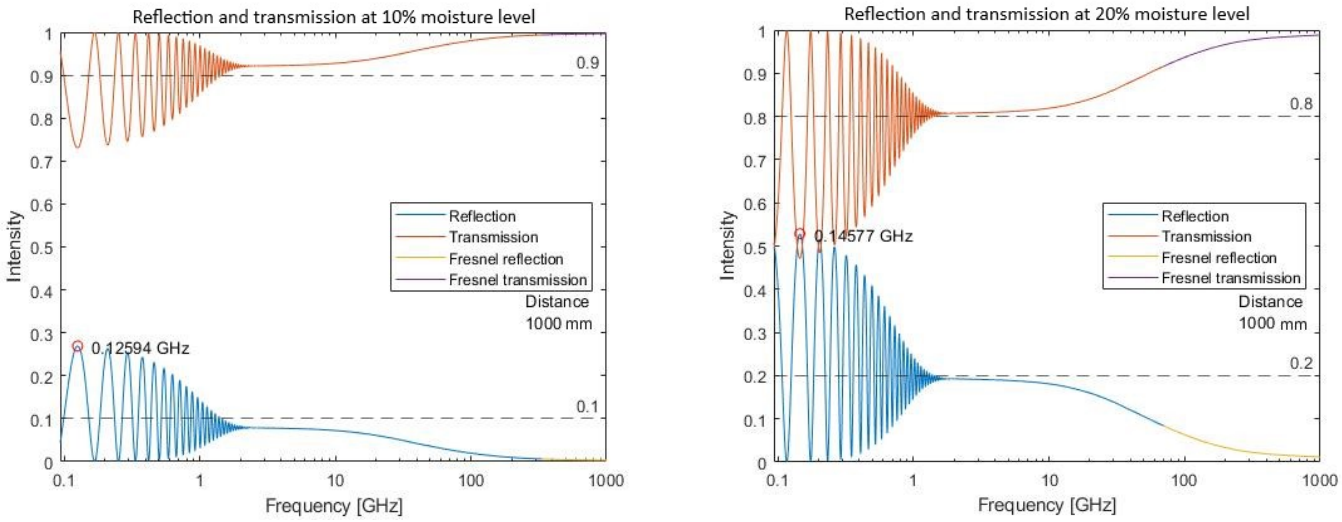

(a) 10 and 20% moisture level

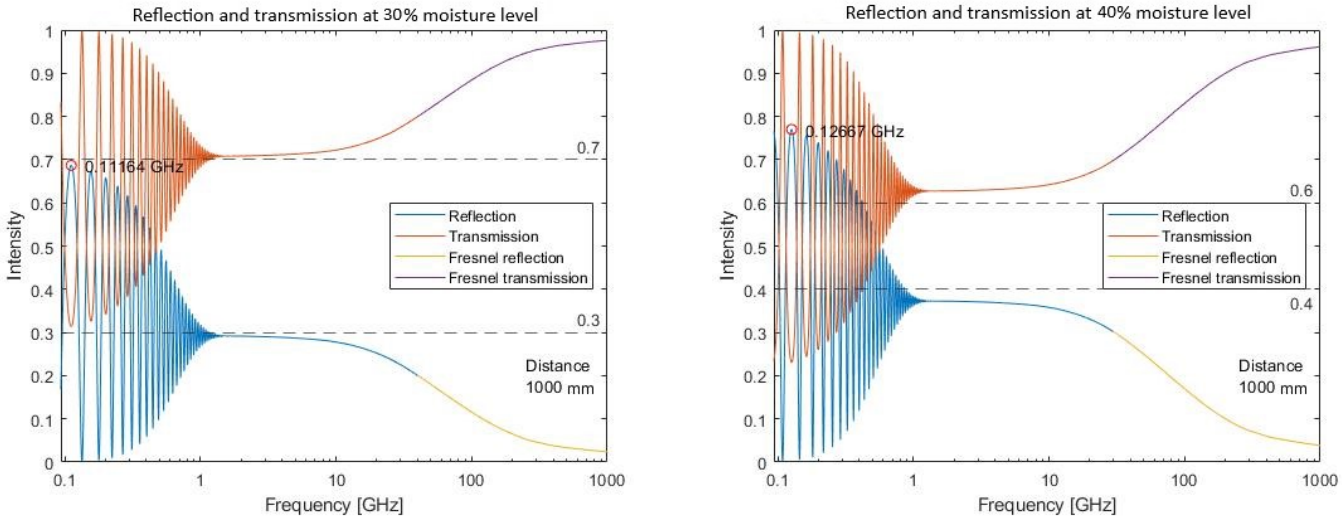

(b) 30 and 40% moisture level

Figure 21: Reflection and transmission intensity of incident radiation as a function of frequency through a material of a distance 1000 mm with moisture levels of 10 through 40%, approximated with Fresnel expressions where the theoretical model produced unidentified values.

Table 4: Power reflectance $\mathfrak{R}$ for a material of distance $d = 1000$ mm in the frequency region where the reflection intensity curve evens out.

Frequency [GHz]	Moisture level [%]	Power reflectance $\mathfrak{R}$ [intensity]
3	10	0.08 (i.e. 8%)
3	20	0.19 (i.e. 19%)
3	30	0.29 (i.e. 29%)
3	40	0.37 (i.e. 37%)

4.1.5 Simulated reflection and transmission through a material of distance 10 m

Figure 22(a)-(b) shows the simulated reflection and transmission spectra through the system described in figure 1 with $d = 10$ m and moisture levels ranging from 10 to 40%. The reflection and transmission spectra in figure 22 exhibit the same response to the increase in distance d as described in sections 4.1.3 and 4.1.4. Without any knowledge about the integer m of the first visible constructive interference fringe, following the steps explained in section 3.1.4 to determine the distance d is now significantly more difficult. For the same reason explained in section 4.1.4, the increase in distance to $d = 10$ m causes the reflection and transmission spectra to produce unidentified values for frequencies above approximately 10 GHz. Figure 22(a)-(b) demonstrates how the missing unidentified values are simulated from the Fresnel equations (15). The key takeaway from figure 22 is that the theoretical model is still valid and provides valuable data about the material's moisture level, even as the distance d extends to 10 metres.

Table 5 shows the power reflectance $\mathfrak{R}$ at $d = 10$ m measured from the spectra in figure 22(a)-(b) for frequencies in the region where the reflection curve evens out. Similarly to the data presented in tables 2-4, the power reflectance $\mathfrak{R}$ showcased in table 5 is increased accordingly with an increase in moisture level. The frequency of 1 GHz was used for all the measurements of the power reflectance $\mathfrak{R}$ in table 5, which is slightly lower compared to the frequencies used for the measurements in tables 2-4. Interestingly, the exact same values for the power reflectance $\mathfrak{R}$ was measured for both $d = 1000$ mm in table 4 and $d = 10$ m in table 5. Where the average deviation between the actual moisture level in the effective medium and the measured power reflectance values $\mathfrak{R}$ in table 5 was found to be 8.96%. Hence the theoretical model was in this instance used to detect the moisture level in the effective medium to a certainty of 91.04%.

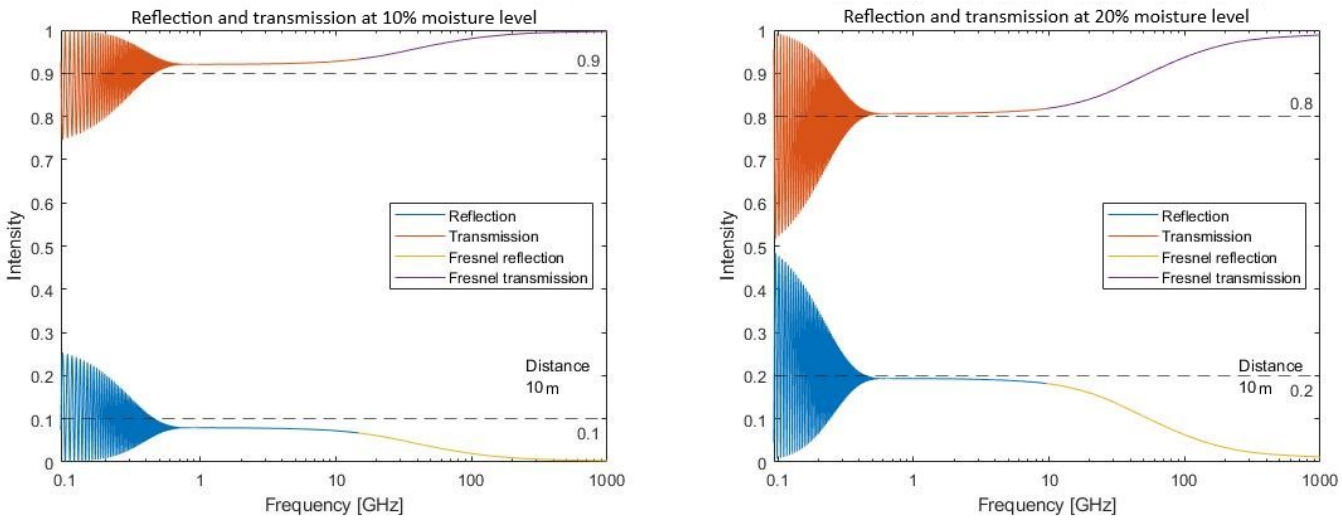

(a) 10 and 20% moisture level

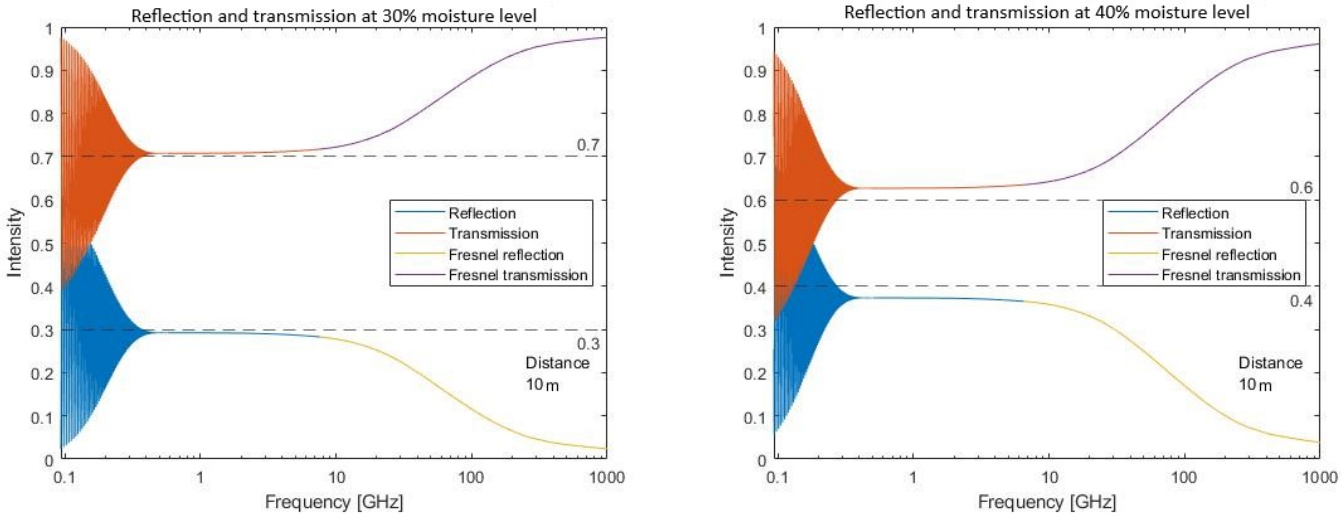

(b) 30 and 40% moisture level

Figure 22: Reflection and transmission intensity of incident radiation as a function of frequency through a material of a distance 10 m with moisture levels of 10 through 40%, approximated with Fresnel expressions where the theoretical model produced unidentified values.

Table 5: Power reflectance $\mathfrak{R}$ for a material of distance $d = 10$ m in the frequency region where the reflection intensity curve evens out.

Frequency [GHz]	Moisture level [%]	Power reflectance $\mathfrak{R}$ [intensity]
1	10	0.08 (i.e. 8%)
1	20	0.19 (i.e. 19%)
1	30	0.29 (i.e. 29%)
1	40	0.37 (i.e. 37%)

4.2 Reflection and transmission spectra simulated of TE and TM polarised off-axis waves

Following the method described in section 3.1.2, the reflection and transmission coefficients for TE and TM polarised waves were determined and used to create the required **M** matrices to simulate reflection and transmission spectra for the chosen frequency range and various levels of moisture ranging from 10 to 40%. Reflection and transmission spectra through the described system in figure 9 with distances $d = 100$ mm and $d = 1000$ mm at the two angles of incidence $\theta_1 = 15°$ and $\theta_1 = 30°$ are presented in this section. The resulting reflection and transmission spectra provide an understanding of how the system responds to an electromagnetic wave which is either TE or TM polarised, as well as how the reflection and transmission process is influenced by changes in the incidence angle θ_1.

4.2.1 Simulated reflection and transmission of TE and TM polarised waves through a material of distance 100 mm

Figure 23(a)-(b) shows the simulated reflection and transmission spectra through the system described in figure 9 with $d = 100$ mm, incidence angle $\theta_1 = 15°$ and moisture levels ranging from 10 to 40%. Reflection and transmission spectra for the same distance d at normal incidence is also included for comparison's sake, represented by the dashed lines. In figure 23, the reflection and transmission curve for normal incidence and TE polarised waves incident at $\theta_1 = 15°$ is relatively similar for the entire frequency spectre. Meaning that the waves at normal incidence and TE polarised waves remain in a similar phase configuration as they propagate through the layered media. TE polarised waves exhibit slightly stronger reflection characteristics and correspondingly slightly weaker transmission characteristics compared to waves at normal incidence.

Figure 23 demonstrates an interesting feature in the reflection and transmission curve for TM polarised waves. In the frequency region where interference effects influence the reflection and transmission curves causing them to oscillate, the reflection and transmission curve for TM polarised waves is out of phase with TE polarised waves and waves at normal incidence. From a physical perspective, this can be explained by considering that the different polarisation and their respective phase configuration is dependent on the angle of incidence θ_1 and refraction θ_2. Where this specific angle of incidence θ_1 introduces a phase shift in the TM polarised waves, resulting in the TM polarised waves to be significantly out of phase with the TE polarised waves and normally incident waves. This feature is present in all the reflection and transmission spectra provided for TE and TM polarised for both distances $d = 100$ mm and $d = 1000$ mm, and both angles of incidence $\theta_1 = 15°$ and $\theta_1 = 30°$. In the frequency region where the interference effects diminish and the reflection and transmission curve evens out, TM polarisation produces slightly weaker reflection characteristics compared to the spectra at normal incidence. Naturally, the differences for TE and TM polarised waves stems from their respective expressions for the reflection and transmission coefficients in equations (13.1)-(13.3).

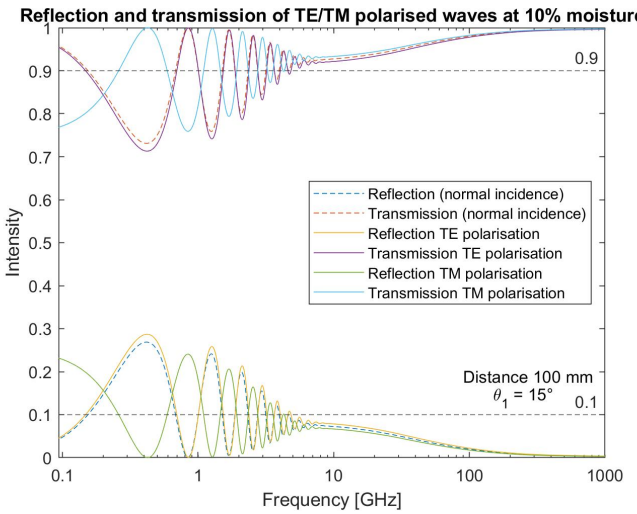

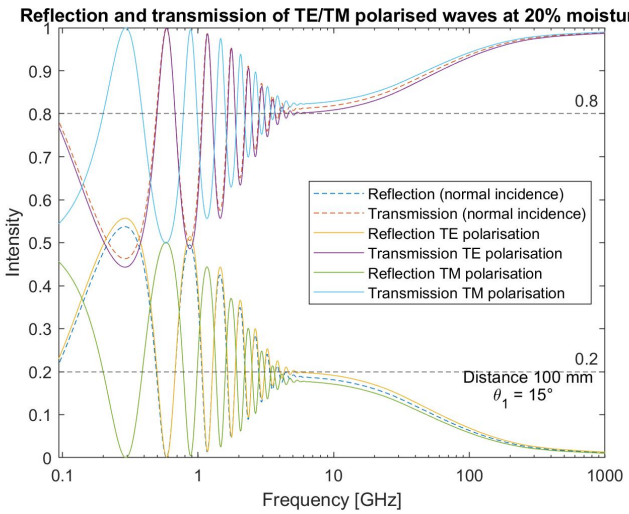

(a) 10 and 20% moisture level

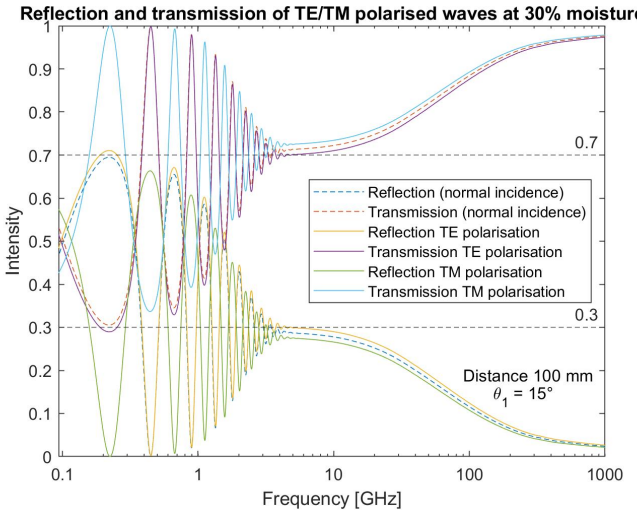

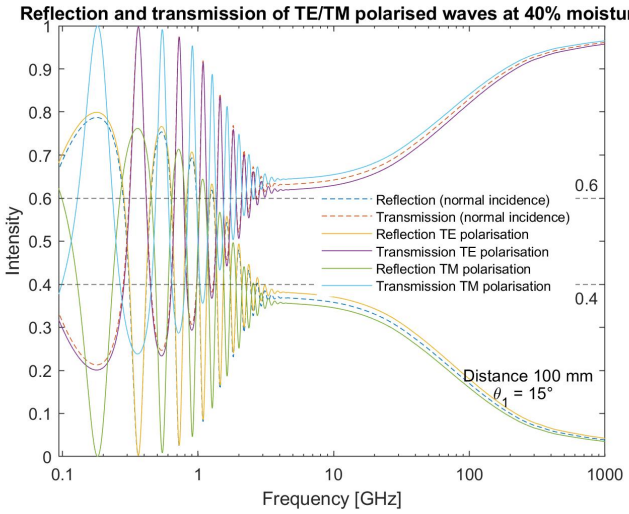

(b) 30 and 40% moisture level

Figure 23: Reflection and transmission intensity of TE and TM polarised waves with incidence angle $\theta_1 = 15°$ as a function of frequency through a material of a distance 100 mm with moisture levels of 10 through 40%.

Table 6 shows the power reflectance $\mathfrak{R}$ at $d = 100$ mm and $\theta_1 = 15°$ measured from the spectra in figure 23(a)-(b) for frequencies in the region where the reflection curve evens out. Which in this case was between 6 and 10 GHz. The data presented in table 6 substantiates the effect an increase in incidence angle θ_1 from normal incidence to $\theta_1 = 15°$ has on the reflection of electromagnetic waves in the layered media. The power reflectance $\mathfrak{R}$ for TE and TM polarised waves is increased in a similar manner to the power reflectance $\mathfrak{R}$ at normal incidence as the level of moisture increases, but with an average deviation of roughly 10%.

Table 6: Power reflectance $\mathfrak{R}$ for a material of distance $d = 100$ mm in the frequency region where the reflection intensity curve evens out.

Frequency [GHz]	Moisture level [%]	Power reflectance $\mathfrak{R}$ ($\theta_1 = 0°$) [intensity]	Power reflectance $\mathfrak{R}$ for TE polarisation ($\theta_1 = 15°$) [intensity]	Power reflectance $\mathfrak{R}$ for TM polarisation ($\theta_1 = 15°$) [intensity]
9	10	0.07 (i.e. 7%)	0.08 (i.e. 8%)	0.06 (i.e. 6%)
9	20	0.18 (i.e. 18%)	0.20 (i.e. 20%)	0.17 (i.e. 17%)
9	30	0.28 (i.e. 28%)	0.30 (i.e. 30%)	0.27 (i.e. 27%)
9	40	0.36 (i.e. 36%)	0.38 (i.e. 38%)	0.35 (i.e. 34%)

Figure 24(a)-(b) shows the simulated reflection and transmission spectra through the system described in figure 9 with $d = 100$ mm, incidence angle $\theta_1 = 30°$ and moisture levels ranging from 10 to 40%. Again the dashed lines represent reflection and transmission of waves at normal incidence. The same observations made for the spectra of TE and TM polarised waves in figure 23 for $\theta = 15°$ are also applicable for the spectra in figure 24. Where TM polarised waves are out of phase with TE polarised waves, almost to the point of having opposite phases (i.e. phase difference $\varphi = \frac{\lambda}{2}$).

In the frequency region where the interference effects diminish and the reflection and transmission curve evens out, TE polarisation produces slightly stronger reflection characteristics, whereas TM polarisation produces slightly weaker reflection characteristics compared to the spectra at normal incidence. Comparing the spectra for TE and TM polarised waves in figure 23 and 24, it is eminent that increasing the angle of incidence θ_1 from 15° to 30° has increased how much the reflection and transmission spectra of TE and TM waves deviate compared to that of normally incident waves. This also substantiated by the data measured in table 7, which shows the power reflectance $\mathfrak{R}$ at $d = 100$ mm and $\theta_1 = 30°$ measured from figure 24(a)-(b) for frequencies in the region where the reflection curve evens out.

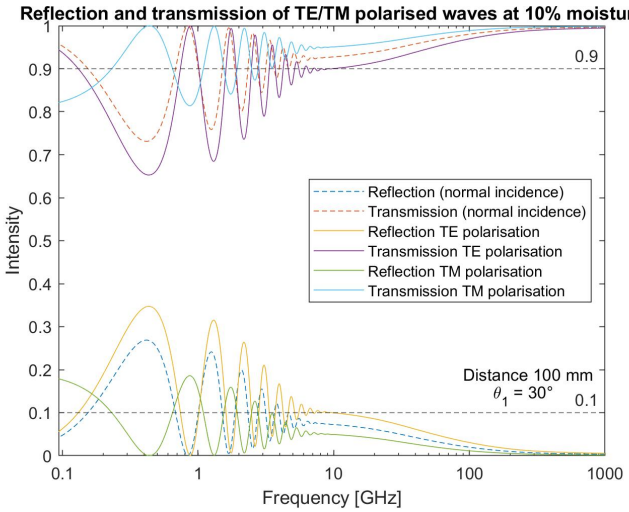

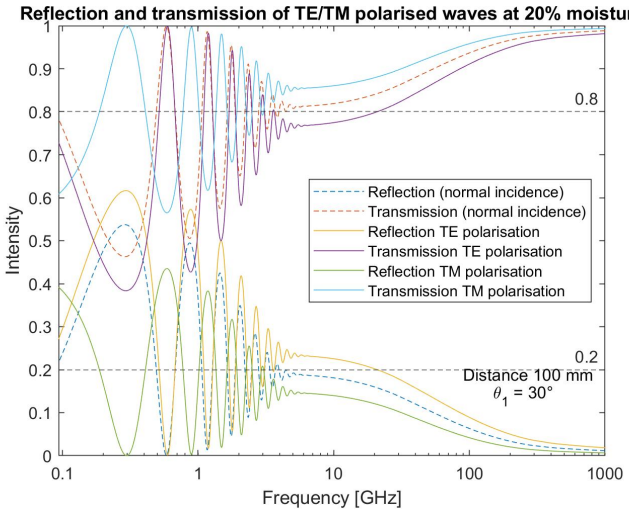

(a) 10 and 20% moisture level

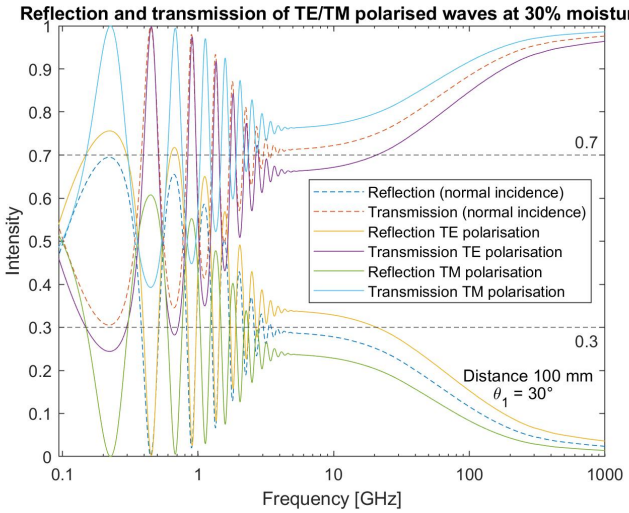

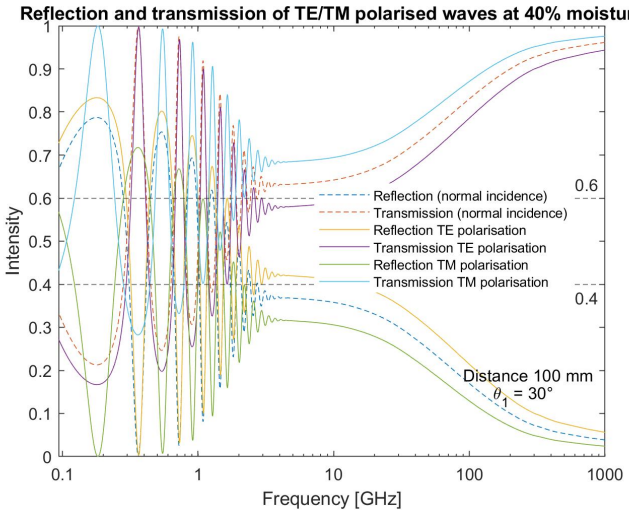

(b) 30 and 40% moisture level

Figure 24: Reflection and transmission intensity of TE and TM polarised waves with incidence angle $\theta_1 = 30°$ as a function of frequency through a material of a distance 100 mm with moisture levels of 10 through 40%.

For the corresponding measurements in table 6 for $\theta_1 = 15°$ and same distance d, the average deviation in power reflectance $\mathfrak{R}$ between normally incident waves and TE/TM polarised waves was found to be roughly 10%. In contrast to the measurements presented in table 7 for $\theta_1 = 30°$, where the average deviation is roughly 27%. Which is an increase of 17% to the corresponding measurements for incidence angle $\theta_1 = 15°$, showcasing that an increase in incidence angle θ_1 implicates a greater deviation of the corresponding reflection and transmission spectra for TE/TM polarised waves compared to the spectra for normally incident waves.

Table 7: Power reflectance $\mathfrak{R}$ for a material of distance $d = 100$ mm in the frequency region where the reflection intensity curve evens out.

Frequency [GHz]	Moisture level [%]	Power reflectance $\mathfrak{R}$ ($\theta_1 = 0°$) [intensity]	Power reflectance $\mathfrak{R}$ for TE polarisation ($\theta_1 = 30°$) [intensity]	Power reflectance $\mathfrak{R}$ for TM polarisation ($\theta_1 = 30°$) [intensity]
9	10	0.07 (i.e. 7%)	0.10 (i.e. 10%)	0.05 (i.e. 5%)
9	20	0.18 (i.e. 18%)	0.23 (i.e. 23%)	0.14 (i.e. 14%)
9	30	0.28 (i.e. 28%)	0.34 (i.e. 34%)	0.24 (i.e. 24%)
9	40	0.36 (i.e. 36%)	0.42 (i.e. 42%)	0.31 (i.e. 31%)

4.2.2 Simulated reflection and transmission of TE and TM polarised waves through a material of distance 1000 mm

As discussed in section 4.1, reflection and transmission spectra of normally incident waves are sensitive to changes in the distance d of the middle layer. Where an increase in distance d caused the interference pattern to oscillate more frequently, as well as a shift of the interference pattern itself towards the lower frequencies. Presented in this section is the simulated reflection and transmission spectra of TE and TM polarised waves, where the distance d of the middle layer in figure 9 has been increased to 1000 mm to determine how changes in distance d influences the resulting reflection and transmission spectra. Figure 25(a)-(b) shows the simulated reflection and transmission spectra through the system described in figure 9 with $d = 1000$ mm, incidence angle $\theta_1 = 15°$ and moisture levels ranging from 10 to 40%. As expected, the interference pattern oscillates more frequently and is shifted towards the lower frequencies in figure 25 compared to the corresponding spectra in figure 23 for $d = 100$ mm.

Figure 25 demonstrates the same characteristics described in the previous section, where TM polarised waves are considerably out of phase with the TE polarised and normally incident waves. TE polarised and normally incident waves constructively interfere for approximately the same frequencies, whereas TM polarised waves destructively interfere at these frequencies, and vice versa. A characteristic which emerges due to the relation between the individual phase configurations of TE and TM polarised waves and the incidence angle θ_1.

Similarly to the simulated spectra provided in the previous section, TE and TM polarised waves exhibit slightly stronger and weaker reflection characteristics, respectively. Substantiated by the measurements of the power reflectance $\mathfrak{R}$ from figure 25 presented in table 8. These measurements were executed at the frequency of 3 GHz, which is roughly where the reflection curve stops oscillating and evens out in figure 25. As stated previously, the power reflectance $\mathfrak{R}$ for TE and TM polarised waves is increased in a similar manner to the power reflectance $\mathfrak{R}$ at normal incidence as the level of moisture increases, but with an average deviation of 6%. Comparing the data presented in table

8 with the corresponding measurements of the power reflectance $\mathfrak{R}$ for $d = 100$ mm in table 6, the increase in distance d from 100 to 1000 mm actually reduced the deviation in power reflectance $\mathfrak{R}$ between the normally incident waves and TE/TM polarised waves with 4%.

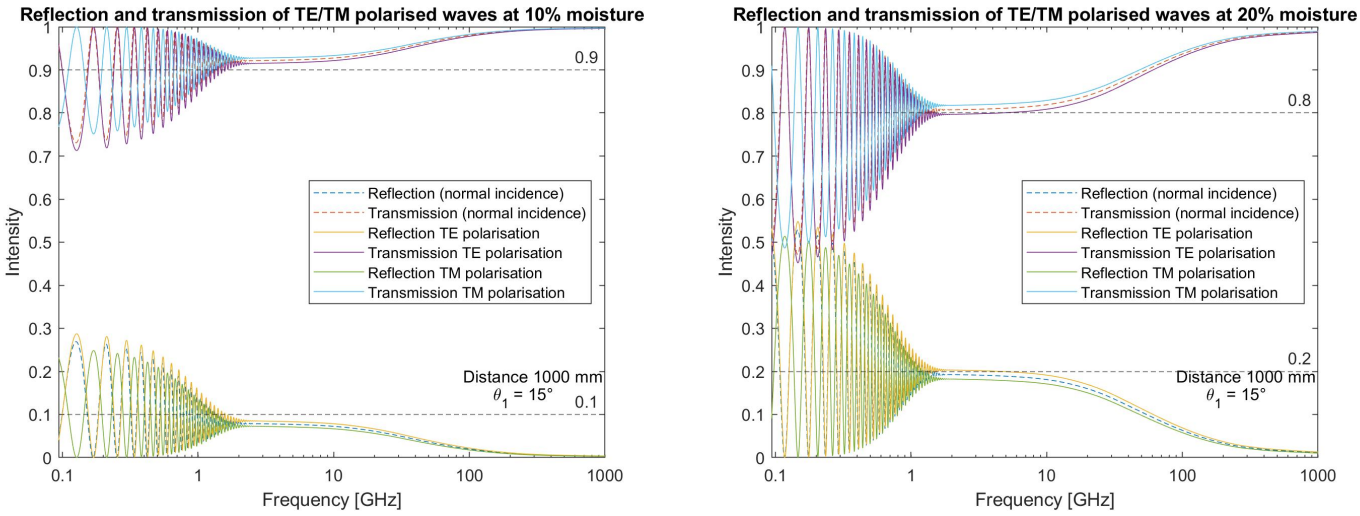

(a) 10 and 20% moisture level

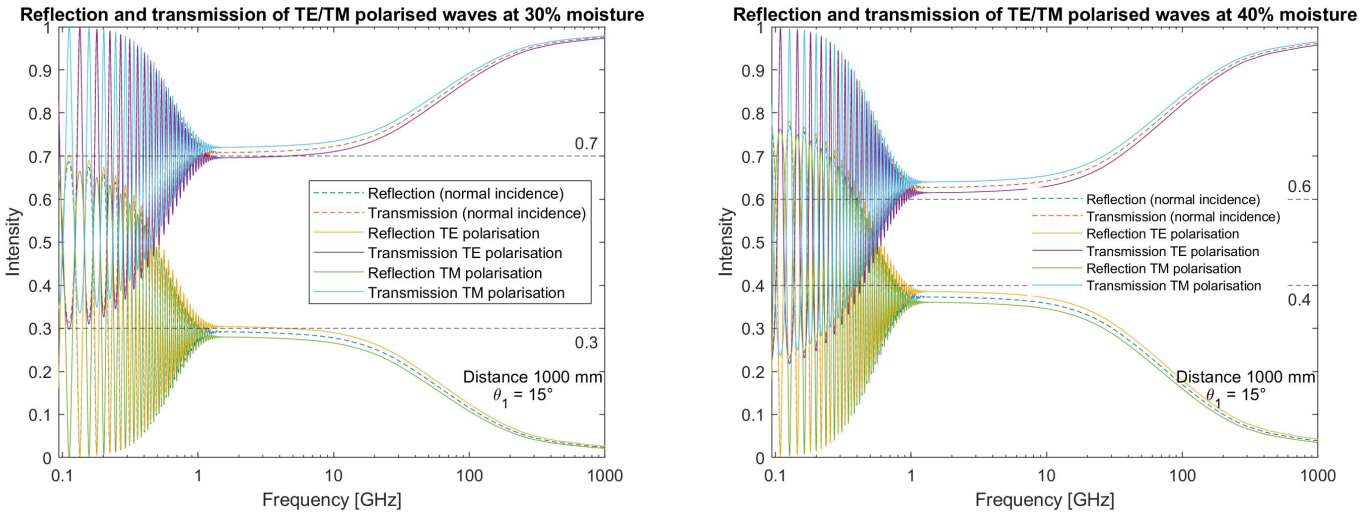

(b) 30 and 40% moisture level

Figure 25: Reflection and transmission intensity of TE and TM polarised waves with incidence angle $\theta_1 = 15°$ as a function of frequency through a material of a distance 1000 mm with moisture levels of 10 through 40%.

Table 8: Power reflectance $\mathfrak{R}$ for a material of distance $d = 1000$ mm in the frequency region where the reflection intensity curve evens out.

Frequency [GHz]	Moisture level [%]	Power reflectance $\mathfrak{R}$ ($\theta_1 = 0°$) [intensity]	Power reflectance $\mathfrak{R}$ for TE polarisation ($\theta_1 = 15°$) [intensity]	Power reflectance $\mathfrak{R}$ for TM polarisation ($\theta_1 = 15°$) [intensity]
3	10	0.08 (i.e. 8%)	0.08 (i.e. 8%)	0.07 (i.e. 7%)
3	20	0.19 (i.e. 19%)	0.20 (i.e. 20%)	0.18 (i.e. 18%)
3	30	0.29 (i.e. 29%)	0.30 (i.e. 30%)	0.28 (i.e. 28%)
3	40	0.37 (i.e. 37%)	0.38 (i.e. 38%)	0.36 (i.e. 36%)

For the simulated reflection and transmission spectra of TE and TM polarised waves shown in figure 26(a)-(b), the incidence angle was increased to $\theta_1 = 30°$. Similarly to the observations made in the previous section, an increase in incidence angle θ_1 coincide with a greater discrepancy in the reflection and transmission spectra between normally incident waves and TE/TM polarised waves. Which is also the case when comparing the spectra in figure 25 for $\theta_1 = 15°$ to the spectra in figure 26 for $\theta_1 = 30°$. Measurements presented in table 9 showcases the discrepancy in power reflectance $\mathfrak{R}$ between normally incident waves and TE/TM polarised waves from figure 26 in the frequency region where the oscillations diminish and the reflection curve evens out. Comparing the corresponding measurements in table 8 and 9, increasing the incidence angle from $\theta_1 = 15°$ to $\theta_1 = 30°$ caused the average deviation in power reflectance $\mathfrak{R}$ between normally incident waves and TE/TM polarised waves to increase from 6% up to 24%. This is an increase of 18%, which is virtually the same observation made in the previous section where the distance was set at $d = 100$ mm.

Comparing the corresponding measurements of power reflectance $\mathfrak{R}$ for the same incidence angle θ_1, but with different distance d, the change in distance from $d = 100$ mm to 1000 mm reduced the deviation by 3%. Hence the increase in distance d actually provides the more accurate results in relation to the detected discrepancy between normally incident waves and TE/TM polarised waves. The key takeaway from the presented results in this section, is the fact that an increase in incidence angle θ_1 has a substantial impact on the resulting reflection and transmission spectra of TE and TM polarised waves compared to the spectra of normally incident waves. Which makes it more difficult to accurately detect the level of moisture in the desired media.

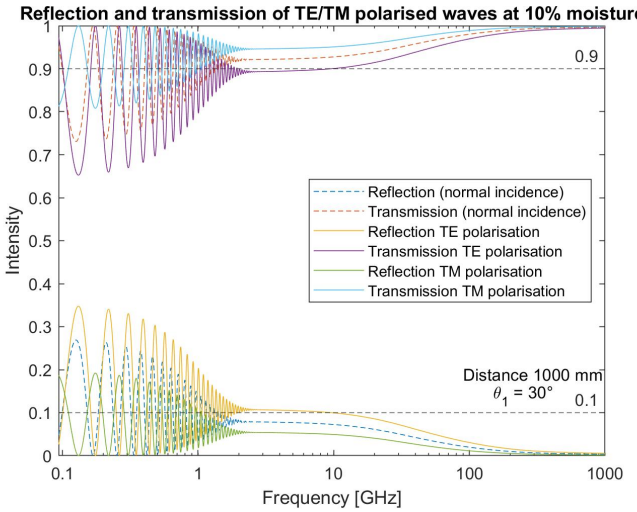

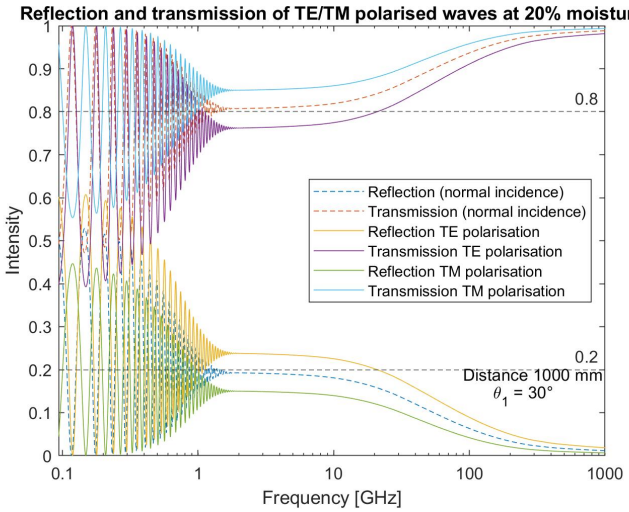

(a) 10 and 20% moisture level

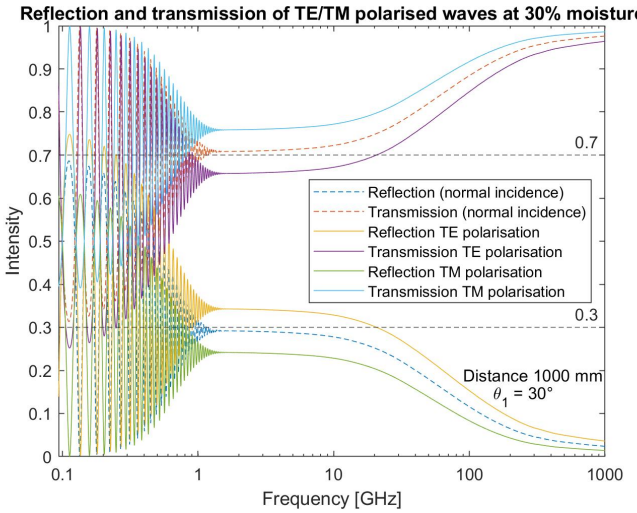

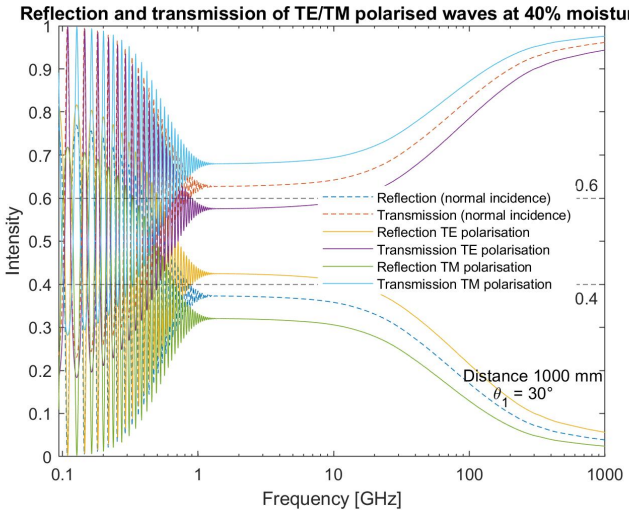

(b) 30 and 40% moisture level

Figure 26: Reflection and transmission intensity of TE and TM polarised waves with incidence angle $\theta_1 = 30°$ as a function of frequency through a material of a distance 1000 mm with moisture levels of 10 through 40%.

Table 9: Power reflectance $\mathfrak{R}$ for a material of distance $d = 1000$ mm in the frequency region where the reflection intensity curve evens out.

Frequency [GHz]	Moisture level [%]	Power reflectance $\mathfrak{R}$ ($\theta_1 = 0°$) [intensity]	Power reflectance $\mathfrak{R}$ for TE polarisation ($\theta_1 = 30°$) [intensity]	Power reflectance $\mathfrak{R}$ for TM polarisation ($\theta_1 = 30°$) [intensity]
3	10	0.08 (i.e. 8%)	0.11 (i.e. 11%)	0.05 (i.e. 5%)
3	20	0.19 (i.e. 19%)	0.24 (i.e. 24%)	0.15 (i.e. 15%)
3	30	0.29 (i.e. 29%)	0.34 (i.e. 34%)	0.24 (i.e. 24%)
3	40	0.37 (i.e. 37%)	0.42 (i.e. 42%)	0.32 (i.e. 32%)

4.3 Experimental measurements of sponge sample

Experimental measurements were executed in the lab following the measurement method described in section 3.2. Where a sponge filled with different volumetric moisture contents θ_w between 10 and 40% was used as sample material. Measurements of the scattering parameter $S11$ were performed using DAKS-3.5 in the described configuration and then converted to the corresponding complex permittivity ε of the sample material in the frequency range 85 MHz - 14 GHz. Determining the complex permittivity ε of the sample material allowed for the simulation of the resulting reflection spectra at different distances d to compare with the corresponding theoretical results presented in section 4.1. Calibration measurements of battery water are presented first, followed by experimental measurements of the complex permittivity ε at different volumetric moisture contents θ_w, and lastly the resulting reflection spectra at different distances d derived from the experimental measurements.

4.3.1 Calibration measurements

Before performing any measurements, the DAK-3.5 setup was calibrated under load using battery water at 24°C. Figure 27 shows the load calibration, where the yellow lines represent the measured values of the dielectric constant ε' and dielectric loss factor ε'' between 85 MHz and 14 GHz. The red lines represent the corresponding target values of water available in the DAK software. With the exception of some noise towards the higher frequencies, the measured values are fairly consistent with the target values for water.

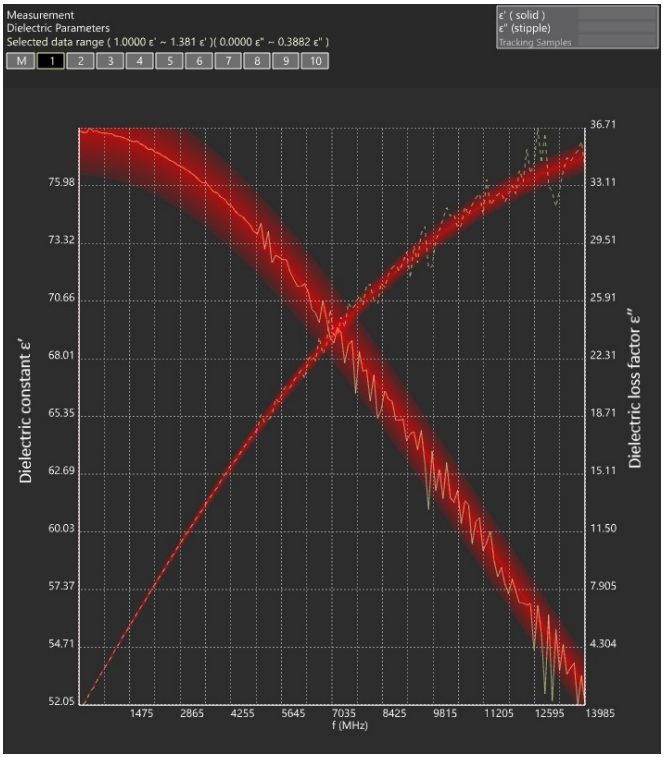

Figure 27: Calibration measurement of the dielectric constant ε' (y-axis on the left) and dielectric loss factor ε'' (y-axis on the right) of battery water as a function of frequency at 24.7°C.

Figure 28 shows the same measured and target values as in figure 27, but in a more readable manner and with the addition of the complex permittivity ε derived from the complex refractive index $\underline{n}$ gathered from Segelstein (1981). A visible trend in figure 28 is that the noise in the measured values increases with frequency, as well as the deviation between the measured values and the values derived from Segelstein (1981). The Segelstein values of the dielectric constant ε' is lower compared to the measured values, with the deviation between the two values increasing with frequency. Whereas the Segelstein, target, and measured values of the dielectric loss factor ε'' are approximately equivalent for the visible frequency range. Values of both the dielectric constant ε' and dielectric loss factor ε'' are shown in table 10. As well as the deviation between the measured battery water values and the target values of water available in the DAK software for frequencies between 1 and 14 GHz. Where the average deviation of the dielectric constant ε' and dielectric loss factor ε'' was 0.4% and 1.43%, respectively. Indicating a slightly higher deviation in the dielectric loss factor ε'', but still relatively low deviation between the measured and target values of both the dielectric constant ε' and dielectric loss factor ε''. [15]

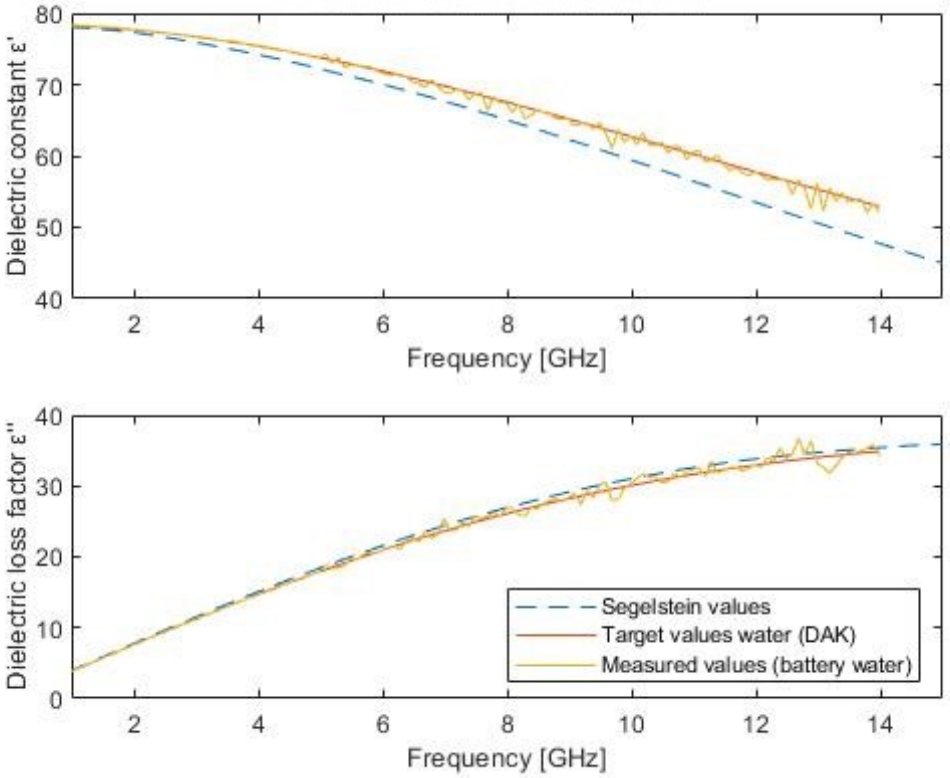

Figure 28: Dielectric constant ε' and dielectric loss factor ε'' derived from Segelstein (1981), experimental measurement of battery water, and target values of water from DAK software as a function of frequency [15].

Table 10: Dielectric constant ε' and dielectric loss factor ε'' derived from Segelstein (1981), experimental measurement values of battery water, and target values of water from DAK software [15].

Frequency [GHz]	Segelstein values		Measured battery water values		Target values water (DAK)		Deviation [%]	
	ε'	ε''	ε'	ε''	ε'	ε''	ε'	ε''
1	78.0	3.9	78.4	3.7	78.3	3.8	0.13	2.6
2	77.3	7.8	77.7	7.5	77.7	7.2	0.0	4.2
4	74.2	15.1	75.4	14.7	75.4	14.6	0.0	0.7
6	70.0	21.6	71.7	21.0	71.9	20.9	0.3	0.5
8	65.0	27.0	67.5	26.2	67.6	26.1	0.1	0.4
10	59.4	31.0	62.1	30.3	62.7	30.1	1.0	0.7
12	53.5	33.8	57.8	33.1	57.8	33.0	0.0	0.3
14	47.7	35.4	52.1	34.2	52.9	34.9	1.5	2.0

4.3.2 Complex permittivity of sponge sample at different volumetric moisture contents

After the calibration process was completed, the complex permittivity ε of the sponge sample was measured at different volumetric moisture contents θ_w between 10 and 40%, showcased in figure 29. While figure 30 shows the corresponding properties based on the derived values of the complex permittivity ε from Segelstein (1981) combined with the effective media approximation to regulate the amount of volumetric moisture content θ_w. The same trends are present in both figures, where an increase in volumetric moisture content θ_w coincides with an increase in both the dielectric constant ε' and dielectric loss factor ε''. This is expected as the sponge exhibit similar dielectric properties to that of air (i.e. $\varepsilon' \approx 1$ and $\varepsilon'' \approx 0$). Whereas water exhibit considerably greater values for both the dielectric constant ε' and dielectric loss factor ε''. Naturally, the measured experimental curves are less smooth in comparison to the curves from Segelstein (1981) due to the presence of noise. [15]

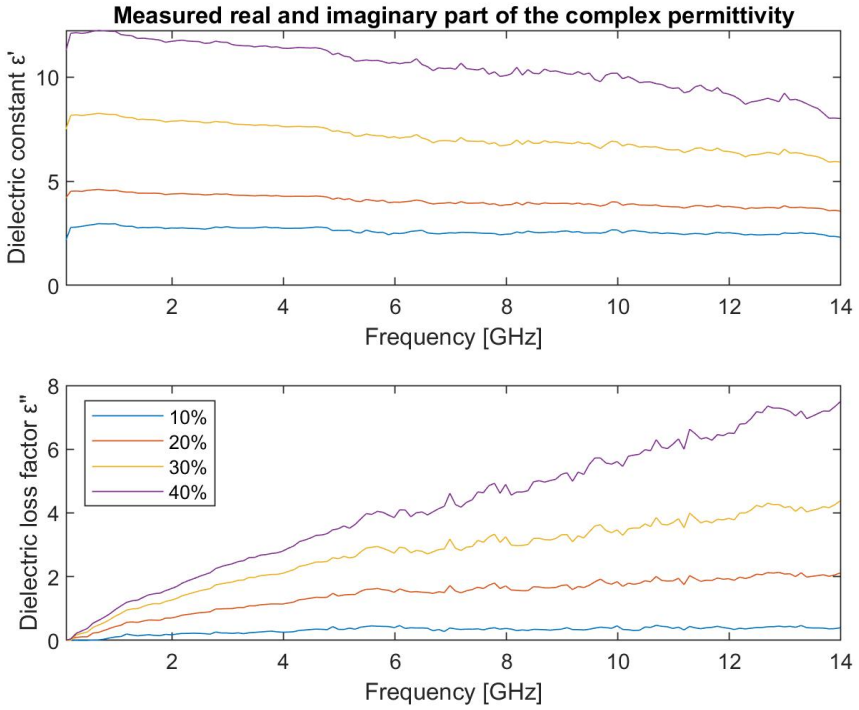

Figure 29: Dielectric constant ε' and dielectric loss factor ε'' measured experimentally of a sponge as a function of frequency with different volumetric moisture contents between 10 and 40%.

The separation between the dielectric constants ε' of the different volumetric moisture contents θ_w is most prominent at the lower end of the frequency range, and become less separated as the frequency increases. The opposite is true for the dielectric loss factor ε'', where the separation is most prominent towards the higher end of the frequency range. This can be understood from the fact that the dielectric constant ε' is inversely proportional to frequency, while the dielectric loss

factor ε'' is proportional to frequency in the considered frequency range.

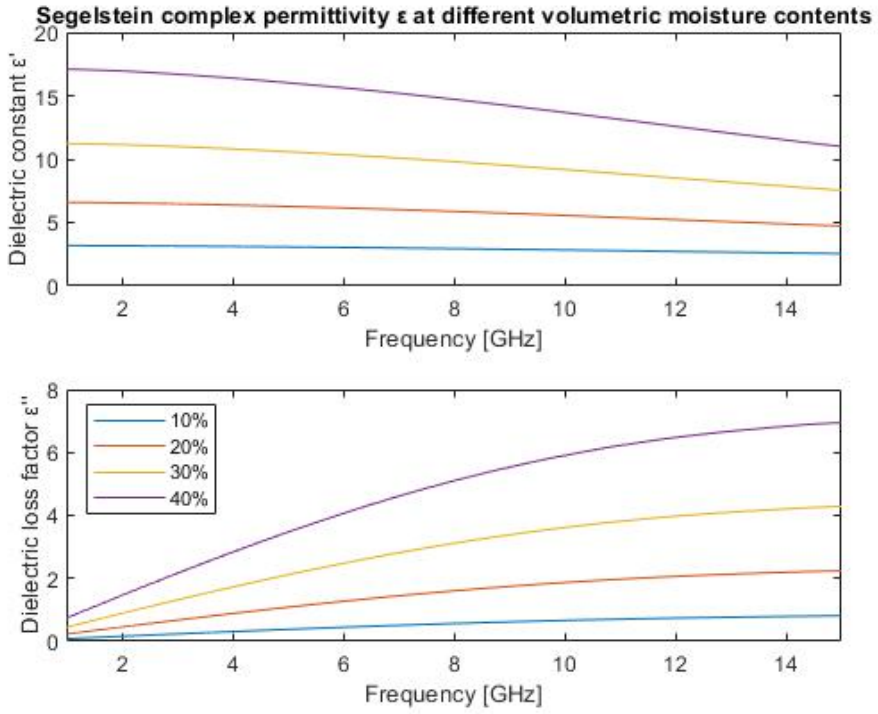

Figure 30: Dielectric constant ε' and dielectric loss factor ε'' derived from Segelstein (1981) as a function of frequency at different volumetric moisture contents between 10 and 40% [15].

Table 11 shows values of the dielectric constant ε' and the dielectric loss factor ε'' at specific frequencies and different volumetric moisture contents θ_w, as well as the deviation between the Segelstein (1981) properties and the measured experimental properties. Where the deviation is considerable for certain values, especially for the dielectric loss factor ε''. The deviation in the dielectric constant ε' is lowest at the volumetric moisture content θ_w of 10% with an average deviation of 11.8%. At the volumetric moisture contents θ_w between 20 and 40%, the deviation in the dielectric constant ε' is substantially higher at roughly 25-30%. These deviations in the dielectric constant ε' and dielectric loss factor ε'' will have an impact on the corresponding reflection spectra provided in the next section. It is not apparent if the deviation is correlated with either frequency or volumetric moisture content θ_w. Other factors such as noise, temperature variations, and inconsistent measurements could be the root of the matter. As the complex permittivity ε is sensitive to small changes in temperature and the Segelstein (1981) properties are valid only for the temperature of 25°. [15]

An important aspect regarding the measured dielectric properties is that the values of the dielectric constant ε' are greater than the values of the dielectric loss factor ε'' in the considered frequency range. Implicating that the dielectric constant ε' is the dominating property in the complex permittivity ε. Which means that even considerable deviations as high as 55.6% in the dielectric loss factor

ε'' has less significance as long as the deviation in the dielectric constant ε' is relatively low.

Table 11: Dielectric constant ε' and dielectric loss factor ε'' derived from Segelstein (1981) and experimental measurement values of battery water, and target values of water from DAK software [15].

Frequency [GHz]	Segelstein values		Measured experimental values		Deviation [%]	
	ε'	ε''	ε'	ε''	ε'	ε''
Volumetric moisture content of 10%						
2	3.17	0.16	2.76	0.18	12.9	12.5
6	3.03	0.44	2.51	0.40	17.2	9.1
10	2.84	0.66	2.66	0.46	6.3	30.0
14	2.60	0.79	2.32	0.40	10.8	49.4
Volumetric moisture content of 20%						
2	6.55	0.45	4.39	0.70	32.98	55.6
6	6.15	1.27	4.00	1.51	34.96	18.9
10	5.56	1.87	4.00	1.70	28.06	9.1
14	4.89	2.19	3.57	2.12	26.00	3.2
Volumetric moisture content of 30%						
2	11.40	0.89	7.88	1.26	30.88	41.6
6	10.35	2.48	7.14	2.74	31.01	10.5
10	9.18	3.61	6.89	3.47	24.95	3.9
14	7.85	4.21	5.93	4.38	24.46	4.0
Volumetric moisture content of 40%						
2	16.95	1.46	11.7	1.62	30.97	11.0
6	15.63	4.06	10.71	3.85	31.48	5.2
10	13.68	5.90	10.19	5.61	25.51	4.9
14	11.53	6.83	8.01	7.49	30.53	9.7

4.3.3 Simulated reflection of the sponge sample

By using the measured experimental values of the complex permittivity ε at the different volumetric moisture contents θ_w, the corresponding reflection spectra were simulated by following the same method used for the theoretical model described in section 3.1.

4.3.3.1 Simulated reflection through a sample material of distance 100 mm

Figure 31(a)-(b) shows resulting reflection spectra simulated for volumetric moisture contents between 10 and 40% through a material of distance $d = 100$ mm. Where the orange curve represents the reflection intensity based on the complex permittivity ε measured experimentally of the sponge sample at different volumetric moisture contents θ_w. For comparisons sake, the corresponding reflection spectra simulated from the theoretical model based on the dielectric properties gathered from Segelstein (1981) is also included as the dashed blue curve in figure 31 [15].

As expected the interference pattern is present towards the lower end of the considered frequency range, represented by oscillations in the reflection intensity curve. Where the peaks and valleys correspond to constructive and destructive interference, respectively. As explained in section 4.1.3, an increase in volumetric moisture level θ_w coincides with an increase of the refractive index n, causing the interference pattern to oscillate at an increased rate. As well as slightly shifting the interference pattern towards the lower frequencies, showcased in the reflection spectra in figure 31.

The discrepancy between the Segelstein reflection and the measured experimental reflection is roughly the same for the different volumetric moisture contents between 20 and 40%, and slightly less so at $\theta_w = 0.1$. This is also consistent with the data given in table 11, where the deviation between the experimental and Segelstein values of the dielectric constant ε' and dielectric loss factor ε'' is roughly the same at each of the volumetric moisture contents θ_w.

Similarly to the simulated reflection spectra from the theoretical model represented by the dashed line in figure 31, an increase in the volumetric moisture content θ_w coincides with an increase in the experimental reflection. A correlation between the volumetric moisture content θ_w and the reflection intensity is found by measuring the reflection intensity of frequencies not influenced by interference effects, showcased in table 12 at the frequency of 9 GHz. As expected, the experimental reflection intensity derived from the complex permittivity ε of the sponge sample provides a less accurate indication of the volumetric moisture content θ_w in the sample material in comparison to the reflection spectra based on the Segelstein (1981) properties [15]. Comparing the volumetric moisture content θ_w to the corresponding experimental reflection intensity in table 12, the maximum and minimum deviation of 42% and 22.5% is found at $\theta_w = 0.1$ and $\theta_w = 0.4$, respectively. Where the average deviation between the two mentioned quantities in table 12 is 30.7%. Indicating that the volumetric moisture content θ_w between 10 and 40% through a sample material of distance $d = 100$ mm is on average determined from the resulting reflection intensity to a certainty of 69.3%.

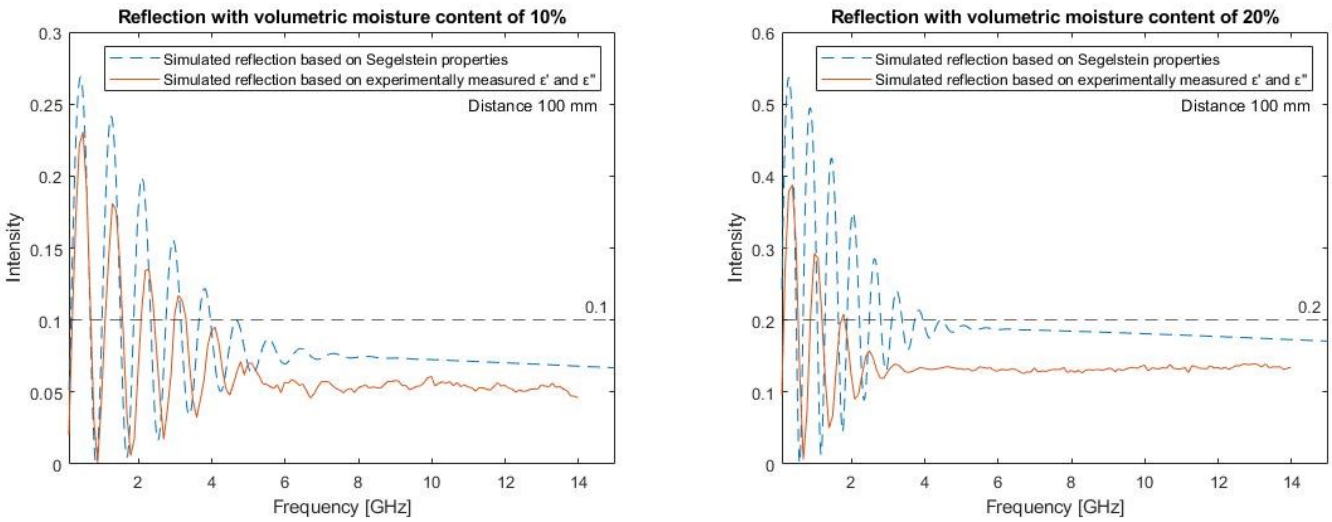

(a) 10 and 20% volumetric moisture content

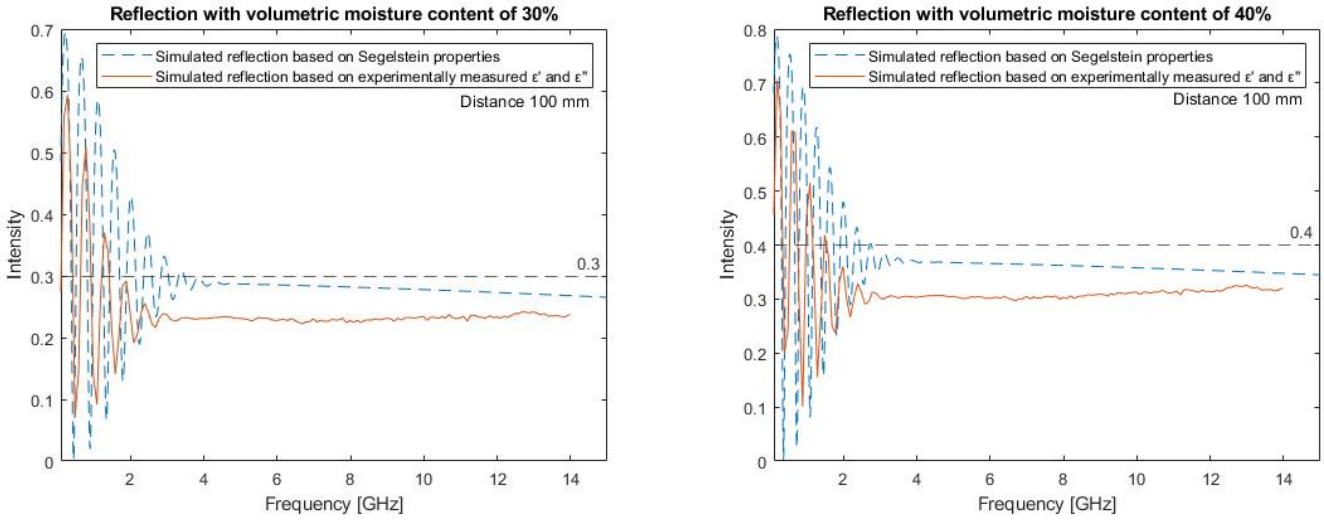

(b) 30 and 40% volumetric moisture content

Figure 31: Reflection based on the complex refractive index $\underline{n}$ of water gathered from Segelstein (1981) and the complex permittivity ε measured experimentally of a sponge as a function of frequency, with the distance set at 100 mm and volumetric moisture contents between 10 and 40% [15].

Table 12: Reflection values at specific frequencies measured from the reflection spectra with the distance set at 100 mm and volumetric moisture contents between 10 and 40%.

Frequency [GHz]	Volumetric moisture content	Segelstein reflection	Experimental (sponge sample)
9	0.1	0.074	0.058
9	0.2	0.18	0.13
9	0.3	0.28	0.23
9	0.4	0.36	0.31

4.3.3.2 Simulated reflection through a sample material of distance 500 mm

Figure 32(a)-(b) shows the reflection spectra simulated for volumetric moisture contents between 10 and 40% through a material of distance $d = 500$ mm. The reflection spectra in figure 32 follow the same trends as in figure 31, with a few minor differences. The most noteworthy difference is that the interference pattern is shifted towards the lower frequencies, as well as the oscillations in the interference pattern becoming more frequent. These changes can be understood from equation (35), where an increase in distance d reduces the spacing in frequency between the different interference fringes denoted by m. A more detailed explanation of this response is provided in section 4.1.3.

As the interference pattern is shifted towards the lower frequencies, so is the frequency where the reflection intensity most accurately provides an indication of the volumetric moisture content θ_w in the sample material. Which is found by measuring the reflection intensity of frequencies not influenced by interference effects, showcased in table 13 at the frequency of 4.5 GHz. In this case, the deviation between the volumetric moisture content θ_w and the corresponding experimental reflection intensity is on average 29.2%%. Meaning that the volumetric moisture content θ_w between 10 and 40% through a sample material of distance $d = 500$ mm is on average determined by measuring the reflection intensity at 4.5 GHz to a certainty of 70.2%. Which is 1.5% more accurate compared to the case for $d = 100$ mm in the previous section.

The deviation in the interference pattern showcased in figure 32 for the simulated reflection based on the experimentally measured dielectric properties is due to the sampling resolution of the DAKS-3.5 setup being too low. The sampling rate was set at frequency intervals of 100 MHz, which is too low to properly sample the features of the interference pattern.

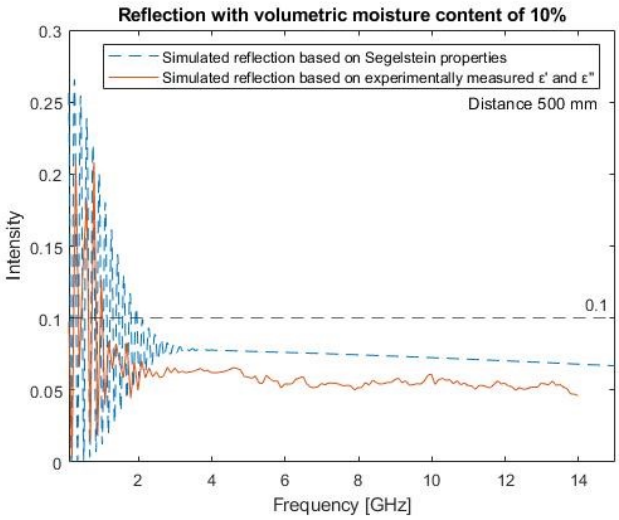

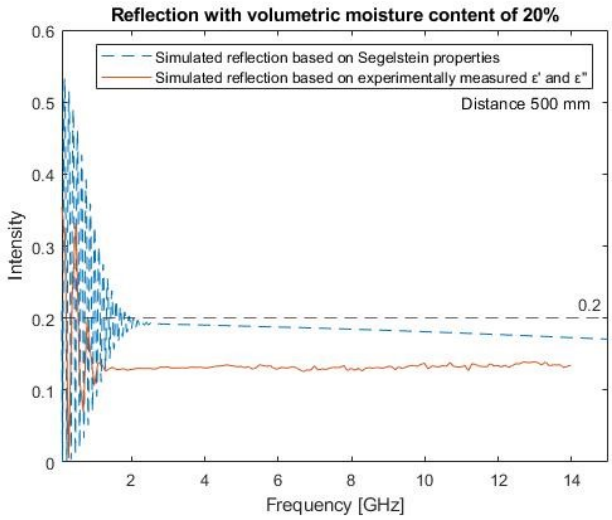

(a) 10 and 20% volumetric moisture content

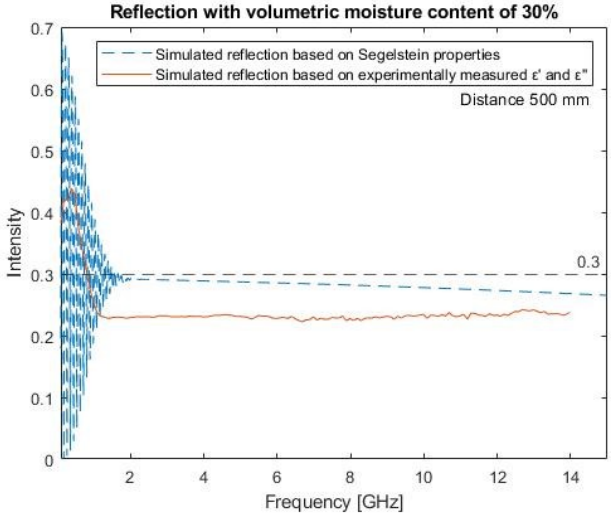

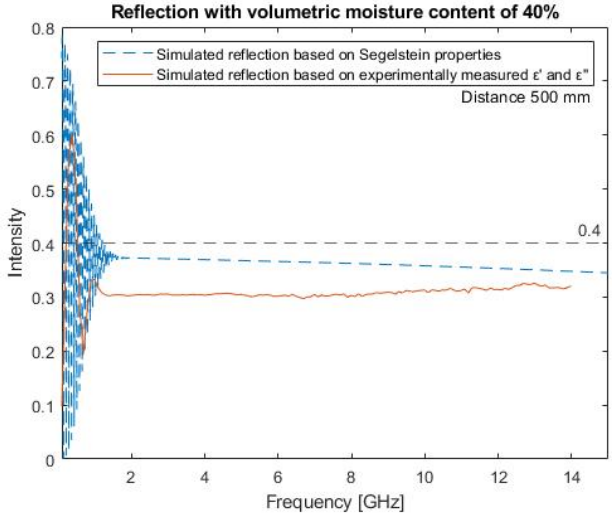

(b) 30 and 40% volumetric moisture content

Figure 32: Reflection based on the complex refractive index $\underline{n}$ of water gathered from Segelstein (1981) and the complex permittivity ε measured experimentally of a sponge as a function of frequency, with the distance set at 500 mm and volumetric moisture contents between 10 and 40% [15]. Deviations in the interference pattern of the simulated reflection of the experimental properties is due to the low sampling resolution of the DAKS-3.5 setup.

Table 13: Reflection values at specific frequencies measured from the reflection spectra with the distance set at 500 mm and volumetric moisture contents between 10 and 40%.

Frequency [GHz]	Volumetric moisture content	Segelstein reflection	Experimental (sponge sample)
4.5	0.1	0.077	0.064
4.5	0.2	0.19	0.13
4.5	0.3	0.29	0.23
4.5	0.4	0.37	0.31

4.3.3.3 Simulated reflection through a sample material of distance 1000 mm

Figure 33(a)-(b) shows the reflection spectra simulated for volumetric moisture contents between 10 and 40% through a material of distance $d = 1000$ mm. Again the reflection spectra showcased in figure 33 is consistent with the behaviour described for the reflection spectra in figure 31 and 32. Where the discrepancy between the Segelstein reflection and the measured experimental reflection is roughly the same for the different volumetric moisture contents θ_w between 10 and 40%.

Comparing with the spectra in figure 31 and 32, the increase in distance d to a 1000 mm coincides with the interference pattern shifting towards the lower end of the frequency range and also oscillating at an increased rate. Increasing the volumetric moisture content θ_w has a similar effect. Meaning that the frequency where the reflection intensity most accurately provides an indication of the volumetric moisture content θ_w is also shifted towards the lower frequencies. Table 14 shows the measured values of the reflection intensity as the interference effects diminish at the frequency 3 GHz. In this case, the deviation between the volumetric moisture content θ_w and the corresponding experimental reflection intensity is on average 28.96%. Meaning that the volumetric moisture content θ_w between 10 and 40% through a sample material of distance $d = 1000$ mm is on average determined by measuring the reflection intensity at 3 GHz to a certainty of 71.04%. Which is 0.84% more accurate compared to the case for $d = 500$ mm in the previous section.

The deviation in the interference pattern showcased in figure 33 for the simulated reflection based on the experimentally measured dielectric properties is due to the sampling resolution of the DAKS-3.5 setup being too low. The sampling rate was set at frequency intervals of 100 MHz, which is too low to properly sample the features of the interference pattern.

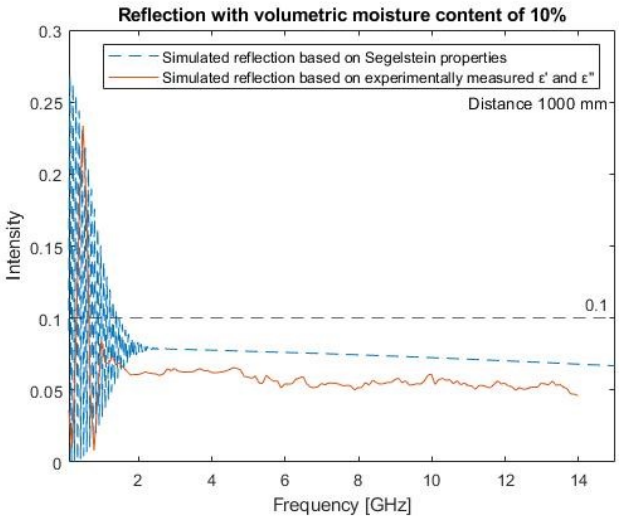

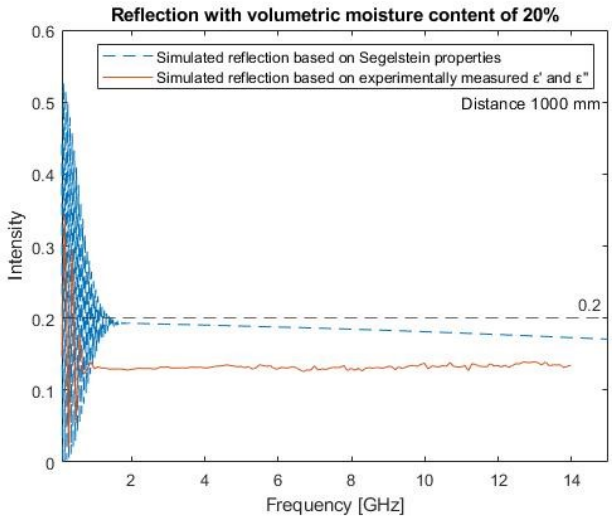

(a) 10 and 20% volumetric moisture content

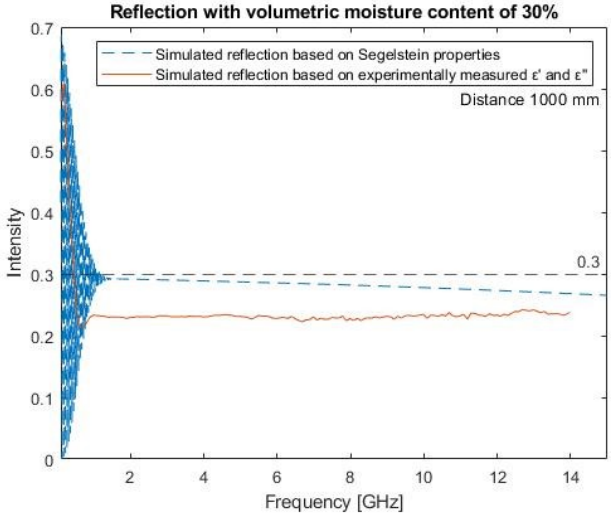

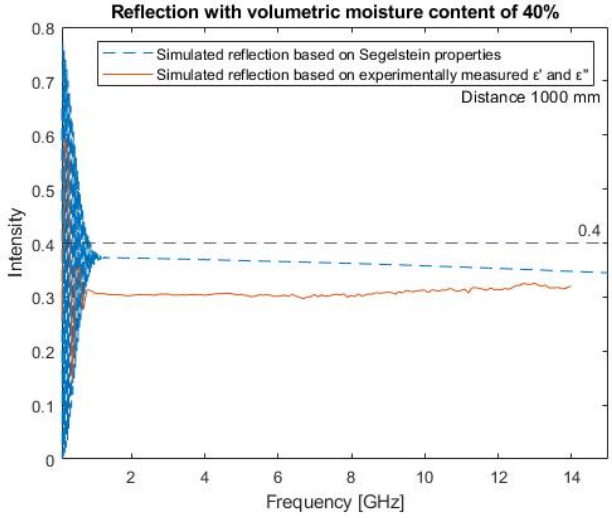

(b) 30 and 40% volumetric moisture content

Figure 33: Reflection based on the complex refractive index $\underline{n}$ gathered from Segelstein (1981) and the complex permittivity ε of water measured experimentally of a sponge as a function of frequency, with the distance set at 1000 mm and volumetric moisture contents between 10 and 40% [15]. Deviations in the interference pattern of the simulated reflection of the experimental properties is due to the low sampling resolution of the DAKS-3.5 setup.

Table 14: Reflection values at specific frequencies measured from the reflection spectra with the distance set at 1000 mm and volumetric moisture contents between 10 and 40%.

Frequency [GHz]	Volumetric moisture content	Segelstein reflection	Experimental (sponge sample)
3	0.1	0.078	0.065
3	0.2	0.19	0.13
3	0.3	0.29	0.23
3	0.4	0.37	0.31

5 Discussion

The aim of this master's thesis was to investigate whether electromagnet waves in the GHz domain could be used for moisture detection in waste materials. In this section, the findings from the theoretical model and the experimental measurements are evaluated and discussed to indicate whether the results serve to answer the initial problem statement. As well as considerations and possible improvement points to both the theoretical model and the experimental measurements.

5.1 Theoretical model

The theoretical model was developed and implemented based on the experimentally measured complex refractive index $\underline{n}$ of water at a temperature of 25°C gathered from Segelstein (1981) in the frequency range 0.1-1000 GHz. Reflection and transmission spectra were simulated in section 4.1 and 4.2 of media with volumetric moisture contents θ_w using the effective media approximation, distances d, and angles of incidence θ_1.

Due to the nature of the considered layered media, interference patterns emerged in the simulated reflection and transmission spectra. Where changes in the distance d caused the interference pattern to be shifted in relation to frequency and also change the oscillation rate in the interference pattern. An increase in distance d coincided with the interference pattern shifting towards the lower frequencies, as well as increasing the oscillation rate of the interference fringes. A detailed explanation to this behaviour is provided in section 4.1.3 by considering the equation (35). Additionally, increasing the moisture level had a similar effect on the interference pattern as increasing the distance d, which was also explained in more detail in section 4.1.3. By measuring the frequency of the first visible constructive interference fringe denoted by m and the corresponding refractive index n at that frequency, the distance d was determined from equation (26). Where the distance $d = 10$ mm was determined with 90% certainty, $d = 100$ mm with 98% certainty, and $d = 1000$ mm with 99.8% certainty. Increasing the distance beyond $d = 100$ mm did however make it more difficult to determine the distance from the interference pattern, as some of the fringes were shifted towards lower frequencies outside of the considered frequency range. Making difficult to identify the number m in equation (26) of the first visible interference fringe.

In the simulated reflection and transmission spectra, the interference pattern was present towards the lower end of the considered frequency range. As the frequency increased, the interference effects diminished and eventually concluded. At this point, both the reflection and transmission intensity levelled out, where the reflection decreased slowly with frequency to almost zero at 1000 GHz. While the transmission intensity increased slowly with frequency to almost unity at 1000 GHz. In the frequency region where the interference effects concluded and the reflection intensity levelled out, there was an apparent relationship between the reflection intensity and the level of moisture in the effective medium. Which seemed reasonable as an increase in moisture level implicated an increase in both the real and imaginary parts of the complex refractive index $\underline{n}$ of the effective

medium, resulting in a greater fraction of the incident electromagnetic waves to be reflected at the boundaries between the different layers in the layered medium. Measuring the reflection intensity in the specified frequency region gave a relatively accurate indication of the moisture level in the effective medium. This specified frequency region was however not the same for all the simulated spectra, as changes in the distance d caused the frequency at which the reflection intensity levelled out to be shifted.

Reflection and transmission spectra were simulated with distances ranging from 10 mm to 10 m, where measuring the reflection intensity in the frequency range of 1-35 GHz gave the best indication of the moisture level in the effective medium. Measuring the reflection intensity at the lower frequencies was best suited for the longer distances d, while the higher frequencies were best suited for the shorter distances d. The deviation between the moisture level in the effective medium and the measured reflection intensity was more significant for the shorter distances d. Increasing the distance d improved the accuracy at which the moisture level was determined by measuring the reflection intensity in the specified frequency region. The average deviation between the actual moisture level in the effective medium and the measured reflection intensity from all the simulated spectra provided in section 4.1 was found to be 14%. Meaning that by interpreting the simulated reflection spectra in the frequency range 1-35 GHz, moisture levels ranging from 10 to 40% in the effective medium was detected to a certainty of 86%.

5.1.1 Considerations and limitations of the theoretical model

The theoretical model used to simulate reflection and transmission spectra from the complex refractive index $\underline{n}$ of water gathered from Segelstein (1981) is based on a few assumptions and simplifications which certainly deviate from reality. Therefore it is uncertain how reliable the theoretical model is in regards to detecting moisture levels. To begin with, dielectric properties such as the complex refractive index $\underline{n}$ is sensitive to small changes in temperature. Where the theoretical model is based on the complex refractive index $\underline{n}$ measured only at the temperature of 25°C. To improve the reliability of the results, simulations using the complex refractive index $\underline{n}$ at different temperatures should be performed.

The theoretical model is also based on the ideal case showcased in figure 1, where the electromagnetic wave is assumed to propagate through a structure of three layers separated by planar boundaries. An electromagnetic wave would rarely travel through these three layers alone. In reality, the electromagnetic wave would most likely propagate through a structure consisting of many different layers. Additionally, the boundaries between the different layers of the considered system in figure 1 are assumed to planar. In reality, all surfaces are rough. As the roughness of the surface is at a similar or smaller scale to the wavelength λ of the incident electromagnetic wave, scattering process occur. These scattering processes at rough surfaces have not been considered in the theoretical model. Which could be useful to consider in future work, as these scattering processes will influence the response of the incident electromagnetic waves.

Results in section 4.2 addresses off-axis waves at two different angles of incidence θ_1 for both TE and TM polarisation. Increasing the incidence angle θ_1 caused the reflection and transmission spectra of TE and TM polarised waves to deviate from the corresponding spectra for normally incident waves, where the deviation became more significant as both the moisture level and incidence angle θ_1 increased. It is therefore desirable to perform moisture measurements at normal incidence if possible.

Another aspect that influences the reliability of the results provided by the theoretical model stems from the use of an effective media approximation to determine the effective complex refractive index $\underline{n}$ of media containing different levels of moisture. This approximation allows for heterogeneous media to be treated as homogeneous media. This simplification does however deviate from reality, as inhomogeneities in media directly influences the propagation of electromagnetic waves. Inhomogeneities and impurities in a media can cause the electromagnetic waves to be scattered in an unpredictable manner. Representing media of different moisture levels through effective media approximation may therefore not be the most reliable approach. However, when considering scattering and absorption in composite materials, no other methods to solve the problem are readily available. The effective media approximation considered in this master's thesis is the volume average of refractive indexes. As there are several other effective media approximations available, trying out different effective media approximations to find the one most suitable for the specific circumstances may improve the reliability of the results.

Lastly, the theoretical model was based on the assumption that electromagnetic waves in the considered frequency range has high transmission in most materials except water and metals. Where the materials mixed with water were assumed to exhibit approximately the same dielectric properties as air (i.e. $n \approx 1$). This is only true to an extent, as certain materials such as polymers have refractive indices typically ranging from 1.3-1.7. Thus, if materials such as metals or polymers are mixed together with the media containing water, the response of the system is affected. Making it more difficult to determine whether the response of the system is caused only by changes in moisture level.

5.2 Experimental measurements

Experimental measurements of dielectric properties at different volumetric moisture contents θ_w between 10 and 40% were executed using a sponge as sample material. Measurements of the complex permittivity ε provided in section 4.3.2 were then used to simulate the corresponding reflection spectra following the same method described for the theoretical model in the frequency range 85 MHz - 14 GHz, provided in section 4.3.3. Such that the validity and accuracy of the theoretical model could be determined by comparing with the corresponding reflection spectra simulated from the experimental measurements. As well as evaluating whether changes in the simulated reflection spectra were correlated to changes in the volumetric moisture content θ_w in the sample material, such that the volumetric moisture content θ_w could be determined by interpreting the corresponding reflection spectra.

The complex permittivity ε measured experimentally at different volumetric moisture levels θ_w was compared to the corresponding complex permittivity ε derived from Segelstein (1981) and the effective media approximation to regulate for different volumetric moisture contents θ_w. Both the experimental and Segelstein (1981) properties followed the same trends in regards to changes in the volumetric moisture content θ_w, as well as frequency. The experimentally measured values of the dielectric constant ε' and dielectric loss factor ε'' presented in figure 29 did contain some noise, especially towards the higher end of the frequency range. Additionally, there was considerable deviation between the measured and Segelstein properties at certain frequencies and volumetric moisture contents, substantiated by table 11. Where the average deviation of all the measurements of the dielectric constant ε' and dielectric loss factor ε'' was found to be 24.94% and 17.4%, respectively. [15]

Using equations (9) and (10), the experimentally measured values of the dielectric constant ε' and dielectric loss factor ε'' were converted to the refractive index n and extinction coefficient κ. Such that the corresponding reflection spectra could be simulated for different distances d and volumetric moisture contents θ_w between 10 and 40%, provided in section 4.3.3. The reflection spectra derived from the theoretical model were also included for comparisons sake. Again, both the experimental and theoretical reflection spectra followed the same trends in regards to changes in the volumetric moisture content θ_w and distance d. The simulated reflection intensity based on the experimentally measured dielectric properties was consistent to some extent in comparisons to the theoretical reflection intensity. However, there was still a noticeable deviation between the two simulated reflection intensities at the different volumetric moisture contents $_w$, which was consistent with the deviation between the Segelstein (1981) and experimental measurements of the dielectric constant ε' and dielectric loss factor ε'' provided in table 11. [15]

The interference pattern was also present in the simulated experimental reflection intensity towards the lower end of the frequency range. Where an increase in both the distance d and volumetric moisture content θ_w caused the interference pattern to be shifted towards the lower frequencies, as

well as increasing the oscillation rate of the interference fringe. A response that was explained in more detail in section 4.1.3 by considering the relationship between the wavelength λ, distance d, and the refractive index n in equation (35). As the distance d was increased beyond 100 mm, there was a deviation in the interference pattern between the simulated reflection intensity based on the experimentally measured values and the theoretical model. This could be explained by considering that the DAKS-3.5 only sampled the dielectric properties of the sample material with 100 MHz intervals. Where the oscillations in the interference pattern through material of distance $d = 1000$ mm was considerably more sensitive to frequency changes than intervals of 100 MHz. Sampling the dielectric properties of the sample material with a higher resolution would reduce the deviation in the interference pattern for the corresponding reflection simulation.

The experimental reflection spectra were interpreted in a similar manner as the reflection spectra of the theoretical model in regards to determining the volumetric moisture level θ_w of the sample material. In doing so, the average deviation between the actual volumetric moisture level θ_w of the sample material and the corresponding measurement of the reflection intensity was found to be 30.7%, 29.2%, and 28.96% for the distances of 100 mm, 500 mm, and 1000 mm, respectively. Giving a total average deviation of 29.62% between the two quantities. Meaning that by interpreting the simulated reflection intensity at any given volumetric moisture level θ_w would indicate the moisture level on average to certainty of 70.38%. Which is only a 15.62% difference to the findings from the theoretical mode. However, the findings from the theoretical model was based on a larger data set compared to the experimental data set. Where the deviation at shorter distances d was greater in comparisons to that of longer distances d. The key takeaway is that even though the experimental results were slightly less accurate in comparisons to the theoretical, the same trends discovered from the theoretical model regarding the relation between the volumetric moisture content θ_w and the corresponding dielectric properties of the effective medium were also present in the experimental results. Where an increase in volumetric moisture content θ_w coincided with an increase in the complex permittivity ε and the corresponding reflection intensity. Giving a fairly accurate indication of the volumetric moisture level θ_w in the sample material.

5.2.1 Considerations for the experimental measurements

The experimental results were measured using DAKS-3.5 consisting of an open ended coaxial probe connected to a R140 VNA, which measured the scattering parameter $S11$ and converts to the corresponding values of the complex permittivity ε. This measurement setup is limited to the frequency range 85 MHz - 14 GHz, which was not ideal considering that the frequency range addressed in this master's thesis extended from 0.1 to 1000 GHz. However, the experimental measurements still provided enough data to give an indication of the moisture level in the sample material, or at least indicate changes in the changes in the volumetric moisture content in the sample material.

As mentioned in section 3.2.4, the chosen measurement method has both advantages and disadvantages. Even though the experimental measurements provided relatively accurate results in terms of

detecting the moisture level, the method still had its limitations. As the probe is primarily designed to perform measurements on homogeneous materials with solid surfaces, which was not the case for the sample material used in the experimental measurements. Pressing the probe on the surface of the sponge drastically impacted the measurements, making it difficult to acquire consistent measurements. As pressing the probe on the soft sponge caused the sponge to deform and make for an uneven surface, leading to heterogeneous features and thereby unreliable measurements. Resting the probe too lightly on the surface could introduce the presence of air bubbles, which is also to the detriment of accurate readings. To achieve somewhat consistent readings, the probe had to be carefully placed on the surface of the sponge without deforming the surface, but still minimising the likelihood of air bubbles to appear.

The sample material itself had limitations that could influence the consistency and reliability of the measurements. For instance, it is hard to tell if the water inside the sponge was uniformly distributed. It is reasonable to assume that water inside the sponge flowed towards the bottom of the sponge due to the gravitational force. In an attempt to counteract this effect, the sponge was flipped in-between measurements. Difficulties were also experienced when performing measurements at high volumetric moisture contents θ_w, as some of the water leaked out of the sponge during measurements.

For consistent measurements, temperature variations should also be kept to a minimum. As the dielectric properties are sensitive to small changes in temperature. Maintaining the same temperature for each measurement is however only possible in a controlled environment, which was not the case for the experimental measurement method used in this master's thesis.

It is also worth mentioning that the reflection spectra simulated for the experimental measurements were based on the method used for the theoretical model and not actual experimental reflection spectra measured from a sample material. The experimental reflection spectra were simulated based on the experimentally measured dielectric properties of the wet sponge to compare with the corresponding reflection spectra simulated based on dielectric properties gathered from Segelstein (1981) and the effective media approximation.

5.3 Future work

As mentioned, the experimental measurement method used in this master's thesis is somewhat limited. Trying different measurement methods such as the free space method could be useful, especially since the free space measuring method does not require the measuring equipment to be in contact with the sample material. Even though this measurement method has its advantages and disadvantages, it would still provide a larger data set to analyse and characterise how sample materials with different volumetric moisture contents θ_w affect the measurements. The free space method would also give a more accurate representation in relation to the method used to develop the theoretical model, as it would measure the reflection of the sample material without requiring

to be in contact with the surface of the sample. Where this specific requirement for the open ended coaxial probe method was to the detriment of accurate readings due to the soft surface of the sponge.

Trying different sample materials filled with water to see if it affects the measured dielectric properties could also be useful. As the theoretical model is based on the assumption that the material containing water had the same dielectric properties as air, which might not always be the case (e.g. polymers). Maintaining a consistent temperature would also make for improved measurements. Although it would most likely require a controlled environment, which does not give an accurate representation of real-world conditions. Thus it might be useful to measure dielectric properties across a wide range of temperatures at different volumetric moisture contents θ_w to get a better understanding of how the measurements are affected by temperature. As well as measuring samples with a non-planar surface, different shapes, sizes, and cross-sectional areas to give a more realistic representation of real-world conditions.

In relation to the theoretical model, trying out different effective media approximations might also be useful to see which one is the most suitable for the specific circumstances. As well as considering how rough surfaces influence the incident electromagnetic waves, especially when the roughness of the surface is at a similar or smaller scale to the wavelength λ.

6 Conclusion

As stated previously, the aim of this master's thesis was to investigate whether electromagnetic waves in the GHz domain could be a viable solution to detect moisture in homogeneous materials. By using the complex frequency-dependent refractive index $\underline{n}(\nu)$ of water combined with matrix theory and effective medium approximation, reflectance and transmittance spectra were simulated for an effective media with different moisture levels.

Simulated reflectance and transmittance spectra based on the theoretical model for different moisture levels and distances d provided in sections 4.1 and 4.2, were analyzed at both normal incidence and with increased incidence angles of $\theta_1 = 15^\circ$ and 30° for TE and TM polarised waves. The simulated spectra from the theoretical model showed promising results in detecting moisture levels, as the measured power reflectance from the simulated spectra increased accordingly with the level of moisture. Especially in the frequency range of 1-35 GHz. From interpreting all the simulated reflection and transmission spectra for normal incidence, the moisture level was detected with an average certainty of 86%. It is worth mentioning that these results are valid only at the temperature of 25°C. Introducing variables such as temperature, pressure, incidence angle θ_1, different polarisation or rough surfaces has direct influence over the corresponding reflection and transmission spectra of the considered system. Where increasing the incidence angle θ_1 beyond 0° at normal incidence lead to considerably less accurate results in terms of detecting the moisture level, see section 4.2.

An interesting by-product of the considered system in figure 1 showed up as interference patterns in the simulated spectra in section 4.1. The frequency of the oscillations in the interference pattern, as well as the position of the interference pattern in relation to frequency was both dependent on the moisture level and distance d of the effective medium. Increasing the distance d or the moisture level also increased the frequency of the oscillations, and shifted the interference pattern towards the lower end of the considered frequency range. By interpreting the interference pattern in the simulated reflection spectra using interference theory explained in section 2.7, the distance d of the effective medium was determined with to a high degree of certainty.

To determine the validity and accuracy of the theoretical model, experimental measurements of dielectric properties were performed in the lab using the DAKS-3.5 measurement setup. A sponge filled with different volumetric moisture contents θ_w was used as sample material. By measuring the dielectric constant ε' and the dielectric loss factor ε'' of the wet sponge for different volumetric moisture contents θ_w ranging from 10 to 40%, the corresponding reflection spectra were simulated using the same method described for the theoretical model. The resulting reflection spectra were then compared to the corresponding reflection spectra simulated from the theoretical model. Where the simulated reflection spectra based on the experimentally measured dielectric properties detected the volumetric moisture content θ_w of the sample material with an average certainty of 70.38%, which is 15.62% less than for the theoretical model. Limitations and inconsistencies of the measurement method could be the source of the deviation between the experimental and theoretical results,

discussed in section 5. The key takeaway is however that an increase in volumetric moisture content θ_w in the sample material was strongly correlated with an increase in the observed reflection intensity in the simulated reflection spectra. Especially in the frequency range of 1-35 GHz in the theoretical results, and 3-14 GHz in the experimental results.

Further studies should be conducted by measuring dielectric properties of sample materials filled with different volumetric moisture contents θ_w in different conditions. As well as trying different measurement methods to verify the validity of the theoretical model. The theoretical model can also be further developed by trying different effective media approximations to determine which one is most suited for moisture detection in sample materials.

References

1. Cheng, H., Zhang, Y., Meng, A. & Li, Q. Municipal Solid Waste Fueled Power Generation in China: A Case Study of Waste-to-Energy in Changchun City. *Environmental Science & Technology* **41.** PMID: 18044534, 7509–7515. https://doi.org/10.1021/es071416g (2007).

2. Chýlek, P., Srivastava, V., Pinnick, R. G. & R. T. Wang, R. T. Scattering of electromagnetic waves by composite spherical particles: experiment and effective medium approximations. *Applied Optics* **27,** 2396–2404. https://doi.org/10.1364/AO.27.002396 (12 June 1988).

3. Ellison, W., Lamkaouchi, K. & Moreau, J.-M. Water: a dielectric reference. *Journal of Molecular Liquids* **68,** 171–279. ISSN: 0167-7322. https://www.sciencedirect.com/science/article/pii/0167732296009269 (1996).

4. Fitzpatrick, R. *Electromagnetism and Optics* Spring 1999.

5. Hutchinson, N. J., Coquil, T., Navid, A. & Pilon, L. Effective optical properties of highly ordered mesoporous thin films. https://www.seas.ucla.edu/~pilon/Publications/TSF2010-numerical.pdf (Sept. 9, 2009).

6. Komilis, D., Kissas, K. & Symeonidis, A. Effect of organic matter and moisture on the calorific value of solid wastes: An update of the Tanner diagram. *Waste Management* **34,** 249–255. ISSN: 0956-053X. https://www.sciencedirect.com/science/article/pii/S0956053X13004601 (2014).

7. Kumar, A. & Samadder, S. A review on technological options of waste to energy for effective management of municipal solid waste. *Waste Management* **69,** 407–422. ISSN: 0956-053X. https://www.sciencedirect.com/science/article/pii/S0956053X17306268 (2017).

8. Kupfer, K. *Electromagnetic Aquametry* (Springer, Amalienstr. 13, 2005).

9. La Gioia, A., Porter, E., Merunka, I., Shahzad, A., Salahuddin, S., Jones, M. & O'Halloran, M. Open-Ended Coaxial Probe Technique for Dielectric Measurement of Biological Tissues: Challenges and Common Practices. *Diagnostics* **8,** 40 (June 2018).

10. Lunkenheimer, P., Emmert, S., Gulich, R., Köhler, M., Wolf, M., Schwab, M. & Loidl, A. Electromagnetic-radiation absorption by water. *Phys. Rev. E* **96,** 062607. https://link.aps.org/doi/10.1103/PhysRevE.96.062607 (6 Dec. 2017).

11. Mohee, R. & Mudhoo, A. in *Waste to Energy: Opportunities and Challenges for Developing and Transition Economies* (ed Karagiannidis, A.) 297–321 (Springer London, London, 2012). ISBN: 978-1-4471-2306-4. https://doi.org/10.1007/978-1-4471-2306-4_12.

12. Oyama, Y., Zhen, L., Tanabe, T. & Kagaya, M. Sub-terahertz imaging of defects in building blocks. *NDT E International* **42,** 28–33. ISSN: 0963-8695. https://www.sciencedirect.com/science/article/pii/S0963869508000911 (2009).

13. Paz, A. M., Trabelsi, S., Nelson, S. O. & Thorin, E. Measurement of the Dielectric Properties of Sawdust Between 0.5 and 15 GHz. *IEEE Transactions on Instrumentation and Measurement* **60,** 3384–3390 (2011).

14. Saleh, B. E. A. & Teich, M. C. *Fundamentals of Photonics* (John Wiley Sons, Incorporated, ProQuest Ebook Central, 2013).

15. Segelstein D, *The complex refractive index of water* (1981). https://mospace.umsystem.edu/xmlui/bitstream/handle/10355/11599/SegelsteinComRefInd.pdf?sequence=4&isAllowed=y.

16. University of Reading. Absorption and extinction coefficient theory. https://www.reading.ac.uk/ir-substrateopticaltheory-absorptionandextinctioncoefficienttheory.aspx (2019).

17. Wooten, F. *Chapter 3 - ABSORPTION AND DISPERSION* (ed Wooten, F.) 42–84. ISBN: 978-0-12-763450-0. https://www.sciencedirect.com/science/article/pii/B9780127634500500088 (Academic Press, 1972).

A Matlab code for generating reflectance and transmittance spectra

```
refractiveIndexAir=1+1i*0;                    %refractive index air

n=100;                                        %100 microns (0.1 mm) between each mie
    scattering computation
wavelength=199:n:3200000;                     %Wavelengths of incident light on
   particles micrometer
DISTANCE_OF_MEDIA = 10000000;                 %distance d of media containing
   moisture in micrometers
y=complexRefInd(wavelength);                  %Complex refractive index data

reflectionLHS_TE = zeros(1, length(wavelength));
reflectionRHS_TE = zeros(1, length(wavelength));
transmissionLHS_TE = zeros(1, length(wavelength));
transmissionRHS_TE = zeros(1, length(wavelength));

reflectionLHS_TM = zeros(1, length(wavelength));
reflectionRHS_TM = zeros(1, length(wavelength));
transmissionLHS_TM = zeros(1, length(wavelength));
transmissionRHS_TM = zeros(1, length(wavelength));

reflectionLHS = zeros(1, length(wavelength));
reflectionRHS = zeros(1, length(wavelength));
transmissionLHS = zeros(1, length(wavelength));
transmissionRHS = zeros(1, length(wavelength));

reflection = zeros(1, length(wavelength));

frequency = zeros(1, length(wavelength));
wavelengthMeters = zeros(1, length(wavelength));

moistureLevel = 0.3;                         %water volume

LIGHT_SPEED = 3*10^8;                         %light speed

ANGLE_OF_INCIDENCE = pi/12;

for q=1:length(wavelength)

effectiveMedia = (1-moistureLevel)*refractiveIndexAir + moistureLevel*y(q);
          %refractive index with effective media approximation

ANGLE_OF_REFRACTION = asin((refractiveIndexAir*sin(ANGLE_OF_INCIDENCE))/
   effectiveMedia);
k0 = 2*pi/wavelength(q);  %free-spave wavenumber

```

```
%Implementation of normally incident waves
r_12 = (refractiveIndexAir - effectiveMedia)/(refractiveIndexAir + effectiveMedia)
    ;     %reflection coefficients at first boundary
r_21 = (effectiveMedia - refractiveIndexAir)/(refractiveIndexAir + effectiveMedia)
    ;

t_12 = sqrt(1-(abs(r_12))^2);       %transmission coeffcients at first boundary
t_21 = sqrt(1-(abs(r_21))^2);

A1 = (t_12*t_21-r_12*r_21)/t_21;    %Conversion between S_1 to M1
B1 = r_21/t_21;
C1 = -r_12/t_21;
D1 = 1/t_21;

A3= (t_12*t_21-r_12*r_21)/t_12; %Conversion between S_3 to M3
B3 = r_12/t_12;
C3 = -r_21/t_12;
D3 = 1/t_12;

a = real(effectiveMedia)*k0*DISTANCE_OF_MEDIA;            %n value
b = imag(effectiveMedia)*k0*DISTANCE_OF_MEDIA;            %k value

A2 = exp(-b - 1i*a);            %Elements of the matrix of the wave
D2 = exp(b + 1i*a);             %propagating through the middle layer

M2 = [A2 0; 0 D2];

M1 = [A1 B1; C1 D1];
M3 = [A3 B3; C3 D3];        %The three wave-transfer matrices M1, M2, and M3

M = M3*M2*M1;                   %Product of M3, M2, and M1

t_123 = (M(1)*M(4) - M(3)*M(2))/M(4);
t_321 = 1/M(4);
r_123 = -M(3)/M(4);              %Converting back to scattering matrix to
r_321 = M(2)/M(4);               %find the overall reflectance and transittance

%Implementation of oblique TE polarised waves
n_1_TE = refractiveIndexAir*cos(ANGLE_OF_INCIDENCE);
n_2_TE = effectiveMedia*cos(ANGLE_OF_REFRACTION);
a_12_TE = 1;
a_21_TE = 1;

r_TE_12 = (n_1_TE-n_2_TE)/(n_1_TE+n_2_TE);
r_TE_21 = (n_2_TE-n_1_TE)/(n_1_TE+n_2_TE);

A1_TE = (n_1_TE+n_2_TE)/(2*a_21_TE*n_2_TE);
B1_TE = (n_2_TE-n_1_TE)/(2*a_21_TE*n_2_TE);
```

```
C1_TE = B1_TE;
D1_TE = A1_TE;

A3_TE = (n_1_TE+n_2_TE)/(2*a_12_TE*n_1_TE);
B3_TE = (n_1_TE-n_2_TE)/(2*a_12_TE*n_1_TE);
C3_TE = B3_TE;
D3_TE = A3_TE;

M_TE_1 = [A1_TE B1_TE; C1_TE D1_TE];
M_TE_3 = [A3_TE B3_TE; C3_TE D3_TE];

a_OFF_AXIS = real(effectiveMedia)*k0*DISTANCE_OF_MEDIA*cos(ANGLE_OF_REFRACTION);
             %n value
b_OFF_AXIS = imag(effectiveMedia)*k0*DISTANCE_OF_MEDIA*cos(ANGLE_OF_REFRACTION);
             %k value

A2_OFF_AXIS = exp(-b_OFF_AXIS - 1i*a_OFF_AXIS);            %Elements of the matrix
    for the wave
D2_OFF_AXIS = exp(b_OFF_AXIS + 1i*a_OFF_AXIS);             %propagating through
    the middle layer

M2_OFF_AXIS = [A2_OFF_AXIS 0; 0 D2_OFF_AXIS];

M_TE = M_TE_3*M2_OFF_AXIS*M_TE_1;                    %Product of M3, M2, and M1

t_TE_123 = (M_TE(1)*M_TE(4) - M_TE(3)*M_TE(2))/M_TE(4);
t_TE_321 = 1/M_TE(4);
r_TE_123 = -M_TE(3)/M_TE(4);              %Converting back to scattering matrix to
r_TE_321 = M_TE(2)/M_TE(4);               %find the overall reflectance and
    transittance

%Implementation of oblique TM polarised waves
n_1_TM = refractiveIndexAir*sec(ANGLE_OF_INCIDENCE);
n_2_TM = effectiveMedia*sec(ANGLE_OF_REFRACTION);
a_12_TM = cos(ANGLE_OF_INCIDENCE)/cos(ANGLE_OF_REFRACTION);
a_21_TM = 1/a_12_TM;

r_TM_12 = (n_1_TM-n_2_TM)/(n_1_TM+n_2_TM);
r_TM_21 = (n_2_TM-n_1_TM)/(n_1_TM+n_2_TM);

A1_TM = (n_1_TM+n_2_TM)/(2*a_21_TM*n_2_TM);
B1_TM = (n_2_TM-n_1_TM)/(2*a_21_TM*n_2_TM);
C1_TM = B1_TM;
D1_TM = A1_TM;

A3_TM = (n_1_TM+n_2_TM)/(2*a_12_TM*n_1_TM);
B3_TM = (n_2_TM-n_1_TM)/(2*a_12_TM*n_1_TM);
C3_TM = B3_TM;
```

```
D3_TM = A3_TM;

M_TM_1 = [A1_TM B1_TM; C1_TM D1_TM];
M_TM_3 = [A3_TM B3_TM; C3_TM D3_TM];

M_TM = M_TM_3*M2_OFF_AXIS*M_TM_1;                    %Product of M3, M2, and M1

t_TM_123 = (M_TM(1)*M_TM(4) - M_TM(3)*M_TM(2))/M_TM(4);
t_TM_321 = 1/M_TM(4);
r_TM_123 = -M_TM(3)/M_TM(4);              %Converting back to scattering matrix to
r_TM_321 = M_TM(2)/M_TM(4);               %find the overall reflectance and
    transittance

%Plotting the Fresnel equations where the theoretical model produces
%invalid results

reflection(q) = (abs(r_123))^2;

if (q > 1)
    k = q-1;
    if isnan(reflection(k))

        reflectionLHS(q) = (abs(r_12))^2;               %Fresnel reflection
        transmissionLHS(q) = 1-(abs(r_12))^2;           %Fresnel transmission

        reflectionLHS_TE(q) = (abs(r_TE_12))^2;         %Fresnel reflection TE
        transmissionLHS_TE(q) = 1-(abs(r_TE_12))^2;     %Fresnel transmission TE

        reflectionLHS_TM(q) = (abs(r_TM_12))^2;         %Fresnel reflection TM
        transmissionLHS_TM(q) = 1-(abs(r_TM_12))^2;     %Fresnel transmission TM
    elseif reflection(k)>0
        reflectionLHS(q) = (abs(r_123))^2;
        reflectionRHS(q) = (abs(r_321))^2;              %Power reflectance

        transmissionLHS(q) = 1-(abs(r_123))^2;
        transmissionRHS(q) = 1-(abs(r_321))^2;          %Power transmittance

        reflectionLHS_TE(q) = (abs(r_TE_123))^2;
        reflectionRHS_TE(q) = (abs(r_TE_321))^2;

        transmissionLHS_TE(q) = 1-(abs(r_TE_123))^2;
        transmissionRHS_TE(q) = 1-(abs(r_TE_321))^2;

        reflectionLHS_TM(q) = (abs(r_TM_123))^2;
        reflectionRHS_TM(q) = (abs(r_TM_321))^2;

        transmissionLHS_TM(q) = 1-(abs(r_TM_123))^2;
        transmissionRHS_TM(q) = 1-(abs(r_TM_321))^2;
```

```
177
178     end
179
180 end
181
182 wavelengthMeters(q) = wavelength(q)*10^(-6);  %wavelength in meters
183 frequency(q) = LIGHT_SPEED/wavelengthMeters(q); %frequency
184
185 end
186
187 semilogx(frequency, reflectionLHS,'--', frequency, transmissionLHS,'--', frequency
    , reflectionLHS_TE, frequency, transmissionLHS_TE,frequency, reflectionLHS_TM,
    frequency, transmissionLHS_TM);
```

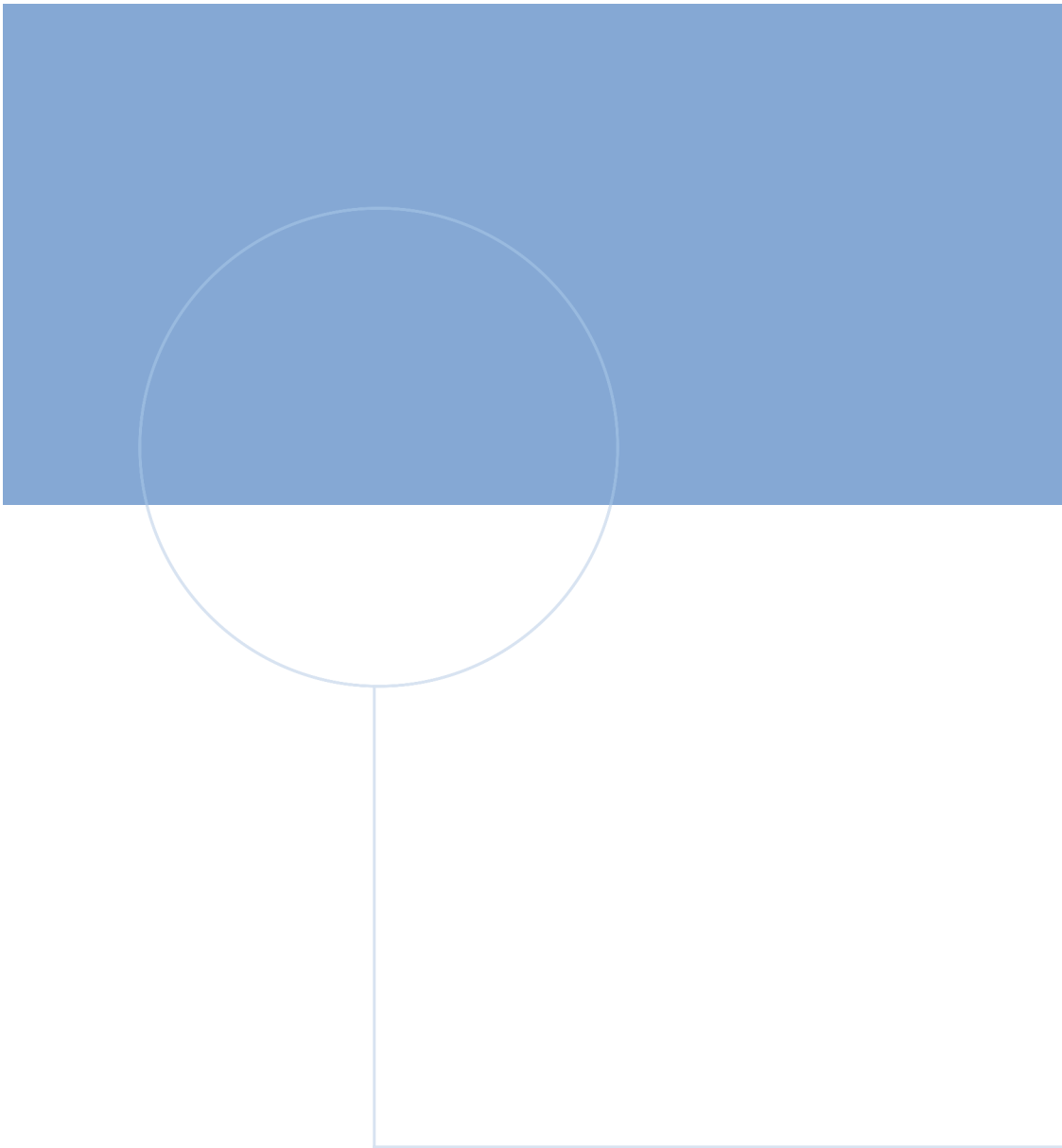

NTNU

Norwegian University of
Science and Technology